Design and Development of Energy Management Strategies for Community and Building Microgrid with Energy Storage and Electric Vehicles

THESIS

Submitted in partial fulfillment of the requirements for the degree of

DOCTOR OF PHILOSOPHY

by

Pavitra Sharma

ID No. 2019PHXF0027P

Under the supervision of

Prof. Hitesh Datt Mathur

and Under the co-supervision of

Prof. Puneet Mishra

BITS Pilani
Pilani | Dubai | Goa | Hyderabad | Mumbai

BIRLA INSTITUTE OF TECHNOLOGY AND SCIENCE

PILANI (RAJASTHAN) INDIA

2024

BITS Pilani
Pilani | Dubai | Goa | Hyderabad | Mumbai

BIRLA INSTITUTE OF TECHNOLOGY AND SCIENCE

DEPARTMENT OF ELECTRICAL AND ELECTRONICS ENGINEERING

PILANI- CAMPUS PILANI (RAJASTHAN) INDIA

CERTIFICATE

This is to certify that the thesis entitled **"Design and Development of Energy Management Strategies for Community and Building Microgrid with Energy Storage and Electric Vehicles"** submitted by **Pavitra Sharma,** ID. No. **2019PHXF0027P** for an award of Ph.D. of the Institute embodies her original work under my supervision.

Signature of the Supervisor

Name	**Prof. Hitesh Datt Mathur**
Designation	**Professor, Department of Electrical & Electronics Engineering Birla Institute of Technology and Science, Pilani, Pilani-Campus Rajasthan, INDIA**
Date	27th September 2024

Signature of the Co-Supervisor

Name	**Prof. Puneet Mishra**
Designation	**Assistant Professor, Department of Electrical & Electronics Engineering Birla Institute of Technology and Science, Pilani, Pilani-Campus Rajasthan, INDIA**
Date	27th September 2024

BIRLA INSTITUTE OF TECHNOLOGY AND SCIENCE

DEPARTMENT OF ELECTRICAL AND ELECTRONICS ENGINEERING

PILANI- CAMPUS PILANI (RAJASTHAN) INDIA

DECLARATION

I hereby declare that this submission is solely my original work. To the best of my knowledge and belief, it does not include any content previously published or authored by another individual, nor does it incorporate material that has substantially contributed to the conferral of any other academic degree or diploma from a university or other institution of higher learning.

I further authorize the Birla Institute of Technology and Science (BITS), Pilani to reproduce this thesis, either in whole or in part, through photocopying or any other means. This authorization extends to fulfilling requests from other institutions or individuals exclusively for scholarly research purposes.

Signature

Name **Pavitra Sharma**

Date 27th September 2024

Acknowledgement

I would like to express my sincere gratitude to all those who have contributed to completing this thesis. First and foremost, I am grateful to my supervisors, Prof. Hitesh Datt Mathur and Dr. Puneet Mishra, for their unwavering support, guidance, and expertise throughout the research process. Their combined insights and encouragement played a crucial role in shaping the direction and quality of this thesis. I am highly thankful to my Doctoral Advisory Committee members, Dr. Bijoy Krishna Mukherjee and Dr. Ashish Patel, for their insightful feedback and constructive criticism. Their expertise greatly enriched the quality of this research.

I am grateful to the EEE department, BITS-Pilani, for providing the necessary resources and facilities to conduct this research. The academic environment and resources offered by the department were instrumental in completing this thesis. I sincerely thank HoD Prof. Navneet Gupta and Ex-HoD Prof. Vinod Kumar Chubey for providing me the requisite facilities to conduct my doctoral research. I am thankful to Prof. Praveen Kumar A. V. (Convener-Departmental Research Committee), Dr. Meetha V. Shenoy, and other faculty colleagues of the EEE department for their constant motivation and encouragement. Special thanks to Prof. V. Ramgopal Rao, Vice-Chancellor of BITS Pilani, and Prof. Sudhir Kumar Barai, Director of BITS Pilani, Pilani campus, for allowing me to pursue my research successfully. I sincerely thank the Department of Science and Technology (DST), New Delhi, for providing financial support for conducting the research.

I am also grateful to my seniors, friends and colleagues Dr. Dhananjay Kumar, Dr. Heema Dave, Dr. Prashant Upadhyay, Dr. Krishna Veer Singh, Dr. Akhilesh Kumar Mishra, Dr. Anukaran Khanna, Dr. Sisir Kumar Yadav, Dr. Rishi Parvanda, Dr. Radha Bhardwaj, Mr. Krishna Kumar Saini, Mr. Somesh Krishna Thanvi, Miss Preeti Sharma and Mr. Shubham Priyadarshi who kept me inspiring and helped in difficult times. Special thanks to my roommates, Dr. Manisha Chaudhary and Dr. Divya Rathore, for always being there for me. I will always cherish the happy moments I spent with my friends at the BITS Pilani campus.

During my teaching assistantship, I got unflinching support from Mr. Ravindra Kumar, Mr. Ashok Saini, and Mr. Tulsiram Sharma for the successful course delivery. I extend my sincere gratitude to Mr. Yogesh Alaria and Mr. Sanjay Bhargava for dealing with all the documentation required for a research scholar. They always made cumbersome processes trouble-free.

I express my deep sense of gratitude, love and respect to my beloved mother Mrs. Veena Sharma and father Mr. Prakash Sharma. I extend my warmest thanks and sincere appreciation to my parents-in-law, Dr. Madhu Jain and Mr. Sudhanshu Mohan Jain, for their unwavering support and understanding throughout this academic endeavour. My heartfelt thanks to my life partner Dr. Tanmay Jain for his unconditional love, support, patience, and cooperation that constantly encouraged me and helped me to deal with my tough days. I would like to express my sincere gratitude and thanks to the entire Sharma and Jain family for their immense love, support and motivation.

Pavitra Sharma Jain

Abstract

The rising electricity demand, the need to reduce greenhouse gas (GHG) emissions, and the continued depletion of fossil fuel reserves require an extra effort by the various countries of the world to bring a paradigm shift in the energy sector. Thus, energy generation from renewable energy resources (RERs) and the installation of battery energy storage systems (BESS) have become very popular. The RERs, BESS and fossil fuel-based traditional generators (TGs) are considered distributed energy sources (DERs) and a micro-scale interconnection of these DERs and loads to make a low voltage electrical network can be termed a microgrid (MG). Furthermore, as electric vehicles (EVs) gained popularity as a viable alternative to fossil fuel-powered vehicles, their penetration has increased significantly. Therefore, to achieve the stable, optimal, sustainable, and efficient operation of the MG with EV integration, an energy management strategy (EMS) is required. The development of EMS is highly dependent on the type of MG, and the most critical MGs are community and building grid-tied MGs. Therefore, it is essential to evaluate energy management aspects for both the MGs.

The stable operation of MG, especially for a community-type MG, is governed by the size and placement of the DERs. To investigate this, multi-bus-based community MG is developed with various renewable & fossil fuel-based DERs, residential, industrial & commercial type voltage-dependent load models, BESS and different EV charging patterns. Further, this thesis formulates a multi-objective function to determine the optimal capacity and location of multiple DERs along with EVS to reduce power losses and voltage fluctuations in the system. Further, to achieve economical, sustainable, and efficient operation of the developed community MG an optimal energy management strategy (OEMS) is developed considering different modes of EV operation, i.e., autonomous charging mode (ACM) and governed charging/discharging mode (GCDM). The developed OEMS aims at maximum utilization of DERs, promotes energy trading between MG and utility grid, performs peak load management through GCDM, and minimizes the dependency of an MG on the utility grid. To attain the maximum utilization of BESS, a coordinated charging/discharging scheduling algorithm is formulated, which takes into account certain operational parameters such as total load demand, state of

charge (SOC) of the previous interval, and power not fulfilled by RERs, and fossil fuel based DERs.

To evaluate the energy management aspects of a building MG (prosumer) data from a real-time system is taken into account. The considered system is a grid-tied MG that consists of solar PV and BESS with EVS, which is designed, developed and deployed at the building of BITS, Pilani, campus. As the BESS accounts for high capital investment and has a limited life cycle, therefore there is a need for an EMS for prosumer buildings that aim at economical and efficient operation of the system. In this regard, this thesis proposed an improved energy management strategy (IEMS) that focuses on increasing the profit of a prosumer building and improving the operating life span of BESS. In addition, a non-linear battery degradation model considering static and dynamic degradation factors, is used to estimate the practical operating life span of BESS. Further, to enhance the efficacy of the proposed IEMS and to achieve the sustainable and more efficient operation of a building MG, a flexible load shifting (FLS) scheme is formulated. It minimizes the burden on BESS and decreases the grid export to MG, which increases the profit of a prosumer building operator, improves the operating life span of BESS, and reduces the dependency of MG on the grid.

The impact of EV penetration on the prosumer building is assessed by advanced probabilistic modelling of EVL, which considers practical situation, i.e., availability of plug-points and uncertain behaviour of EV owner in terms of time duration after which EV may leave the EVS. Further, along with ACM, a new mode of EV operation is introduced, i.e., governed charging/discharging with demand response mode (GCD_DRM). It combines vehicle-to-grid power transfer services and a vehicle demand response strategy to manage the load on the prosumer building. Finally, the performance of IEMS is evaluated by integrating the proposed FLS and the modes of EV operation.

Table of Contents

List of Figures

List of Tables

List of Abbreviations

ACM	Autonomous Charging Mode
BEMS	Basic Energy Management Strategy
BESS	Battery Energy Storage System
CEMS	Conventional Energy Management Strategy
COP	Conference of Parties
DEG	Dispatchable Energy Generator
DER	Distributed Energy Resource
DOD	Depth of Discharge
DR	Demand Response
DSM	Demand Side Management
EEMS	Existing Energy Management Strategy
EMA	Energy Management Architecture
EMS	Energy Management Strategy
EV	Electric Vehicle
EVL	Electric Vehicle Load
EVPL	Electric Vehicle Penetration Level
EVS	Electric Vehicle Station
FLS	Flexible Load Shifting
GCD_DRM	Governed Charging/Discharging with Demand Response Mode
GCDM	Governed Charging/Discharging Mode
GHG	Greenhouse Gas
IEA	International Energy Agency
IEMS	Improved Energy Management Strategy
MG	Microgrid
MGO	Microgrid Operator
OEMS	Optimal Energy Management Strategy

RBA	Rule Based Algorithm
RER	Renewable Energy Resource
SOC	State of Charge
Solar PV	Solar Photovoltaic
TAPL	Total Active Power Loss
TG	Traditional Generator
TVD	Total Voltage Deviation
WTG	Wind Turbine Generator

List of Symbols

Indices and Sets

$t \in \mathcal{T}$	Time interval, $\mathcal{T} \subseteq \mathbb{N}, \mathcal{T} = \{1,2,3,\dots,T\}$
$n \in \mathcal{N}_{EV}$	Number of EVs, $\mathcal{N}_{EV} \subseteq \mathbb{N}, \mathcal{N}_{EV} = \{1,2,3,\dots,N_{EV}\}$
$d \in \mathcal{D}_{EV}$	Type of EVs, $\mathcal{D}_{EV} \subseteq \mathbb{N}, \mathcal{D}_{EV} = \{1,2,3,\dots,D_{EV}\}$

Parameters

P_{PV}^{R}	Rated power of the solar PV generator in kW
η_{PV}	Performance coefficient of the PV power converter
$P_{L}^{\acute{m}}$ and $P_{L}^{\acute{M}}$	Minimum and maximum limits of load demand in kW
η_{PV}	Efficiency of solar PV system
G_{m}^{t}	Measured solar radiation at time 't'
G_{N}	Nominal solar radiation in W/m^2
$\theta_{A,m}^{t}$	Measured ambient temperature at time 't'
θ_{N}	Panel temperature in standard test conditions at ◦C
K_{θ}	Temperature coefficient in ◦C^{-1}
P_{WTG}^{R}	Rated power of the WTG in kW
V_i	Voltage at the i^{th} load bus
$V_{i}^{\acute{m}}$ and $V_{i}^{\acute{M}}$	Minimum and Maximum bus voltage limits
N_b	Total number of buses in the network
N_{br}	Total number of branches present in the network
ρ_B	Self-discharge rate of BESS
$\eta_{B,Ch/DCh}$	Charging and Discharging efficiency of BESS
E_{B}^{R}	Rated energy capacity of BESS.
$P_{B,Ch/Dch}^{\acute{M}}$	Maximum limit of charging and discharging power of BESS
$SOC_{B}^{\acute{m}}$ and $SOC_{B}^{\acute{M}}$	Minimum and Maximum limits of the SOC of the BESS

$SOC_{B,th}$	Threshold value of SOC of the BESS
$P_{B,Ch}^{\acute{M}}$ and $P_{B,Dch}^{\acute{M}}$	Maximum charging and discharging limit of the BESS
T_S	Shelf life of BESS
T_{OL}	Total operating life of BESS
BDf_S	Static degradation of BESS
$\Phi_B^{O\&M}$ and $\Psi_B^{O\&M}$	Variable and fixed O&M cost coefficients of BESS
$\mathbb{C}_{PV}$	Hourly O&M cost of solar PV system
$\zeta_{PV}^{O\&M}$	Operation and maintenance coefficient for the installed PV system
$E_{EV}^{R,d}$	Rated capacity of dth type EV battery
$\eta_{EV,Ch}/\eta_{EV,Dch}$	Charging and Discharging efficiency of EV
N_{EV_P}	Number of EV plug-points at EVS
$P_{EV,Ch/Dch}^{d}$	Rated charging/ discharging power of EV in kW/h
$SOC_{EV}^{\acute{M}}$	Maximum value of SOC of EV battery
$SOC_{EV,Dch}^{th}$	Threshold limit of SOC of EV battery till which discharging can be performed
$S_{EV}^{\acute{M},d}$	Maximum distance EV can travel in one charge
$TD_L^{\acute{m}}$	Minimum value of leave time duration required for V2G operation
N_{EV}^{E}, N_{EV}^{R}, N_{EV}^{V}	Number of EVs of employees, residential people and visitors
α_E, α_V and α_R	Ratios of employees, visitors, and residential EV owners.
$\pi_{PV}^{t,s}$ and $\pi_L^{t,s}$	Probabilities of each scenario 's' for time instant 't' for PV and load

Variables

P_L^t	Load demand of the system in kW at time 't'
P_{PV}^t	Power generated by solar PV in kW at time 't'
P_{WTG}^t	Power generated by WTG in kW at time 't'
P_{DEG}^t	Power generated by DEG in kW at time 't'

P_G^t	Power exchanged with grid in kW at time 't'
P_{Loss}^t	Real power loss occurring in system in kW at time 't'
v_w^t	Speed of wind in m/sec at time 't'
$P_{B,Ch}^t / P_{B,Dch}^t$	Charging and discharging power of the BESS at time instant 't'
SOC_B^t and SOC_B^{t+1}	SOC of BESS at 't' and 't+1' instant
BDf_D^t	Dynamic degradation of BESS for time interval 't'
$\mathbb{C}_{MG}^t$	Total operation cost of MG in $
$\mathbb{C}_G^t$	Cost of energy exchanged with the grid in $
$\mathbb{C}_B^t$	O&M cost of BESS in $
λ_G^t	Energy trading price of the grid at a time 't' in $/kWh
P_{EP}^t	Equivalent power in kW at a time 't'
T_{PI}^n	Plug-in time of EV
T_{AT}^n	Arrival time of EV
T_{PO}^n	Actual plug-out time of EV
T_{EPO}^n	Estimated plug-out time of EV
T_{DPO}^n	Desired plug-out time of EV
$S_{EV}^{n,d}$	Distance travelled by n^{th} EV of d^{th} type
TD_{Ch}^n	Time duration required by the EV for getting fully charged
$TD_{Dch}^{\acute{M},n}$	Maximum discharging time duration of EV
TD_{Dch}^n	Actual discharging duration of EV
$SOC_{EV,PI}^{n,d}$	SOC of EV at the time of plug-in
TD_L^n	Leave time duration of n^{th} EV
ξ_{G2V}^n	EV owner's input regarding G2V operation
ξ_{DRS}^n	EV owner's input regarding participation in DRS operation
$K_{\mathrm{V2G\_DRS}}^n$	Decision variable of EV aggregator
$T_{Dch,end}^n$	Time at which discharging of EV ends
$T_{Ch,starts}^n$	Time at which charging starts after discharging process of EV

$P_{EV,ACM}^{t}$, $P_{EV,GCDM}^{t}$, and P_{EV,GCD_DRM}^{t}	Daily EVL of N_{EV} EVs in case of ACM, GCDM and GCD_DRM

Chapter 1

Introduction

1.1. Background

The availability of electrical energy significantly impacts a society's present and future progress. The daily depletion of fossil fuel reserves, increasing electricity demand, and the need to reduce greenhouse gas (GHG) emissions necessitate a paradigm shift in the energy industry. It was reported by the European scientists from Copernicus and the World Meteorological Organization (WMO) that the past 10 decades were the hottest years on record, with 1.40°C above the pre-industrial average (1850-1900) [1][2]. It was also found that for the first time in 2022, global average CO_2 concentrations exceeded pre-industrial values by 50% and continued to rise in 2023 [3]. Therefore, promoting energy generation using indigenous resources, especially renewable energy resources (RERs) and low-carbon technology, has gained immense popularity. In this regard, at the 26th annual summit of COP (Conference of Parties), i.e., COP26, more than 200 countries pledged to keep temperature rises within 1.5°C and to reach net zero emissions by 2050 [4]. Scientists estimated that the goal can be achieved by reducing GHG emissions by 45% by 2030, compared with 2010 levels, and from there to net zero emissions by 2050. Further, COP28 discussed measures to accelerate efforts towards net zero by around mid-century and reduce non-CO2 emissions, e.g., methane emissions globally by 2030 [5]. It is suggested to triple the renewable energy capacity by 2030 (to at least 11,000 GW by 2030) and collectively double the global energy efficiency improvements from around 2% to over 4% annually until 2030, as shown in Fig. 1.1 [6]. The International Energy Agency (IEA) discussed the roadmap to achieve Net Zero by 2050 and expects a surge in solar photovoltaic (PV) and wind energy source

capacity addition (including households with rooftop), battery storage installations and sales share of electric vehicles (EVs) as shown in Fig. 1.2 respectively [7][8]. These RERs, such as solar PV systems, wind generators, battery energy storage systems (BESS) and fossil fuel-based traditional generators (TGs), are considered distributed energy sources (DERs) [9]–[11]. However, their integration with each other, and with the electrical network, requires a smart energy management strategy (EMS) to achieve the optimal, efficient, and stable operation of the system [12]. The interconnection of the DERs to make an electrical network is called a microgrid (MG).

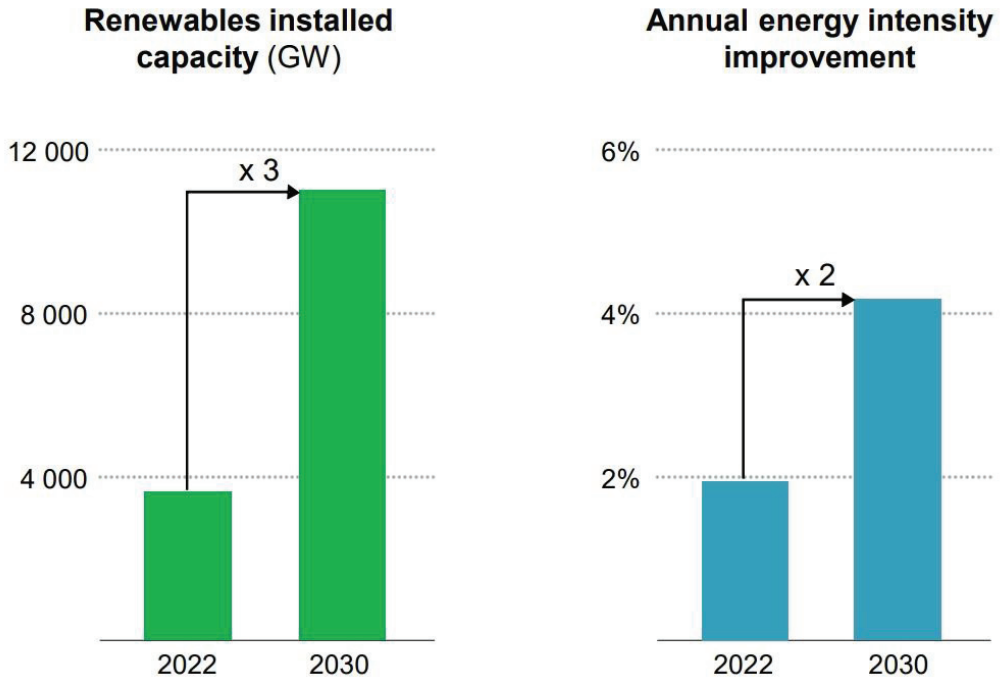

Figure 1.1 Expected growth in installed capacity of renewables and in annual energy intensity improvement [6]

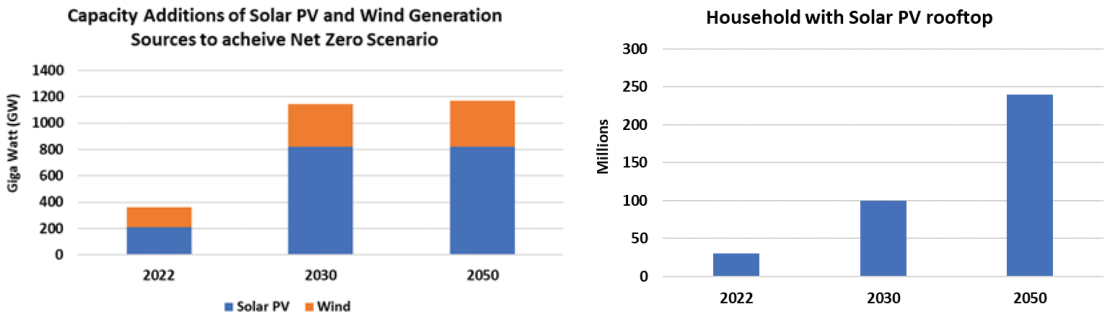

(a) (b)

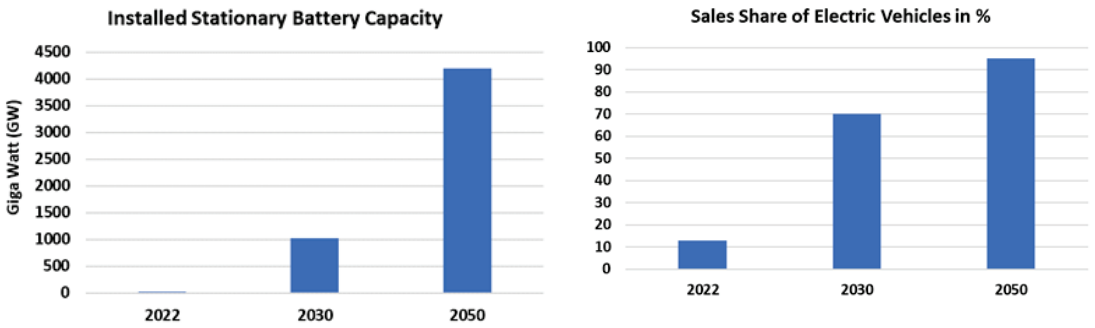

(c) (d)

Figure 1.2 Expected growth in (a) solar PV and wind energy source capacity addition (b) households with solar PV rooftops, (c) battery storage installations and (d) sales share of electric vehicles (EVs)

1.2. Microgrids (MGs)

A micro-scale interconnection of the DERs and loads developing a low-voltage electrical network can be termed a MG [13]–[15]. The International Electrotechnical Commission and the U.S. Department of Energy define a MG as a group of interconnected loads and DERs within clearly specified electrical boundaries forming a local electric power system at distribution voltage levels that act as a single controllable entity for the grid [16], [17]. It can operate in grid-connected and an islanded mode [16]–[20]. The basic architecture of an AC-DC community MG with its main components is shown in Fig. 1.3.

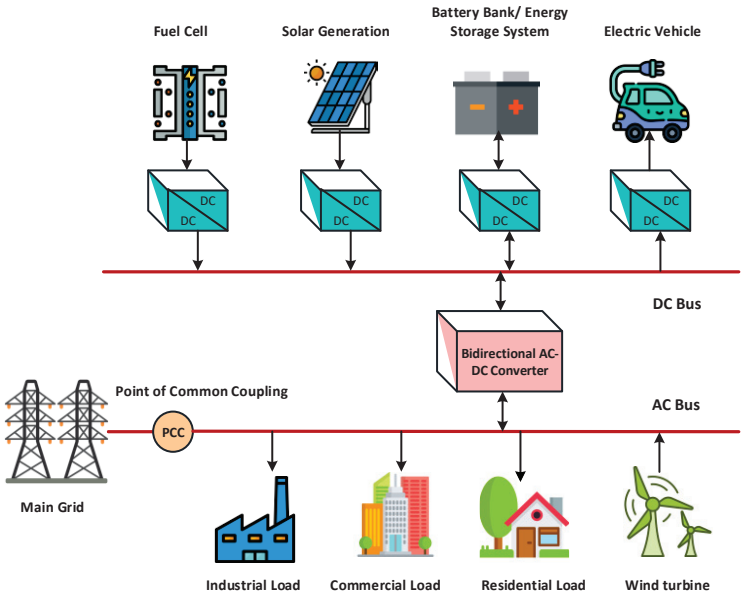

Figure 1.3 Basic architecture of an AC-DC community MG

There are several benefits of MG, such as it reduces CO_2 emission due to utilization of RERs, it provides ancillary support to the main grid, it feeds local demand, which can reduce the distribution losses and cost of transmission of the power network, it can provide the adequacy of generation as it has control over its generation and internal loads, etc. A typical MG classification is shown in Fig. 1.4. While integrating the DERs into MG, it is crucial to take care of uncertainties associated with RERs, as well as optimal sizing and effective scheduling of DERs. Therefore, MG demands an energy management architecture (EMA) to maintain its optimal, efficient, sustainable and stable operation.

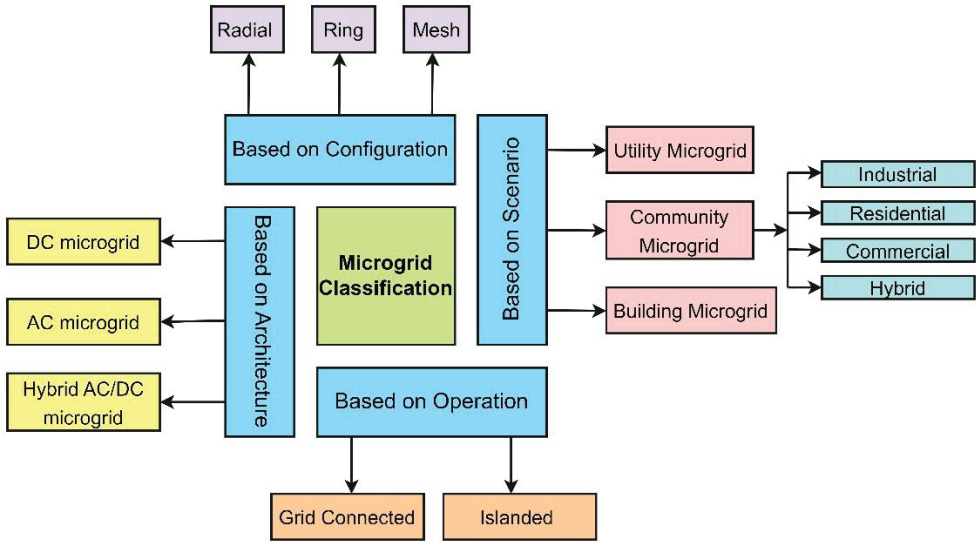

Figure 1.4 Typical MG classification

1.3. Energy Management Architecture (EMA) of MGs

According to the IEC standard 61970, associated with the application of energy management program in power systems, EMA is a computer system containing a software platform providing essential support services and a set of applications providing the functionality needed for the effective operation of electrical generation and transmission facilities to assure adequate security of energy supply at minimum cost [21],[22]. The main functions of an EMA for MGs are to assign generation schedules for DERs, monitor and forecast their generation, perform load forecasting, manage the controllable loads to control energy production and consumption and analyze energy market prices[23],[24]. The EMA in MG has been considered the most promising

solution to attain MGs' resilient, reliable, optimized, and cost-effective operation while satisfying the technical constraints [25]–[27].

An EMA makes use of various modules such as forecast, optimization, data analysis, and human-machine interface (HMI) to perform optimal decisions with the help of an energy service interface (ESI) and communications protocols, and these decisions are communicated to grid side and customer side units as shown in Fig.1.5 [19],[28]–[30]. These modules look after different areas, such as forecast deals with DERs/load forecasting and energy market prices. Further, forecasted data and historical data are analyzed using a data analysis module. The optimization module, which is considered to be the most important system of the EMA, deals with the optimal and efficient operation of the MG. It works as the brain of an EMA, which can operate/control the MG as per the desired objectives. Further, the HMI module helps in data visualization and real-time control.

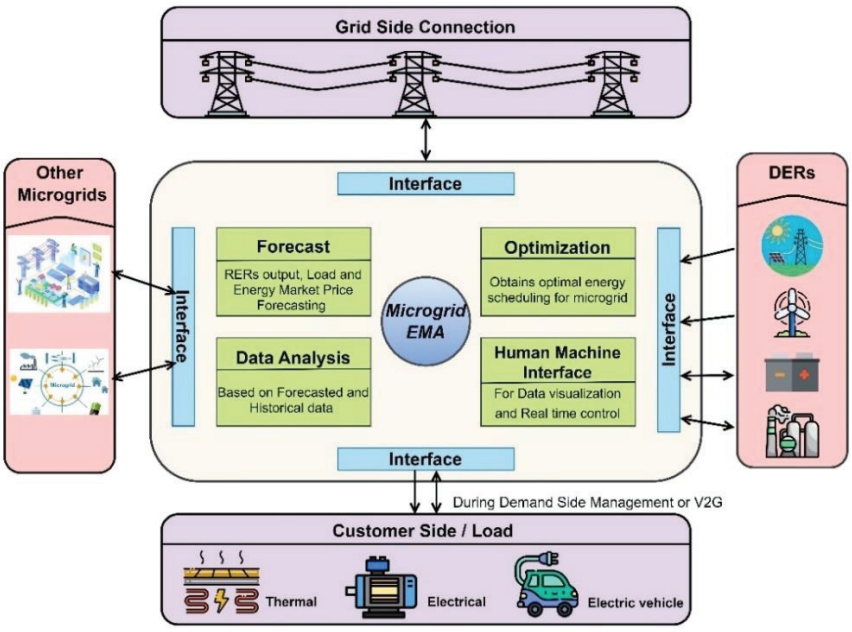

Figure 1.5 Energy management architecture for an MG

Energy management of MGs has numerous benefits, including increased efficiency, reliability, sustainability, and economic viability of energy systems [31]. Some of the main benefits are as follows:

- Energy efficiency: Energy management optimises the use of available resources in MGs, which leads to higher energy efficiency. MGs can be more efficient

than standard centralised grids by reducing waste and optimising energy distribution and consumption.

- Cost savings: Effective energy management can significantly reduce costs for MG operators and end users [32]. MGs can reduce dependency on expensive peak-demand electricity by optimising energy generation, storage, and distribution, lowering energy bills and mitigating the impact of volatile energy prices.
- Integration of renewable energy: MGs incorporate renewable energy sources such as solar, wind, and hydroelectric power [33]. EMA allows optimal integration of these intermittent resources, maximising their utilisation while maintaining grid stability and reliability.
- Grid resilience: MGs are more resilient and reliable than centralized grids, particularly in disruptions such as disasters, grid outages, or cyber-attacks. Energy management offers proactive monitoring, rapid response to disruptions, and islanding capabilities to keep critical systems operational during emergencies.
- Carbon emission reduction: MG energy management helps to reduce carbon emissions and mitigate the effects of climate change by encouraging the use of renewable energy and optimising energy consumption patterns. MGs play an important part in achieving a low-carbon energy future.
- Demand response: EMA enables MGs to change energy consumption patterns in response to changing grid circumstances, electricity costs, or environmental issue [12]. Demand response programmes help to balance supply and demand, optimise grid operations, and decrease stress on the power system during peak times.
- Enhanced grid stability: MG energy management improves grid stability by actively controlling generation, storage, and demand in the system [34]. Advanced control algorithms and predictive analytics help mitigate voltage fluctuations, frequency deviations, and other instabilities, delivering a reliable and consistent power supply for connected users.

- Grid independence: MGs can function independently or in conjunction with the main power grid, providing greater energy security and grid independence. Energy management systems enable MGs to optimise local resources, balance supply and demand, and provide crucial services even when isolated from the main grid.
- Remote and off-grid applications: MGs are ideal for providing dependable power to communities, industries, and infrastructure in remote areas [35]. EMA enables the optimal use of local resources, lowering dependence on imported fuels and increasing energy availability in underserved areas.
- Technological innovation and economic development: Investing in MG energy management promotes technological innovation, job creation, and economic development in the energy industry. Renewable energy, energy storage, smart grid technology, and data analytics contribute to growth and competitiveness while creating opportunities for sustainable development.

1.4. Classification of EMA for MGs

An EMA in MG can be broadly classified according to three main categories, i.e., based on supervisory control, operating time platform, and the decision-making strategy adopted to achieve effective and optimal operation of MG, as shown in Fig. 1.6.

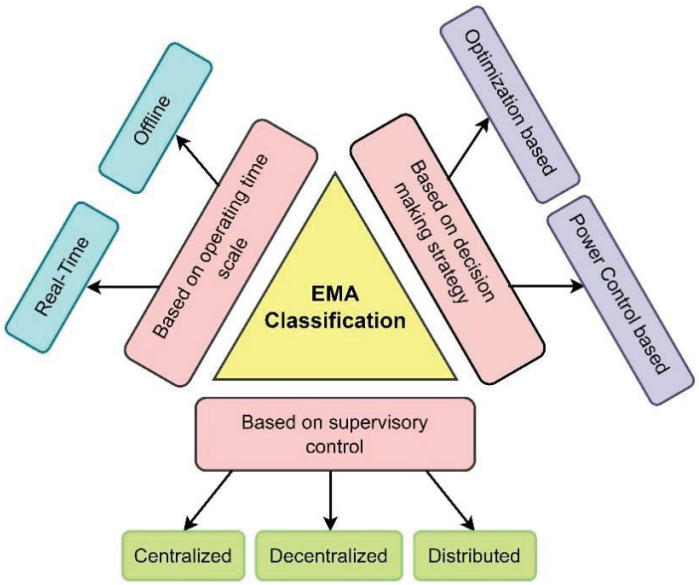

Figure 1.6 Classification of the energy management architecture

1.4.1. EMA based on Supervisory Control

Supervisory control can be referred to the overall monitoring of the individual process operations occurring in the system. It is responsible for the complete monitoring of the system and the effective interconnection between individual controllers [36],[37]. Based on supervisory control, EMA can be broadly divided into three types, i.e., centralized, decentralized, and distributed, as shown in Fig. 1.7. The circles in Fig. 1.7 show the various nodes or units of the MG system.

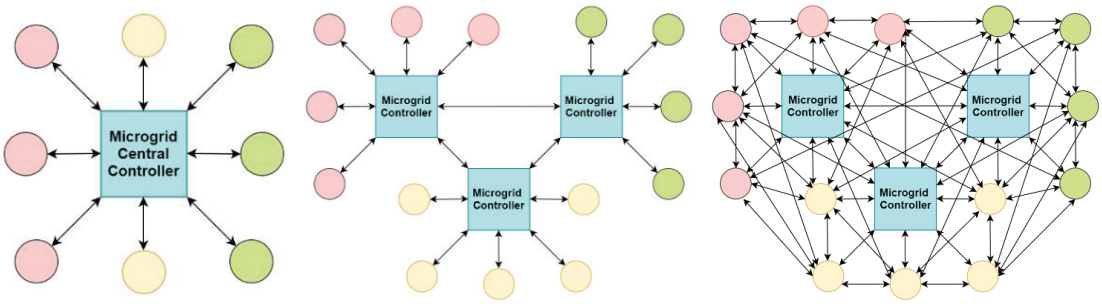

Figure 1.7 Various supervisory control approaches for EMA in MG (a) Centralized (b) Decentralized (c) Distributed

The centralized EMA consists of a central controller that gathers all the necessary information about DERs, load, electricity market, weather, etc. and performs optimal scheduling of MG. Later, the decision is sent to the local controllers (LC) of units [38],[39]. Whereas, in decentralized EMA, there are multiple central controllers, and they communicate with each other and their respective LCs in real-time. Every LC puts forward a present and future generation or demand request to the central controller.

Further, it performs the optimal scheduling and communicates it back to the LC of MG [40]. This process keeps on going until local and global objectives are achieved. The third approach, distributed EMA, is an advanced version of decentralized EMA and eliminates the concept of centralization. In this control approach, along with the central controller, each LC unit also communicates and exchanges local information like voltage and frequency with each other [41],[42]. This helps the central controllers to obtain a global solution while using the two-way communication link of the local controllers [33].

1.4.2. EMA based on the operating time platform

For developing an efficient and effective EMA, the time taken for implementation and execution of a new decision/adaptation is the most critical parameter that needs to be selected carefully [43]. The two most commonly used operating time platforms for the EMA decision-making process are offline and real-time (RT) platforms.

1.4.2.1. EMA based on the offline time platform

This operating time platform is usually preferred during the planning of the system or performing day ahead scheduling when it is assumed that forecasted parameters (RERs generation, load demand, market price) are already known. Then, the offline EMA obtains an optimal schedule for all the sub-sections of the system [44]–[49]. The offline EMA lacks consideration of uncertainties in MGs; therefore, commonly used probabilistic methods for uncertainty quantifications, such as Monte Carlo and scene reduction techniques, are adopted to manage the uncertainty of RERs and load demand. Then, a random or deterministic optimization technique can be used to determine the optimal solution [47].

1.4.2.2. EMA based on the real-time platform

Although day-ahead scheduling may provide the global optimal solution, as the actual values are slightly different from forecasted values due to unavoidable forecasted errors, therefore, it is difficult to achieve the expected results. Further, the high uncertainty of RERs and load demand leads to the complex design of the EMA. Thus, many researchers are focussing on real-time (RT) scheduling to reduce the impact of uncertainties on the EMA and make it simpler from the design perspective [50]–[58]. For grid-connected MGs, the RT scheduling should also optimize the traded energy between the grid and MG.

The offline EMA has several disadvantages, but it still acts as auxiliary support to the RT EMA for any MG. The results of offline EMA are fed to RT EMA to test its convergence [59],[60]. The objective function of offline EMA is decomposed into smaller sub-problems to reduce the computational complexity, which can be solved further using a distributed optimization approach [61],[62].

1.4.3. EMA based on decision-making approaches

Decision-making approaches are adopted to achieve effective, stable, and optimal operation of MG. Based on these approaches, EMA can be majorly segregated into two categories, i.e., optimization and power control approach, as shown in Fig. 1.8. The optimization-based approach includes classical programming methods, meta-heuristic approaches, stochastic/robust programming approaches, and artificial intelligence-based approaches. The power control-based approach is subdivided into model predictive control techniques and other power control methods such as droop control, hierarchical control, master-slave control, peer-to-peer (P2P) control, voltage-frequency control, etc.

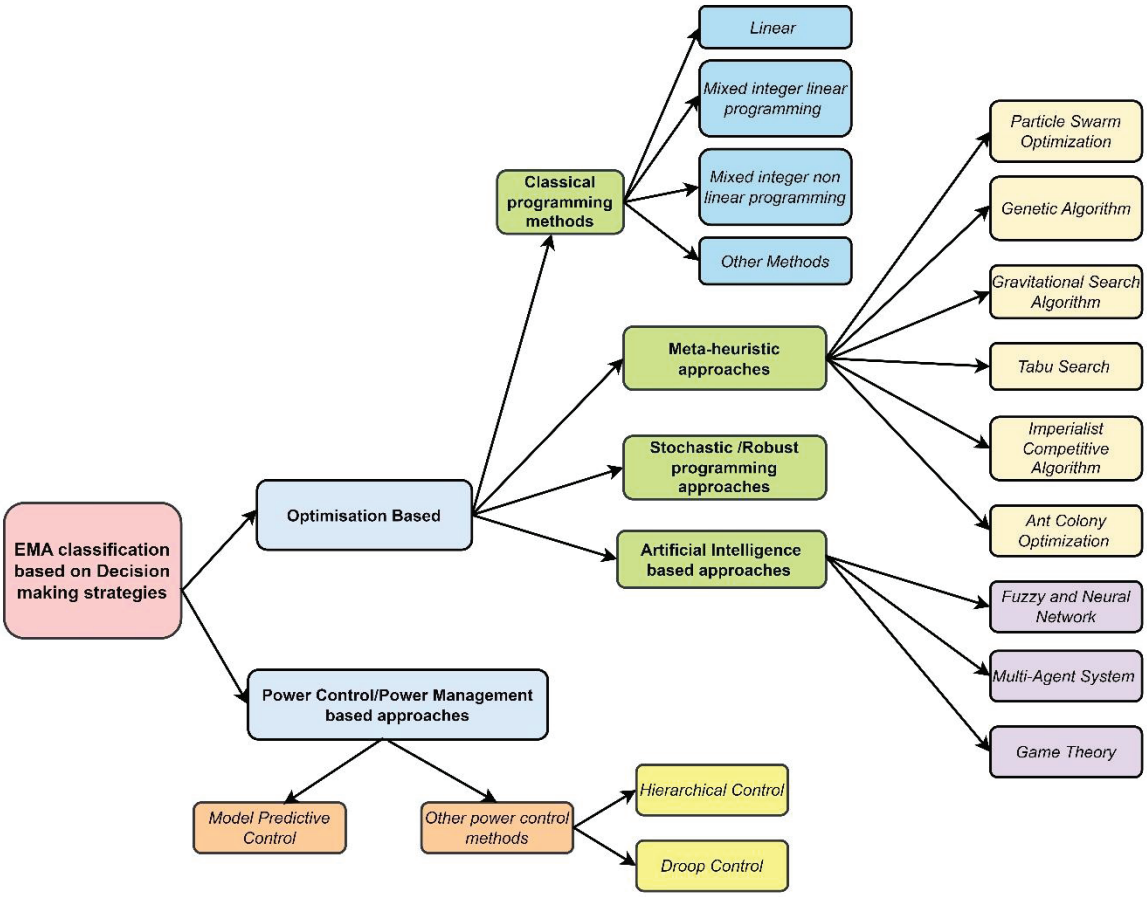

Figure 1.8 EMA classification based on a decision-making approach.

1.5. Motivation and problem statement

The main component of the MG EMA is the optimization module because it consists of an energy management strategy (EMS), which is entirely responsible for the optimal, efficient, stable and sustainable operation of the MG. However, the development of EMS

for MGs faces numerous challenges due to the complexity of integrating many energy sources, controlling dynamic loads, including EVs, and assuring grid stability, which motivated this research. Some of the significant challenges are:

- MGs frequently use intermittent renewable energy sources such as solar and wind, which are weather-dependent. Managing the fluctuation of these sources necessitates complex EMSs, including forecasting and scheduling operations, to efficiently balance supply and demand.
- Energy storage devices, such as batteries, are critical in stabilizing MG operations because they store excess energy for later use or smooth out supply and demand fluctuations. However, integrating energy storage involves challenges for an MG EMS in terms of its proper sizing, management, and maintenance in order to maximize efficiency and life span.
- MGs serve a wide range of customers with variable energy needs that might vary frequently and unpredictably. Managing these dynamic loads necessitates demand forecasting and demand response mechanisms in EMSs to provide a reliable power supply without overloading the grid.
- EV charging raises the MG's load, which could strain the present distribution infrastructure and lead to increasing peak demand. An MG EMS should be able to balance EV charging demand with other electrical demand to prevent overloads, voltage fluctuations, and grid congestion.
- Community MGs are usually comprised of various DERs, such as solar panels, wind turbines, and smaller generators. Coordinating the operation of these DERs while ensuring grid stability and reliability can be difficult, particularly in systems with multiple owners and controls. Further, ensuring grid stability and resilience in MGs is critical, especially during disruptions such as power outages or unexpected changes in load or generation. EMS must have advanced voltage regulation and power loss minimization algorithms that can prevent grid instabilities or cascading failures.
- Deployment of the MG with EMA, especially on a large-scale building, involves a huge initial investment and continuous operational costs. The MG EMS should

balance the costs of technology deployment with the expected benefits in terms of energy savings, efficiency, and system longevity.

The development of EMS is highly dependent on the type of MG, and the most critical are community and building MGs. Therefore, it is essential to evaluate energy management aspects for both types of MGs.

Thus, this research focuses on developing an EMS to achieve the economical, efficient, and stable operation of the community MG consisting of various DERs and for a prosumer building MG having solar PV rooftop and BESS with the integration of EV load.

1.6. Organization of thesis

Chapter 1 discusses the background, motivation, problem statement and objectives of the research carried out in the thesis.

Chapter 2 presents an exhaustive literature survey of the previously reported studies that consider community MGs, prosumer buildings, and the modelling of the electric vehicle load (EVL). Further, few research limitations are identified.

Chapter 3 designs the community MG consisting of various DERs and electric vehicle stations (EVSs). Moreover, it formulates a multi-objective function with the purpose of determining the optimal capacity and location of multiple DERs along with EVS to reduce power losses and voltage fluctuations in the system.

Chapter 4 proposed an optimal energy management strategy (OEMS) that aims at maximum utilization of DERs, promotes energy trading between MG and the utility grid, performs peak load management, and minimizes the dependency of an MG on the utility grid. It mainly focuses on achieving economic, efficient, and sustainable operation of community MG.

Chapter 5 is about designing a grid-connected AC-DC hybrid MG for a building and deploying it on its rooftop to develop a prosumer building. Further, an improved energy management strategy (IEMS) is developed to optimize the operating cost of MG and improve the operating life span of BESS by its effective utilization. It aims to achieve the economical and efficient operation of the system.

Chapter 6 formulates a flexible load shifting (FLS) scheme for a prosumer building aiming at shifting the flexible loads to improve the utilization of RERs and increase the sustainability of the system. Moreover, it discusses the advanced probabilistic modelling of EVL, which considers the practical events and the uncertain behaviour of EV owners. Further, the performance assessment of IEMS is studied with FLS and EVL.

Chapter 7 concludes the research work by outlining the main contributions and discusses the future scope of the research.

Figure 1.9 shows the pictorial representation of the organization of the thesis.

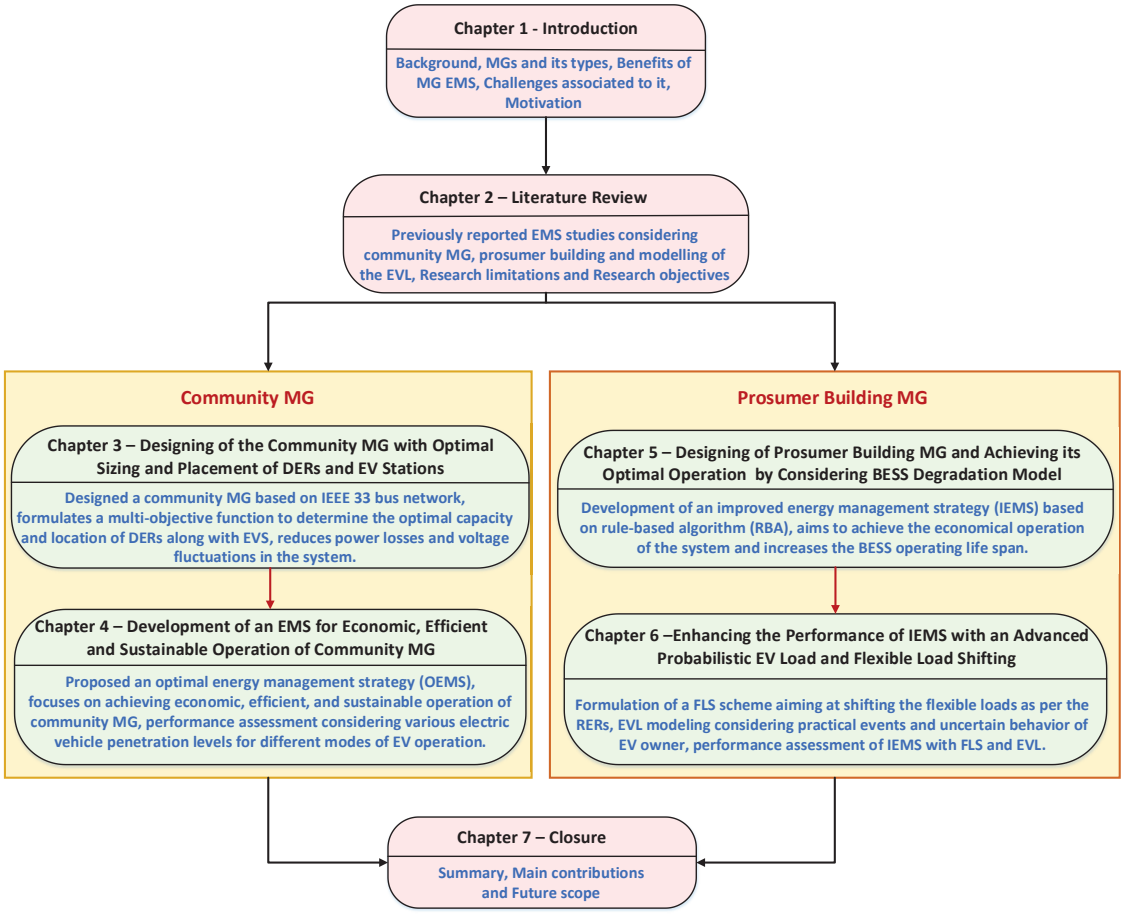

Figure 1.9 Pictorial representation of organization of thesis

Bibliography

[1] "article67824016 @ www.thehindu.com." [Online]. Available: https://www.thehindu.com/sci-tech/science/january-2024-warmest-on-record-european-climate-agency/article67824016.ece.

[2] "1141937 @ news.un.org." [Online]. Available: https://news.un.org/en/story/2023/10/1141937.

[3] Z. Liu, Z. Deng, S. Davis, and P. Ciais, "Monitoring global carbon emissions in 2022," Nat. Rev. Earth Environ., vol. 4, no. 4, pp. 205–206, 2023, doi: 10.1038/s43017-023-00406-z.

[4] "Cop26 @ Www.Un.Org." [Online]. Available: https://www.un.org/en/climatechange/cop26#:~:text=The UN Climate Change Conference in Glasgow,climate change — the science%2C the solutions%2C.

[5] "b45dac09463c2a2c7d9f7040d41789548054d845 @ unric.org." [Online]. Available: https://unric.org/en/climate-highlights-of-cop28/.

[6] United Nations Climate Change, "Summary of global climate action at COP27," Glob. Clim. Action, pp. 1–16, 2022, [Online]. Available: https://unfccc.int/sites/default/files/resource/GCA_COP27_Summary_of_Global_Climate_Action_at_COP_27_1711.pdf.

[7] International Energy Agency, "Net Zero by 2050: A Roadmap for the Global Energy Sector," p. 70, 2021.

[8] IEA, "Net Zero Roadmap," Int. Energy Agency, pp. 1–226, 2023.

[9] S. Parhizi, H. Lotfi, A. Khodaei, and S. Bahramirad, "State of the art in research on microgrids: A review," IEEE Access, vol. 3, pp. 890–925, 2015, doi: 10.1109/ACCESS.2015.2443119.

[10] H. D. Mathur, N. C. Hien, N. Mithulananthan, D. Joshi, and R. C. Bansal, "Distributed Generation: A Power System Perspective," in Handbook of Renewable Energy Technology, pp. 563–585.

[11] A. F. Zobaa and R. C. Bansal, Handbook of Renewable Energy Technology. WORLD SCIENTIFIC, 2011.

[12] P. Sharma, H. Dutt Mathur, P. Mishra, and R. C. Bansal, "A critical and comparative review of energy management strategies for microgrids," Appl. Energy, vol. 327, no. May, p. 120028, 2022, doi: 10.1016/j.apenergy.2022.120028.

[13] S. Ali, Z. Zheng, M. Aillerie, J. P. Sawicki, M. C. Péra, and D. Hissel, "A review of dc microgrid energy management systems dedicated to residential applications," Energies, vol. 14, no. 14, pp. 1–26, 2021, doi: 10.3390/en14144308.

[14] D. Kumar, H. D. Mathur, S. Bhanot, and R. C. Bansal, "Modeling and frequency control of community micro-grids under stochastic solar and wind sources," Eng. Sci. Technol. an Int. J., vol. 23, no. 5, pp. 1084–1099, 2020, doi: https://doi.org/10.1016/j.jestch.2020.02.005.

[15] T. Adefarati, R. C. Bansal, and J. J. Justo, "Reliability and economic evaluation of a microgrid power system," Energy Procedia, vol. 142, pp. 43–48, 2017, doi: 10.1016/j.egypro.2017.12.008.

[16] J. Buck, "International electrotechnical commission," Handb. Transnatl. Econ. Gov. Regimes, no. 617, pp. 573–584, 2009, doi: 10.1163/ej.9789004163300.i-1081.

[17] D. T. T. and M. A. S. I., "Doi:10.1016/J.Tej.2012.09.013," 2012, [Online]. Available: http://dx.doi.org/10.1016/j.tej.2012.09.013.

[18] S. Bacha, D. Picault, B. Burger, I. Etxeberria-Otadui, and J. Martins, "Photovoltaics in microgrids:

An overview of grid integration and energy management aspects," IEEE Ind. Electron. Mag., vol. 9, no. 1, pp. 33–46, 2015, doi: 10.1109/MIE.2014.2366499.

[19] N. T. Mbungu, R. M. Naidoo, R. C. Bansal, and V. Vahidinasab, "Overview of the Optimal Smart Energy Coordination for Microgrid Applications," IEEE Access, vol. 7, pp. 163063–163084, 2019, doi: 10.1109/ACCESS.2019.2951459.

[20] M. F. Zia, E. Elbouchikhi, and M. Benbouzid, "Microgrids energy management systems: A critical review on methods, solutions, and prospects," Appl. Energy, vol. 222, no. May, pp. 1033–1055, 2018, doi: 10.1016/j.apenergy.2018.04.103.

[21] "iec-61970-12005-energy-management-system-application-program-interface-ems-api-part-1 @ joinup.ec.europa.eu." [Online]. Available: https://joinup.ec.europa.eu/collection/ict-standards-procurement/solution/iec-61970-12005-energy-management-system-application-program-interface-ems-api-part-1-guidelines-and/distribution/iec-61970-12005-energy-management-system-application-program-interf.

[22] R. C. Bansal, Small signal analysis of isolated hybrid power systems reactive power and frequency control analysis. Oxford, UK: Alpha Science Int. Ltd., 2008.

[23] S. A., R. Kumar, and R. C. Bansal, "Multiagent-Based Autonomous Energy Management System With Self-Healing Capabilities for a Microgrid," IEEE Trans. Ind. Informatics, vol. 15, no. 12, pp. 6280–6290, 2019, doi: 10.1109/TII.2018.2889692.

[24] N. Nikmehr and S. Najafi Ravadanegh, "Reliability evaluation of multi-microgrids considering optimal operation of small scale energy zones under load-generation uncertainties," Int. J. Electr. Power Energy Syst., vol. 78, no. C, pp. 80–87, 2016, doi: 10.1016/j.ijepes.2015.11.094.

[25] N. Javaid, G. Hafeez, S. Iqbal, N. Alrajeh, M. S. Alabed, and M. Guizani, "Energy Efficient Integration of Renewable Energy Sources in the Smart Grid for Demand Side Management," IEEE Access, vol. 6, pp. 77077–77096, 2018, doi: 10.1109/ACCESS.2018.2866461.

[26] A. M. Jadhav, N. R. Patne, and J. M. Guerrero, "A Novel Approach to Neighborhood Fair Energy Trading in a Distribution Network of Multiple Microgrid Clusters," IEEE Trans. Ind. Electron., vol. 66, no. 2, pp. 1520–1531, 2019, doi: 10.1109/TIE.2018.2815945.

[27] W. Su, J. Wang, and J. Roh, "Stochastic Energy Scheduling in Microgrids With Intermittent Renewable Energy Resources," IEEE Trans. Smart Grid, vol. 5, no. 4, pp. 1876–1883, 2014, doi: 10.1109/TSG.2013.2280645.

[28] E. K. Lee, W. Shi, R. Gadh, and W. Kim, "Design and implementation of a microgrid energy management system," Sustain., vol. 8, no. 11, pp. 1–19, 2016, doi: 10.3390/su8111143.

[29] P. Sharma, P. Mishra, and H. D. Mathur, "Optimal energy management in microgrid including stationary and mobile storages based on minimum power loss and voltage deviation," Int. Trans. Electr. Energy Syst., vol. 31, no. 12, p. e13182, 2021, doi: https://doi.org/10.1002/2050-7038.13182.

[30] Ç. Iris and J. S. L. Lam, "Optimal energy management and operations planning in seaports with smart grid while harnessing renewable energy under uncertainty," Omega, vol. 103, p. 102445, 2021, doi: https://doi.org/10.1016/j.omega.2021.102445.

[31] G. Ma and J. Li, "A Review on Optimal Energy Management of Multimicrogrid System Considering Uncertainties," no. July, pp. 77081–77098, 2022.

[32] V. Sidharthan Panaparambil, Y. Kashyap, and R. Vijay Castelino, "A review on hybrid source energy management strategies for electric vehicle," Int. J. Energy Res., vol. 45, no. 14, pp. 19819–

19850, 2021, doi: 10.1002/er.7107.

[33] M. Meliani, A. El Barkany, I. El Abbassi, A. M. Darcherif, and M. Mahmoudi, "Energy management in the smart grid: State-of-the-art and future trends," Int. J. Eng. Bus. Manag., vol. 13, pp. 1–26, 2021, doi: 10.1177/18479790211032920.

[34] N. Eghtedarpour and E. Farjah, "Power Control and Management in a Hybrid AC/DC Microgrid," IEEE Trans. Smart Grid, vol. 5, no. 3, pp. 1494–1505, 2014, doi: 10.1109/TSG.2013.2294275.

[35] M. Marzband, M. Javadi, J. L. Domínguez-García, and M. Mirhosseini Moghaddam, "Non-cooperative game theory based energy management systems for energy district in the retail market considering DER uncertainties," IET Gener. Transm. \& Distrib., vol. 10, no. 12, pp. 2999–3009, 2016, doi: https://doi.org/10.1049/iet-gtd.2016.0024.

[36] A. Kumar et al., "Strategic integration of battery energy storage systems with the provision of distributed ancillary services in active distribution systems," Appl. Energy, vol. 253, p. 113503, 2019, doi: https://doi.org/10.1016/j.apenergy.2019.113503.

[37] J. B. Almada, R. P. S. Leão, R. F. Sampaio, and G. C. Barroso, "A centralized and heuristic approach for energy management of an AC microgrid," Renew. Sustain. Energy Rev., vol. 60, pp. 1396–1404, 2016, doi: https://doi.org/10.1016/j.rser.2016.03.002.

[38] B. Amrutha Raju, S. Vuddanti, and S. R. Salkuti, "Review of energy management system approaches in microgrids," Energies, vol. 14, no. 17, pp. 1–32, 2021, doi: 10.3390/en14175459.

[39] M. A. Mosa and A. A. Ali, "Energy management system of low voltage dc microgrid using mixed-integer nonlinear programing and a global optimization technique," Electr. Power Syst. Res., vol. 192, p. 106971, 2021, doi: https://doi.org/10.1016/j.epsr.2020.106971.

[40] J. P. Torreglosa, P. García-Triviño, L. M. Fernández-Ramirez, and F. Jurado, "Decentralized energy management strategy based on predictive controllers for a medium voltage direct current photovoltaic electric vehicle charging station," Energy Convers. Manag., vol. 108, pp. 1–13, 2016.

[41] T. Morstyn, B. Hredzak, and V. G. Agelidis, "Control Strategies for Microgrids with Distributed Energy Storage Systems: An Overview," IEEE Trans. Smart Grid, vol. 9, no. 4, pp. 3652–3666, 2018, doi: 10.1109/TSG.2016.2637958.

[42] T. R. Oliveira, W. W. A. Gonçalves Silva, and P. F. Donoso-Garcia, "Distributed Secondary Level Control for Energy Storage Management in DC Microgrids," IEEE Trans. Smart Grid, vol. 8, no. 6, pp. 2597–2607, 2017, doi: 10.1109/TSG.2016.2531503.

[43] H. Zou, S. Mao, Y. Wang, F. Zhang, X. Chen, and L. Cheng, "A Survey of Energy Management in Interconnected Multi-Microgrids," IEEE Access, vol. 7, pp. 72158–72169, 2019, doi: 10.1109/ACCESS.2019.2920008.

[44] N.-O. Song, J.-H. Lee, and H.-M. Kim, "Optimal Electric and Heat Energy Management of Multi-Microgrids with Sequentially-Coordinated Operations," Energies, vol. 9, no. 6, 2016, doi: 10.3390/en9060473.

[45] C. Lupangu, J. J. Justo, and R. C. Bansal, "Model Predictive for Reactive Power Scheduling Control Strategy for PV–Battery Hybrid System in Competitive Energy Market," IEEE Syst. J., vol. 14, no. 3, pp. 4071–4078, 2020, doi: 10.1109/JSYST.2020.2968926.

[46] A. M. Jadhav and N. R. Patne, "Priority-Based Energy Scheduling in a Smart Distributed Network With Multiple Microgrids," IEEE Trans. Ind. Informatics, vol. 13, no. 6, pp. 3134–3143, 2017.

[47] H. Farzin, M. Fotuhi-Firuzabad, and M. Moeini-Aghtaie, "A Stochastic Multi-Objective Framework for Optimal Scheduling of Energy Storage Systems in Microgrids," IEEE Trans. Smart

Grid, vol. 8, no. 1, pp. 117–127, 2017, doi: 10.1109/TSG.2016.2598678.

[48] S. Areekkara, R. Kumar, and R. C. Bansal, "An Intelligent Multi Agent based Approach for Autonomous Energy Management in a Microgrid," Electr. Power Components Syst., vol. 49, no. 1–2, pp. 18–31, Jan. 2021, doi: 10.1080/15325008.2021.1937390.

[49] T. Adefarati, R. C. Bansal, M. Bettayeb, and R. Naidoo, "Optimal energy management of a PV-WTG-BSS-DG microgrid system," Energy, vol. 217, p. 119358, 2021.

[50] A. Parisio, C. Wiezorek, T. Kyntäjä, J. Elo, K. Strunz, and K. H. Johansson, "Cooperative MPC-Based Energy Management for Networked Microgrids," IEEE Trans. Smart Grid, vol. 8, no. 6, pp. 3066–3074, 2017, doi: 10.1109/TSG.2017.2726941.

[51] N. T. Mbungu, R. C. Bansal, R. M. Naidoo, M. Bettayeb, M. W. Siti, and M. Bipath, "A dynamic energy management system using smart metering," Appl. Energy, vol. 280, p. 115990, 2020, doi: https://doi.org/10.1016/j.apenergy.2020.115990.

[52] E. Loukarakis, C. J. Dent, and J. W. Bialek, "Decentralized multi-period economic dispatch for real-time flexible demand management," IEEE Trans. Power Syst., vol. 31, no. 1, pp. 672–684, 2016, doi: 10.1109/TPWRS.2015.2402518.

[53] Y. Wang, S. Mao, and R. M. Nelms, "On Hierarchical Power Scheduling for the Macrogrid and Cooperative Microgrids," IEEE Trans. Ind. Informatics, vol. 11, no. 6, pp. 1574–1584, 2015, doi: 10.1109/TII.2015.2417496.

[54] Y. Zhang, T. Zhang, R. Wang, Y. Liu, B. Guo, and T. Zhang, "Dynamic dispatch of isolated neighboring multi-microgrids based on model predictive control," in 2016 International Conference on Smart Grid and Clean Energy Technologies (ICSGCE), 2016, pp. 50–55.

[55] D. An, Q. Yang, W. Yu, X. Yang, X. Fu, and W. Zhao, "SODA: Strategy-Proof Online Double Auction Scheme for Multimicrogrids Bidding," IEEE Trans. Syst. Man, Cybern. Syst., vol. 48, no. 7, pp. 1177–1190, 2018, doi: 10.1109/TSMC.2017.2651072.

[56] Y. Liu et al., "Distributed Robust Energy Management of a Multimicrogrid System in the Real-Time Energy Market," IEEE Trans. Sustain. Energy, vol. 10, no. 1, pp. 396–406, 2019.

[57] S. Raimondi Cominesi, M. Farina, L. Giulioni, B. Picasso, and R. Scattolini, "A Two-Layer Stochastic Model Predictive Control Scheme for Microgrids," IEEE Trans. Control Syst. Technol., vol. 26, no. 1, pp. 1–13, 2018, doi: 10.1109/TCST.2017.2657606.

[58] V. S. Tabar, S. Ghassemzadeh, and S. Tohidi, "Energy management in hybrid microgrid with considering multiple power market and real time demand response," Energy, vol. 174, pp. 10–23, 2019, doi: https://doi.org/10.1016/j.energy.2019.01.136.

[59] G. Li, D. Wu, J. Hu, Y. Li, M. S. Hossain, and A. Ghoneim, "HELOS: Heterogeneous Load Scheduling for Electric Vehicle-Integrated Microgrids," IEEE Trans. Veh. Technol., vol. 66, no. 7, pp. 5785–5796, 2017, doi: 10.1109/TVT.2016.2636874.

[60] D. An, Q. Yang, W. Yu, X. Yang, X. Fu, and W. Zhao, "Sto2Auc: A Stochastic Optimal Bidding Strategy for Microgrids," IEEE Internet Things J., vol. 4, no. 6, pp. 2260–2274, 2017.

[61] A. R. Malekpour and A. Pahwa, "Stochastic Networked Microgrid Energy Management With Correlated Wind Generators," IEEE Trans. Power Syst., vol. 32, no. 5, pp. 3681–3693, 2017.

[62] D. Gregoratti and J. Matamoros, "Distributed Energy Trading: The Multiple-Microgrid Case," IEEE Trans. Ind. Electron., vol. 62, no. 4, pp. 2551–2559, 2015, doi: 10.1109/TIE.2014.2352592.

Chapter 2

Literature Review

This chapter details the comprehensive literature review of the previously reported studies considering community MG, prosumer building and modelling of the EVL. The community MGs are studied for optimal placement & capacity estimations of DERs and developments of their EMSs. The building MGs are investigated for the development of EMSs considering battery degradation and demand side management (DSM). Further, few research limitations are identified based on which objectives of the thesis are formed.

2.1. Community MG

2.1.1. Optimal placement and capacity estimations of DERs

In the past few years, many algorithms have been formulated to optimize the placement and capacity of DERs to minimize overall power losses in the distribution network [1-5]. In [1], the authors proposed an analytical technique to calculate the optimal location and size of DERs. In [2], the authors utilize an artificial bee colony algorithm to estimate the optimum location, power factor, and size of DERs. The study in [3] was focused on the optimal allocation and sitting of solar PV cells in radial distribution systems based on the Ant Lion optimizer algorithm. The multi-objective function is formulated for the optimization problem, but the authors did not present any information regarding the efficiency of the algorithm compared with other optimization algorithms. In [4], the optimal allocation of DERs is done using a hybrid particle swarm optimization algorithm (HPSO). To place DERs at a suitable position, loss sensitivity analysis is performed, and for optimum sizing, the HPSO algorithm is used, and the results obtained are compared with other optimization algorithms. The work in [5]

applied a hybrid method based on loss sensitivity factors and Moth-Flame optimization to determine the optimal placement and size of DERs. The loss sensitivity factors are used to estimate the candidate bus for DER allocation, and Moth-Flame optimization is used to determine the optimal size and placement of solar and wind-based DER.

Further, the authors of [6] aim to cut down the total investment value by optimal placement of wind-based DER and BESS. The cost of investment for BESS and DERs is taken to be proportional to their size. It is reported in [7], that Hybrid Grey Wolf Optimization (HGWO) is suitable to solve discrete, non-convex problems. Also, there is a considerable reduction in loss and improvement in voltage profile. The results are compared with various metaheuristic algorithms and show that the HGWO algorithm outshines all the other algorithms. The authors in [8] utilize the grasshopper optimization technique to determine the optimal place and size of DERs. The multi-objective function is formulated to minimize the active power losses and to improve the voltage profile of the system.

The voltage-dependent electric load demand and seasonal variations of wind and solar-based DERs are considered but didn't take into account the impact of EV charging load demand and optimal placement of EV charging stations. A genetic algorithm-based optimization problem is formulated in [9] to determine the optimal site and size of EV parking lots. The optimization problem considers the distribution system's reliability and power losses along with investment costs. However, this article didn't consider renewable DERs and various electric vehicle charging patterns based on the location of parking lots in the system. Further, an approach for simultaneous optimal allocation of renewable energy sources and EVS in smart grids is proposed in [10]. A multi-objective optimization problem is formulated to reduce power losses, charging and demand supplying costs, and voltage fluctuations. A hybrid genetic algorithm and particle swarm optimization are used to solve this multi-objective optimization problem, but the authors didn't discuss the impact of different EV charging patterns.

By the conducted literature survey, we remark that the researchers did not focus on optimal capacity estimation and allocations of DERs together with appropriate placement of EVS simultaneously and considering different charging patterns and voltage-dependent load.

2.1.2. EMS considering community MG

The cost optimization-based EMS has been formulated that focuses on minimizing the MG's total cost, which includes DERs and storage system costs, worst scenario transaction cost stemming from the uncertainty in RERs, and utility of dispatchable loads [11]. Further, in [12], the authors present a deterministic EMS that functions in 2 groups: local power management at the customer side and central energy management of the MG. With the help of communication between these two groups, the power flow is managed between the various sources. Whereas, a new concept for community MGs with zero grid impact is introduced to improve the MG's efficiency [13]. To achieve this aim, an intelligent system is developed based on a DC/AC converter that is connected to the building point of coupling with the main grid.

Similarly, few other EMSs are proposed in the literature that focus on energy efficiency, energy trading, and demand profile improvement [14]–[17]. An optimal billing mechanism has been developed, which includes the concepts of fairness, optimality, and user privacy in the DSM of the system [14]. The developed billing mechanism is fair because it distributes the total energy cost among the users depending on their contribution in minimizing the total cost of the system. Authors in [15] formulate an economic model that consists of functional links between properly linked shiftable and shifted load, which minimizes the operation energy costs. A unified demand-side management model is proposed to reduce the operating cost, diminish the peak-to-average power ratio and curtail peak hour's demand with minimized distribution losses [16]. Haffez et al. in [17] presented an autonomous system focusing on the effective and efficient management of different energy sources. The authors concluded that the proposed EMS has desirable performance as it results in saving energy and minimizing the load on the grid.

Few studies of literature have reported an energy management algorithm to optimize the energy flow in the MG by using various techniques [18]–[22]. Like, authors of [18] have employed the Markov decision principle, whereas a fuzzy logic-based advanced system has been proposed in [19] to ensure near optimally managed energy flows. An EMS is formulated based on multi-objective particle swarm optimization to maximize the penetration of renewable energy sources while simultaneously minimizes the

operating cost of MG [20]. Paul et al. in [21] have formulated an economic dispatch problem based on quadratic programming that claims optimal power and BESS scheduling in end-user-MG. A day-ahead energy management scheme is developed for optimal scheduling of RERs and diesel generators by formulating a non-linear programming problem [22]. It co-optimizes the costs associated with both active and reactive powers of diesel generators while simultaneously considering the reactive power capability of inverter-interfaced DERs.

It has also been mentioned in the literature that uncoordinated charging of EVs results in a rise of network losses & peak demand, overloads lines & transformers, and violates voltage range as well [23]. Therefore, network reinforcement is one of the effective solutions to deal with the large deployment of EVs, but it is expensive and infeasible [24]. Another possible solution to resolve these issues is to adopt coordinated or governed charging/discharging algorithms for non-commercial EVs because, 90% of the time, these types of EVs are parked or idle [23].

In this regard, few EMSs are presented in the literature, which aim to achieve efficient operation of MG while simultaneously fulfilling the charging and discharging requirements of EVs [25]–[30]. Like, smart plug-in EV charging strategies, including a unified grid-to-vehicle and vehicle-to-grid (V2G) charging framework, are presented to optimally integrate EVs within the existing distribution system [25]. In addition, the authors of [26] develop an optimal charging/discharging control of EVs that aims to reduce operating costs and considers the constraints of power systems, EVs, and battery degradation costs. An event-triggered-based mathematical model is developed for the V2G scheduling scheme based on the stochastic EVs connection to the smart grid [27]. L. Jian et al. in [28] consider a large-scale EVs V2G scenario and formulate an optimization problem to minimize the load variance of the system. Due to the high computational complexity with large-scale EVs, a double-layer optimal charging strategy is proposed, which effectively solves the problem. Whereas to improve the technical and economic performance of the grid, an EV charging model is developed based on optimal power flow, EV owners' degree of satisfaction, statistical characteristics of EVs, and the power grid cost [29].

Likewise, a smart PHEVs charging strategy utilizing solar power is presented in [30]. In addition, to decrease the dependency of the MG on the utility grid, the challenge of proper sizing of BESS is also addressed. The strategy presented in [30] aims to minimise the energy exchanged between MG and the utility grid by minimizing the energy drawn and energy supplied to the utility grid.

However, these previously reported strategies, such as mentioned in [30] may fail to perform satisfactorily under various scenarios due to certain limitations. These few common limitations are as follows.

1) restriction in the maximum utilization of DERs & energy trading between the MG and utility grid; 2) underutilization of the MG's capability to support the utility grid during contingencies occurring in the system; 3) inability to minimize active power loss (APL) and voltage deviation (VD).

2.2. Prosumer building MG

2.2.1. EMS considering Battery Energy Storage System (BESS) degradation

With the increased popularity of BESS, their integration into the MG network has significantly increased. Therefore, various studies have been conducted on MG energy management and its optimal operation, considering different generation sources and storage systems [31]–[37].

In [33], distributed economic dispatch is performed for a grid-connected MG with high renewable energy penetration and demand-side management. The developed algorithm aims to minimize MG's net cost, including the utility of dispatchable loads, the cost of distributed generation and storage units, and worst-case transaction costs stemming from the uncertainty in renewable energy sources. A. Elgammal et al. [34] developed an efficient EMS for a PV, wind, fuel cell, and battery energy scheme to minimize the operation cost of the MG and maximize the power generated by each source. In [35], an energy management algorithm has been formulated which is based on a mixed integer linear programming problem for grid-connected and islanded MGs integrated with PV, wind turbine, fuel cell, microturbine, diesel generator, and BESS to minimize the

operating cost. Zupančič et al.[36] develops a home energy management system consisting of solar PV, battery and grid. It aims to lower the operating cost of the system as well as maximize the green factor. It was found that the proposed management system decreased the cost objective by 17% and significantly improved the performance ratio. An energy management system for a grid-connected MG consisting of solar PV and BESS is proposed in [37] to minimize the operating cost by controlling battery charge/discharge operations based on the load of MG. These studies focus on minimizing MG's operating cost but do not focus on reducing battery degradation.

In addition to the above-mentioned points, various studies have developed an energy management algorithm for MG considering battery degradation [38]–[45]. In [38] and [39], a linear model of the battery degradation cost is considered that assumes a proportional relationship with the amount of energy exchanged by the battery, regardless of the charge-discharge cycle depth and the current state of charge (SOC) level. In [40], a unit commitment model is formulated that aims at cost minimization considering the battery degradation model based on cycle depth. Authors of [41] proposed a regression-based battery degradation cost model that considers the battery's temperature and cycle depth, i.e., depth of discharge (DOD). However, these studies do not consider the current SOC of each cycle.

Further, in [42],[43], piece-wise linearization of the life cycle function (number of cycle v/s DOD) of the battery is proposed for a BESS sizing of an under-planning MG to achieve the convexity of the formulated problem. Authors of [44] and [45] use the rainflow cycle counting algorithm based on the piece-wise approximation model of battery degradation. A novel battery degradation cost model is developed in [46] that uses the concept of auxiliary SOC of the battery with the cycle depth and formulates a cost minimization objective function. However, the authors use piece-wise linear approximation to incorporate the degradation model into an optimization problem.

It is worth mentioning that all aforementioned studies use piece-wise linear approximation to linearise the life cycle function of BESS, and some ignore calendar ageing that significantly governs the operating life of BESS. Therefore, these models fail to depict the practical degradation and estimation of the life span of BESS.

2.2.2. EMS with Demand Side Management (DSM)

Traditionally, generation was controlled in such a way that the load was met, i.e., generation follows load [4],[7]. However, with the extensive integration of intermittent renewable energy sources into the grid, generation is no longer controllable. Therefore, it becomes necessary that the load itself should contribute to energy management. This is called DSM, and DR strategies are part of it. It models consumer consumption behavior in such a way that the electricity bills are minimized [8]. DSM can be employed in three ways: energy efficiency, demand response (DR) programs, and strategic load management. Among them, DR programs are widely used and include incentive-based and price-based programs. Methods like Direct Load Control (DLC), demand bidding, and interruptible/curtailable load fall under incentive-based DR programs. These methods are mainly applied to thermostatic loads to directly control/curtail the flexible loads [47]. The price-based DR programs mostly consist of time of use (TOU), real time pricing (RTP) and critical peak pricing (CPP).

Recently, many researchers have presented EMS that considers DR programs, such as DLC and various pricing methods [48]–[51]. These strategies optimize the energy cost of consumers. Further, their DR programs aim to shift/control the loads based on the cost of energy or minimize the peak-to-average ratio of load demand, i.e., try to flatten the load demand. However, for prosumer building MGs, these DR strategies may not improve the efficiency of the system because, in these methods, the load is shifted/controlled as per the grid energy prices and does not consider the RERs utilization.

2.3. Modelling of Electric Vehicle Load (EVL)

The rise in the penetration of EVs has motivated researchers to develop an MG scheduling strategy that also considers EV load along with consumer load [52]. However, the modelling of the EV load profile has created further challenges for the development of an adequate MG scheduling strategy. Numerous studies have been conducted to model the EV load profile accurately, and it is generally performed using three major techniques: historical data regression method, machine learning prediction model, and stochastic simulation method based on probability distribution [53].

The historical data regression approach [54] includes the regression analysis prediction model [55] and the day prediction model [56]. The disadvantages of this strategy include a lack of historical data and conflicting statistical criteria, which can lead to errors in mathematical equations and reduce prediction accuracy. Further, machine learning prediction algorithms have been widely employed in recent years to anticipate short-term load for EV charging. Intelligent algorithms such as neural networks [57]–[60], support vector machines [61]–[63], and deep learning [64], [65] are frequently utilized. However, the integrity and the accuracy of historical data have a significant impact on forecast results. While the Monte Carlo approach from the stochastic simulation method [66], [67] is currently the most extensively used method to estimate EV charging demand [68], can simulate random processes and is suitable for macro prediction of unpredictable behaviors of EV users. Based on this, more factors could be added to the EV load profile model.

Like Zhang et al. [68] proposed an improved EV charging load forecast approach that considers demographic and socioeconomic factors. The findings show that the gender, age, and education level of the consumers had a significant impact on the EV charging load. Authors of ref. [69] proposed an EV charging load prediction model by taking into account numerous random parameters such as place, temperature, and road conditions. Most of these studies assume that 1) As the EV arrives at the station, it starts charging instantaneously, irrespective of the available number of EV plug points, and 2) the EV leaves the station only after it is fully charged. However, these assumptions limit the practical modelling of the EVL profile.

2.4. Gaps in the existing research

2.4.1. Considering community MG

- Optimal capacity estimation and allocations of DER units, along with appropriate placement of EVS simultaneously considering different charging patterns and voltage-dependent load, needs to be addressed.
- Previously reported EMS for community MG mainly focused on operating cost minimization, i.e., economical operation of MG, but failed to perform satisfactorily under various scenarios, including stability of the MG due to

certain limitations. These limitations include 1) restriction in the maximum utilization of DERs & energy trading between the MG and utility grid; 2) underutilization of the MG's capability to support the utility grid during contingencies occurring in the system; 3) inability to APL and VD to maintain the stability of MG.

2.4.2. Considering prosumer building MG

- Most of the existing EMSs consider battery degradation in the optimization model to achieve optimal operation of MG. However, they use piece-wise linear approximation to linearize the life cycle function of BESS, and some of them ignore calendar ageing because of that it fails to depict the practical degradation and estimation of the life span of BESS. Therefore, there is a need of EMSs that attain economical and efficient operation of MG while considering a non-linear battery degradation model.
- Former studies have developed EMSs by integrating DR programs such as DLC, TOU, RTP, and CPP. Their DR programs aim to shift/control the loads based on the cost of energy or minimization of the peak-to-average ratio of load demand, i.e., try to flatten the load demand. Though for building MGs, these DR strategies will result in a reduction in power imported from the grid, but they fail to improve the sustainability and efficiency of the system in terms of RER utilization.

2.4.3. Considering modelling of EVL

- Various studies have modelled the EVL profile considering numerous uncertain parameters such as demographic, socioeconomic, and environmental factors. However, these studies didn't consider the availability of EV plug points and the uncertain behavior of EV owners regarding leaving the station even before their EV is fully charged.

2.5. Objectives of the proposed work

- Designing an optimal and stable community MG model based on a multi-bus network with renewable energy sources, battery energy storage system (BESS), and EVs with V2G/G2V features.
- Development of an energy management algorithm for the designed community MG to maximize the profit of MG operator through the efficient utilization of DERs considering probabilistic modelling of EV load.
- Formulation of an improved energy management algorithm for a prosumer building that optimizes the operating cost of MG and improves the BESS operating life span.
- Integration of a flexible load shifting (FLS) scheme and advanced probabilistic EV load modelling (V2G/G2V feature) with improved energy management algorithm to further enhance its performance.

Bibliography

[1] N. Acharya, P. Mahat, and N. Mithulananthan, "An analytical approach for DG allocation in primary distribution network," *Int. J. Electr. Power Energy Syst.*, vol. 28, no. 10, pp. 669–678, 2006, doi: 10.1016/j.ijepes.2006.02.013.

[2] R. Palanisamy and S. K. Muthusamy, "Optimal Siting and Sizing of Multiple Distributed Generation Units in Radial Distribution System Using Ant Lion Optimization Algorithm," *J. Electr. Eng. Technol.*, vol. 16, no. 1, pp. 79–89, 2021, doi: 10.1007/s42835-020-00569-5.

[3] A. Ali, A. Youssef, T. George, and S. Kamel, "Optimal DG allocation in distribution systems using Ant lion optimizer," *2018 Int. Conf. Innov. Trends Comput. Eng.*, pp. 324–331, 2018.

[4] M. A. Tolba, V. N. Tulsky, and A. A. Zaki Diab, "Optimal allocation and sizing of multiple distributed generators in distribution networks using a novel hybrid particle swarm optimization algorithm," in *2017 IEEE Conference of Russian Young Researchers in Electrical and Electronic Engineering (EIConRus)*, 2017, pp. 1606–1612, doi: 10.1109/EIConRus.2017.7910880.

[5] H. Abdel-mawgoud, S. Kamel, M. Ebeed, and M. M. Aly, "An efficient hybrid approach for optimal allocation of DG in radial distribution networks," in *2018 International Conference on Innovative Trends in Computer Engineering (ITCE)*, 2018, pp. 311–316, doi: 10.1109/ITCE.2018.8316643.

[6] J. Qiu, Z. Xu, Y. Zheng, D. Wang, and Z. Y. Dong, "Distributed generation and energy storage system planning for a distribution system operator," *IET Renew. Power Gener.*, vol. 12, no. 12, pp. 1345–1353, 2018.

[7] R. Sanjay, T. Jayabarathi, T. Raghunathan, V. Ramesh, and N. Mithulananthan, "Optimal allocation of distributed generation using hybrid grey wolf optimizer," *Ieee Access*, vol. 5, pp. 14807–14818, 2017.

[8] K. S. Rani, B. K. Saw, P. Achargee, and A. K. Bohre, "Optimal Sizing and Placement of Renewable DGs using GOA Considering Seasonal Variation of Load and DGs," in *2020 International Conference on Computational Intelligence for Smart Power System and Sustainable Energy (CISPSSE)*, 2020, pp. 1–6.

[9] M. Moradijoz, M. Parsa Moghaddam, M. R. Haghifam, and E. Alishahi, "A multi-objective optimization problem for allocating parking lots in a distribution network," *Int. J. Electr. Power Energy Syst.*, vol. 46, pp. 115–122, 2013, doi: https://doi.org/10.1016/j.ijepes.2012.10.041.

[10] M. R. Mozafar, M. H. Moradi, and M. H. Amini, "A simultaneous approach for optimal allocation of renewable energy sources and electric vehicle charging stations in smart grids based on improved GA-PSO algorithm," *Sustain. Cities Soc.*, vol. 32, pp. 627–637, 2017, doi: https://doi.org/10.1016/j.scs.2017.05.007.

[11] Y. Zhang, N. Gatsis, and G. B. Giannakis, "Robust energy management for microgrids with high-penetration renewables," *IEEE Trans. Sustain. Energy*, vol. 4, no. 4, pp. 944–953, 2013, doi: 10.1109/TSTE.2013.2255135.

[12] H. Kanchev, D. Lu, F. Colas, V. Lazarov, and B. Francois, "Energy management and operational planning of a microgrid with a PV-based active generator for smart grid applications," *IEEE Trans. Ind. Electron.*, vol. 58, no. 10, pp. 4583–4592, 2011, doi: 10.1109/TIE.2011.2119451.

[13] P. Arboleya *et al.*, "Efficient energy management in smart micro-grids: ZERO grid impact buildings," *IEEE Trans. Smart Grid*, vol. 6, no. 2, pp. 1055–1063, 2015, doi:

10.1109/TSG.2015.2392071.

[14] Z. Baharlouei and M. Hashemi, "Efficiency-fairness trade-off in privacy-preserving autonomous demand side management," *IEEE Trans. Smart Grid*, vol. 5, no. 2, pp. 799–808, 2014, doi: 10.1109/TSG.2013.2296714.

[15] G. Ferruzzi, G. Graditi, F. Rossi, and A. Russo, "Optimal Operation of a Residential Microgrid: The Role of Demand Side Management," *Intell. Ind. Syst.*, vol. 1, no. 1, pp. 61–82, 2015, doi: 10.1007/s40903-015-0012-y.

[16] S. Ahmad, M. Naeem, and A. Ahmad, "Unified optimization model for energy management in sustainable smart power systems," *Int. Trans. Electr. Energy Syst.*, vol. 30, no. 4, p. e12144, 2020, doi: https://doi.org/10.1002/2050-7038.12144.

[17] H. Ahmad, A. Ahmad, and S. Ahmad, "Efficient Energy Management in a Microgrid," *4th Int. Conf. Power Gener. Syst. Renew. Energy Technol. PGSRET 2018*, no. September, pp. 10–12, 2019, doi: 10.1109/PGSRET.2018.8685946.

[18] H. Berlink and A. H. R. Costa, "Batch reinforcement learning for smart home energy management," in *IJCAI International Joint Conference on Artificial Intelligence*, 2015, vol. 2015-Janua, pp. 2561–2567.

[19] A. Chaouachi, R. M. Kamel, R. Andoulsi, and K. Nagasaka, "Multiobjective intelligent energy management for a microgrid," *IEEE Trans. Ind. Electron.*, vol. 60, no. 4, pp. 1688–1699, 2013, doi: 10.1109/TIE.2012.2188873.

[20] A. Elgammal and M. El-Naggar, "Energy management in smart grids for the integration of hybrid wind–PV–FC–battery renewable energy resources using multi-objective particle swarm optimisation (MOPSO)," *J. Eng.*, vol. 2018, no. 11, pp. 1806–1816, 2018, doi: 10.1049/joe.2018.5036.

[21] T. G. Paul, S. J. Hossain, S. Ghosh, P. Mandal, and S. Kamalasadan, "A Quadratic Programming Based Optimal Power and Battery Dispatch for Grid-Connected Microgrid," *IEEE Trans. Ind. Appl.*, vol. 54, no. 2, pp. 1793–1805, 2018, doi: 10.1109/TIA.2017.2782671.

[22] S. M. Sadek, W. A. Omran, M. A. M. Hassan, and H. E. A. Talaat, "Day-Ahead Energy Management for Isolated Microgrids Considering Reactive Power Capabilities of Distributed Energy Resources and Reactive Power Costs State of Charge Value of Curtailment," vol. 10, no. 4, 2020.

[23] A. Dubey and S. Santoso, "Electric Vehicle Charging on Residential Distribution Systems: Impacts and Mitigations," *IEEE Access*, vol. 3, pp. 1871–1893, 2015, doi: 10.1109/ACCESS.2015.2476996.

[24] L. Pieltain Fernández, T. Gomez San Roman, R. Cossent, C. Mateo Domingo, and P. Frías, "Assessment of the Impact of Plug-in Electric Vehicles on Distribution Networks," *IEEE Trans. Power Syst.*, vol. 26, no. 1, pp. 206–213, 2011, doi: 10.1109/TPWRS.2010.2049133.

[25] R. Mehta, D. Srinivasan, A. M. Khambadkone, J. Yang, and A. Trivedi, "Smart Charging Strategies for Optimal Integration of Plug-In Electric Vehicles Within Existing Distribution System Infrastructure," *IEEE Trans. Smart Grid*, vol. 9, no. 1, pp. 299–312, 2018, doi: 10.1109/TSG.2016.2550559.

[26] R. Leou, "Optimal Charging/Discharging Control for Electric Vehicles Considering Power System Constraints and Operation Costs," *IEEE Trans. Power Syst.*, vol. 31, no. 3, pp. 1854–1860, 2016, doi: 10.1109/TPWRS.2015.2448722.

[27] L. Jian, Y. Zheng, X. Xiao, and C. C. Chan, "Optimal scheduling for vehicle-to-grid operation with stochastic connection of plug-in electric vehicles to smart grid," *Appl. Energy*, vol. 146, pp. 150–161, May 2015, doi: 10.1016/j.apenergy.2015.02.030.

[28] L. Jian, X. Zhu, Z. Shao, S. Niu, and C. C. Chan, "A scenario of vehicle-to-grid implementation and its double-layer optimal charging strategy for minimizing load variance within regional smart grids," *Energy Convers. Manag.*, vol. 78, pp. 508–517, Feb. 2014, doi: 10.1016/j.enconman.2013.11.007.

[29] J. Yang, L. He, and S. Fu, "An improved PSO-based charging strategy of electric vehicles in electrical distribution grid," *Applied Energy*, vol. 128. Elsevier Ltd, pp. 82–92, Sep. 01, 2014, doi: 10.1016/j.apenergy.2014.04.047.

[30] G. R. Chandra Mouli, P. Bauer, and M. Zeman, "System design for a solar powered electric vehicle charging station for workplaces," *Appl. Energy*, vol. 168, no. 2016, pp. 434–443, 2016, doi: 10.1016/j.apenergy.2016.01.110.

[31] S. Suthar and N. M. Pindoriya, "Energy management platform for integrated battery-based energy storage – solar PV system: a case study," *IET Energy Syst. Integr.*, vol. 2, no. 4, pp. 373–381, 2020, doi: 10.1049/iet-esi.2020.0035.

[32] P. K. Gayen, R. Majumdar, and S. Mondal, "Development and implementation of adaptive solar module– and battery characteristics–based real-time power management for solar battery system under grid-connected and -islanded conditions," *Int. Trans. Electr. Energy Syst.*, vol. 30, no. 3, p. e12240, 2020, doi: https://doi.org/10.1002/2050-7038.12240.

[33] Y. Zhang, N. Gatsis, and G. B. Giannakis, "Robust Energy Management for Microgrids With High-Penetration Renewables," *IEEE Trans. Sustain. Energy*, vol. 4, no. 4, pp. 944–953, 2013, doi: 10.1109/TSTE.2013.2255135.

[34] A. Elgammal and M. El-Naggar, "Energy management in smart grids for the integration of hybrid wind–PV–FC–battery renewable energy resources using multi-objective particle swarm optimisation (MOPSO)," *J. Eng.*, vol. 2018, no. 11, pp. 1806–1816, 2018, doi: 10.1049/joe.2018.5036.

[35] V. V. S. N. Murty and A. Kumar, "Multi-objective energy management in microgrids with hybrid energy sources and battery energy storage systems," *Prot. Control Mod. Power Syst.*, vol. 5, no. 1, pp. 1–20, 2020, doi: 10.1186/s41601-019-0147-z.

[36] J. Zupančič, B. Filipič, and M. Gams, "Genetic-programming-based multi-objective optimization of strategies for home energy-management systems," *Energy*, vol. 203, 2020, doi: 10.1016/j.energy.2020.117769.

[37] R. J. J. Molu, S. Raoul Dzonde Naoussi, P. Wira, W. F. Mbasso, S. T. Kenfack, and S. Kamel, "Optimization-based energy management system for grid-connected photovoltaic/battery microgrids under uncertainty," *Case Stud. Chem. Environ. Eng.*, vol. 8, no. June, p. 100464, 2023, doi: 10.1016/j.cscee.2023.100464.

[38] X. Pan, R. Khezri, A. Mahmoudi, A. Yazdani, and G. M. Shafiullah, "Energy Management Systems for Grid-Connected Houses with Solar PV and Battery by Considering Flat and Time-of-Use Electricity Rates," *Energies*, vol. 14, no. 16, 2021, doi: 10.3390/en14165028.

[39] M. A. Hossain, H. R. Pota, S. Squartini, F. Zaman, and K. M. Muttaqi, "Energy management of community microgrids considering degradation cost of battery," *J. Energy Storage*, vol. 22, no. February, pp. 257–269, 2019, doi: 10.1016/j.est.2018.12.021.

[40] A. Rezaee Jordehi, "An improved particle swarm optimisation for unit commitment in microgrids

with battery energy storage systems considering battery degradation and uncertainties," *Int. J. Energy Res.*, vol. 45, no. 1, pp. 727–744, 2021, doi: 10.1002/er.5867.

[41] M. F. Zia, E. Elbouchikhi, and M. Benbouzid, "Optimal operational planning of scalable DC microgrid with demand response, islanding, and battery degradation cost considerations," *Appl. Energy*, vol. 237, pp. 695–707, 2019, doi: https://doi.org/10.1016/j.apenergy.2019.01.040.

[42] M. Seydenschwanz, K. Majewski, C. Gottschalk, and R. Fink, "Linear Approximation of Cyclic Battery Aging Costs for MILP-Based Power Dispatch Optimization," in *2019 IEEE PES Innovative Smart Grid Technologies Europe (ISGT-Europe)*, 2019, pp. 1–5.

[43] I. Alsaidan, A. Khodaei, and W. Gao, "A Comprehensive Battery Energy Storage Optimal Sizing Model for Microgrid Applications," *IEEE Trans. Power Syst.*, vol. 33, no. 4, pp. 3968–3980, 2018.

[44] S. Cordova, C. Canizares, A. Lorca, and D. E. Olivares, "An Energy Management System with Short-Term Fluctuation Reserves and Battery Degradation for Isolated Microgrids," *IEEE Trans. Smart Grid*, vol. 12, no. 6, pp. 4668–4680, 2021, doi: 10.1109/TSG.2021.3103783.

[45] Y. Shi, B. Xu, Y. Tan, and B. Zhang, "A Convex Cycle-based Degradation Model for Battery Energy Storage Planning and Operation," in *2018 Annual American Control Conference (ACC)*, 2018, pp. 4590–4596, doi: 10.23919/ACC.2018.8431814.

[46] J. O. Lee and Y. S. Kim, "Novel battery degradation cost formulation for optimal scheduling of battery energy storage systems," *Int. J. Electr. Power Energy Syst.*, vol. 137, no. October 2021, p. 107795, 2022, doi: 10.1016/j.ijepes.2021.107795.

[47] J. Corbett, K. Wardle, and C. Chen, "Toward a sustainable modern electricity grid: The effects of smart metering and program investments on demand-side management performance in the US electricity sector 2009-2012," *IEEE Trans. Eng. Manag.*, vol. 65, no. 2, pp. 252–263, 2018.

[48] D. Zhang, H. Zhu, H. Zhang, H. H. Goh, H. Liu, and T. Wu, "Multi-Objective Optimization for Smart Integrated Energy System Considering Demand Responses and Dynamic Prices," *IEEE Trans. Smart Grid*, vol. 13, no. 2, pp. 1100–1112, 2022, doi: 10.1109/TSG.2021.3128547.

[49] L. Wang, C. Hou, B. Ye, X. Wang, C. Yin, and H. Cong, "Optimal Operation Analysis of Integrated Community Energy System Considering the Uncertainty of Demand Response," *IEEE Trans. Power Syst.*, vol. 36, no. 4, pp. 3681–3691, 2021, doi: 10.1109/TPWRS.2021.3051720.

[50] S. Zheng, Y. Sun, B. Qi, and B. Li, "Incentive-Based Integrated Demand Response Considering S&C Effect in Demand Side With Incomplete Information," *IEEE Trans. Smart Grid*, vol. 13, no. 6, pp. 4465–4482, 2022, doi: 10.1109/TSG.2022.3149959.

[51] H. Zhang, C. Gong, W. Ju, G. Pan, and W. Wang, "Optimization Dispatch Modeling for Demand Response Considering Supply and Demand balance and Security Constraints," in *2021 Power System and Green Energy Conference (PSGEC)*, 2021, pp. 166–170, doi: 10.1109/PSGEC51302.2021.9542507.

[52] O. Sadeghian, A. Oshnoei, B. Mohammadi-ivatloo, V. Vahidinasab, and A. Anvari-Moghaddam, "A comprehensive review on electric vehicles smart charging: Solutions, strategies, technologies, and challenges," *J. Energy Storage*, vol. 54, p. 105241, 2022.

[53] A. S. Al-Ogaili *et al.*, "Review on Scheduling, Clustering, and Forecasting Strategies for Controlling Electric Vehicle Charging: Challenges and Recommendations," *IEEE Access*, vol. 7, pp. 128353–128371, 2019, doi: 10.1109/ACCESS.2019.2939595.

[54] M. Majidpour, C. Qiu, P. Chu, H. R. Pota, and R. Gadh, "Forecasting the EV charging load based on customer profile or station measurement?," *Appl. Energy*, vol. 163, pp. 134–141, 2016, doi:

https://doi.org/10.1016/j.apenergy.2015.10.184.

[55] C. Wang, G. Grozev, and S. Seo, "Decomposition and statistical analysis for regional electricity demand forecasting," *Energy*, vol. 41, no. 1, pp. 313–325, 2012, doi: https://doi.org/10.1016/j.energy.2012.03.011.

[56] A. Ebrahimi and A. Moshari, "Holidays short-term load forecasting using fuzzy improved similar day method," *Int. Trans. Electr. Energy Syst.*, vol. 23, no. 8, pp. 1254–1271, 2013, doi: https://doi.org/10.1002/etep.1650.

[57] D. Panahi, S. Deilami, M. A. S. Masoum, and S. M. Islam, "Forecasting plug-in electric vehicles load profile using artificial neural networks," *2015 Australas. Univ. Power Eng. Conf. Challenges Futur. Grids, AUPEC 2015*, pp. 1–6, 2015, doi: 10.1109/AUPEC.2015.7324879.

[58] Y. Li, Y. Huang, and M. Zhang, "Short-Term Load Forecasting for Electric Vehicle Charging Station Based on Niche Immunity Lion Algorithm and Convolutional Neural Network," *Energies*, vol. 11, no. 5, 2018, doi: 10.3390/en11051253.

[59] J. Zhu *et al.*, "Electric Vehicle Charging Load Forecasting: A Comparative Study of Deep Learning Approaches," *Energies*, vol. 12, no. 14, 2019, doi: 10.3390/en12142692.

[60] X. Zhang, K. W. Chan, H. Li, H. Wang, J. Qiu, and G. Wang, "Deep-Learning-Based Probabilistic Forecasting of Electric Vehicle Charging Load With a Novel Queuing Model," *IEEE Trans. Cybern.*, vol. 51, no. 6, pp. 3157–3170, 2021, doi: 10.1109/TCYB.2020.2975134.

[61] E. S. Xydas, C. E. Marmaras, L. M. Cipcigan, A. S. Hassan, and N. Jenkins, "Forecasting Electric Vehicle charging demand using Support Vector Machines," *Proc. Univ. Power Eng. Conf.*, no. May 2014, 2013, doi: 10.1109/UPEC.2013.6714942.

[62] K. Lu *et al.*, "Load forecast method of electric vehicle charging station using SVR based on GA-PSO," *IOP Conf. Ser. Earth Environ. Sci.*, vol. 69, no. 1, 2017.

[63] M. Duan, A. Darvishan, R. Mohammaditab, K. Wakil, and O. Abedinia, "A novel hybrid prediction model for aggregated loads of buildings by considering the electric vehicles," *Sustain. Cities Soc.*, vol. 41, pp. 205–219, 2018, doi: https://doi.org/10.1016/j.scs.2018.05.009.

[64] J. Zhu, Z. Yang, Y. Guo, J. Zhang, and H. Yang, "Short-Term Load Forecasting for Electric Vehicle Charging Stations Based on Deep Learning Approaches," *Appl. Sci.*, vol. 9, no. 9, 2019, doi: 10.3390/app9091723.

[65] S. Powell, G. Vianna Cezar, E. Apostolaki-Iosifidou, and R. Rajagopal, "Large-scale scenarios of electric vehicle charging with a data-driven model of control," *Energy*, vol. 248, p. 123592, 2022, doi: https://doi.org/10.1016/j.energy.2022.123592.

[66] M. Pantos, "Exploitation of Electric-Drive Vehicles in Electricity Markets," *IEEE Trans. Power Syst.*, vol. 27, no. 2, pp. 682–694, 2012, doi: 10.1109/TPWRS.2011.2172005.

[67] Q. Gao *et al.*, "Charging Load Forecasting of Electric Vehicle Based on Monte Carlo and Deep Learning," in *2019 IEEE Sustainable Power and Energy Conference (iSPEC)*, 2019, pp. 1309–1314, doi: 10.1109/iSPEC48194.2019.8975364.

[68] J. Zhang, J. Yan, Y. Liu, H. Zhang, and G. Lv, "Daily electric vehicle charging load profiles considering demographics of vehicle users," *Appl. Energy*, vol. 274, p. 115063, 2020, doi: https://doi.org/10.1016/j.apenergy.2020.115063.

[69] T. Yi, C. Zhang, T. Lin, and J. Liu, "Research on the spatial-temporal distribution of electric vehicle charging load demand: A case study in China," *J. Clean. Prod.*, vol. 242, p. 118457, 2020, doi: https://doi.org/10.1016/j.jclepro.2019.118457.

Chapter 3

Designing of the Community MG with Optimal Sizing and Placement of DERs and EV Stations

3.1. Introduction

In recent years, the integration of DERs to the conventional grid has increased rapidly due to its advantages in technical, environmental, and economic aspects. Along with DERs, EVs are also getting popular as a potential alternative to fossil-fuel-driven transportation. The penetration of EVs in the network increases the system's total load which is a challenge for the current distribution system [1]. It is observed that power loss and voltage stability of an electrical network is dependent on DER's sizing, EVs charging load, location of DERs, and EV stations (EVSs) in a network. Therefore, if the sizing of DERs and their integration with EVS are planned optimally and strategically in a network then they are always committed to reduce the network's power losses, enhancement of voltage stability margin, improvement of voltage profile and power quality of supplied power [2].

By the conducted literature survey, discussed in Chapter 2, we remark that the researchers did not focus on optimal capacity estimation and allocations of DER units together with appropriate placement of EVS simultaneously, and considering different charging patterns and voltage-dependent load. To investigate these issues, this chapter formulates a multi-objective function with a purpose to determine the optimal capacity and location of multiple DERs along with EVS, to reduce power losses and voltage

fluctuations in the system. The considered test system includes voltage-dependent load models, renewable energy-based DER units, and different EV charging patterns.

3.2. Modelling of various DER units and electrical load

The DER units are usually modeled as a constant power factor model. Power electronic and synchronous generator-based DERs are referred to as controllable DERs [3]. In this study, all DERs are modelled as constant power factor model having a power factor of 0.9 lagging. The details of modelling of various DERs units and electric load are discussed below.

3.2.1. Solar Photovolatic (PV) system

The power of solar PV systems is expressed in terms of solar irradiance and temperature using (3.1) [4].

$$P_{PV}^{t} = \eta_{PV}.P_{PV}^{R}.\frac{G_m^t}{G_N}\left[1 + K_\theta\left\{\theta_{A,m}^{t} - \theta_N\right\}\right] \quad \forall t \in \mathcal{T} \tag{3.1}$$

where, P_{PV}^{R} is the rated power of the PV generator which is considered to be 5 kW, G_m^t is the measured solar radiation at time t, G_N is the nominal solar radiation, which is assumed to be 1000W/m^2, K_θ is a constant equal to -0.0357%/◦C, $\theta_{A,m}^{t}$ is the measured ambient temperature at time t, θ_N is the panel temperature in standard test conditions, which is assumed to be 25°C and η_{PV} is the performance coefficient of the PV power converter which is considered to be 95%. $\mathcal{T}$ is a subset of $\mathbb{N}$, represents time intervals, defined as $\mathcal{T} = [1,2,3 \ldots, T]$. T is the total number of time intervals.

3.2.2. Wind turbine generator (WTG)

The power output of a WTG is a function of wind speed and is expressed by (3.2) [4].

$$P_{WTG}^{t} = \begin{cases} 0\,; \quad v_w^t \le v_{ci,}, v_w^t \ge v_{co,} \\ P_{WTG}^{R} * \left(\frac{v_w^t - v_{ci}}{v_r - v_{ci}}\right)^3;\ v_{ci} < v_w^t \le v_r \\ P_{WTG}^{R} + \left(\frac{P_{WTG}^{co} - P_{WTG}^{R}}{v_{co} - v_r}\right) * (v_w^t - v_r);\ v_r < v_w^t < v_{co} \end{cases} \quad \forall t \in \mathcal{T} \tag{3.2}$$

where P_{WTG}^{t} is the active power output of WTG for time 't'. Also, P_{WTG}^{co} and P_{WTG}^{R} represents the active power output of WTG at cut-out and rated wind speed respectively. Furthermore, v_w^t, v_r, v_{ci} and v_{co} are measured, rated, cut-in, and cut-out wind speeds in m/sec respectively. The specifications of the considered WTG, including rated, cut-in, and cut-out wind speeds are 12.5 m/sec, 3.5 m/sec, 25 m/sec respectively. The WTG (Bonus 150/30) having a specified rated power of 150 kW is considered in this study [5].

3.2.3. Dispatchable energy generator (DEG)

The dispatchable energy generator having a constant power factor of 0.9 lagging is considered. The fossil fuel-dependent energy sources are mainly considered as DEG. In this work, natural gas combined cycle based DEG is taken into account for the simulation studies. Further, the hourly fuel cost of a natural gas generator can be determined using the equation in (3.3).

$$FC_{DEG}(t) = (FC_{unit} * FC_{consumed})/1000 \tag{3.3}$$

where FC_{DEG} refers to the cost of natural gas consumed per hour of operation in \$/h, FC_{unit} represents the purchase price of natural gas per thousand cubic feet in \$ / thousand cubic feet and $FC_{consumed}$ is the natural gas consumption in cubic feet per hour (ft^3 /h).

3.2.4. Electrical load modelling

In a practical distribution system, the load is continuously changing. Therefore, this study considers voltage-dependent load i.e., residential, commercial, and industrial load models to simulate the practical scenario. In load flow problems, the exponential-based static load modeling is more appropriate with respect to dynamic load modeling [17]. In the static load model, load behavior is represented as an algebraic function of voltage magnitude [6]. In the case of exponential load, the mathematical relation between the load parameters and voltage magnitude is shown in (3.4) & (3.5) [7].

$$P_{L,i} = P_{L0} V_i^{n_p} \quad i = 1,2,\ldots..N_b \tag{3.4}$$

$$Q_{L,i} = Q_{L0} V_i^{n_q} \quad i = 1,2,\ldots..N_b \tag{3.5}$$

where, n_p and n_q are active and reactive power exponents which vary according to different load classes i.e., residential, commercial, and industrial respectively. $P_{L,i}$ and $Q_{L,i}$ refers to real and reactive power load at i^{th} bus, while P_{L0} and Q_{L0} are the values of active and reactive power load at initial working conditions, respectively. V_i is the magnitude of the voltage at the i^{th} load bus. Table 3.1 shows the exponent values corresponding to different load types. For constant power loads these exponent values remain zero.

Table 3.1 Exponent values corresponding to different load types[7]

Load Type		**Residential**		**Commercial**		**Industrial**	
		n_{pr}	n_{qr}	n_{pc}	n_{qc}	n_{pi}	n_{qi}
Summer	Day	0.72	2.96	1.25	3.5	0.18	0.6
	Night	0.92	4.04	0.99	3.95	0.18	0.6
Winter	Day	1.04	4.19	1.5	3.15	0.18	0.6
	Night	1.3	4.38	1.51	3.4	0.18	0.6

3.3. Probabilistic modelling of EVL

The stochastic behavior of EVs is an outcome of numerous factors, such as battery capacity, the number of vehicles, charging speeds, time at which it is plugged in or plugged out, daily distance traveled by an EV, type of vehicle, and charging patterns [8]. In this study, the load modeling of EVs is based on few factors, i.e., daily distance traveled by an EV, the number of vehicles, time at which it is plugged in i.e., arrival time and plugged out i.e. departure time.

The parameters such as daily distance traveled by an EV and arrival time are extracted by using Monte Carlo simulation from their respective probability density functions and information regarding these probability density functions are reported in [9]. All the EVs are assumed to be private vehicles and are charged/ discharged according to three different EV stations/parking nodes i.e., residential charging station (RCS), commercial charging station (CCS) and industrial charging station (ICS). It is assumed that EVs considered in this study are private vehicles. It is also assumed; the charging of EVs will start as soon as they reach their residence/workplace until the battery is fully charged.

At RCS, the EV charging starts at 4:00 pm after the owner arrives at the residence, whereas, for CCS it begins at 8:00 am when the owner arrives at the workplace. Usually, industrial employees have three kinds of working shifts therefore for ICS, at morning 6:00 am first shift's EV charging starts, similarly, the second shift and the third shift start at 2:00 pm and 10:00 pm respectively. The SOC of EV for each n^{th} EV at the time of arrival can be calculated using (3.6). The time duration of charging (TD_{Ch}^{n}) for each n^{th} EV can be obtained from (3.7)[9].

$$SOC_{EV,PI}^{n} = 1 - \left(\frac{S_{EV}^{n}}{S_{EV}^{\acute{M}}}\right) \; \forall n \in \mathcal{N}_{EV} \tag{3.6}$$

$$TD_{Ch}^{n} = \frac{\left(1-SOC_{EV,PI}^{n}\right)*E_{EV}^{R}}{\eta_{EV,Ch}*P_{EV,Ch}} \quad \forall n \in \mathcal{N}_{EV} \tag{3.7}$$

S_{EV}^{n} and $S_{EV}^{\acute{M}}$ are the distance travelled by the n^{th} EV and maximum distance EV can travel in one charge. $SOC_{EV,PI}^{n}$ is the SOC of n^{th} EV at the time of plug-in; E_{EV}^{R} represents the rated energy capacity of EV in kWH, $P_{EV,Ch}$ is the charging rate of EV in kW; $\eta_{EV,Ch}$ is the charging efficiency of EVs. $\mathcal{N}_{EV}$ is a subset of $\mathbb{N}$, represents number of EVs and is defined as $\mathcal{N}_{EV} = [1,2,3,\dots,N_{EV}]$. N_{EV} represents the total number of EVs.

The plug-out time (T_{PO}^{n}) of EVs can be further calculated using (3.8) [9].

$$T_{PO}^{n} = T_{PI}^{n} + TD_{Ch}^{n} \quad \forall n \in \mathcal{N}_{EV} \tag{3.8}$$

where T_{PI}^{n} represents the time at which EV charging begins. The charging power ($P_{Ch}^{t,n}$) required to charge the EV can be estimated using equation (3.9). The associated time interval to this charging power can be calculated using equation (3.8) and T_{PI}^{n} .

$$P_{Ch}^{t,n} for\ each\ 't'\ interval\ of\ TD_{Ch}^{n} = P_{EV,Ch} \quad \forall t \in \mathcal{T}, \forall n \in \mathcal{N}_{EV} \tag{3.9}$$

As EVs charging time intervals are independent of each other, therefore they can be accumulated. The daily EVL of a large number of EVs can be calculated using (3.10) as follows:

$$P_{EV}^{t} = \sum_{n=1}^{N_{EV}} P_{Ch}^{t,n} \quad \forall t \in \mathcal{T}, \forall n \in \mathcal{N}_{EV} \tag{3.10}$$

where P_{EV}^{t} is the daily EVL profile of N_{EV} EVs.

3.4. Objective function formulation and operational constraints

In order to formulate the objective function, power flow calculation is an initial step. Conventional power flow algorithms such as Gauss-Seidel, Newton Raphson are incompetent for distribution network as it has low X/R ratio.

Hence, the Backward-Forward sweep power flow algorithm is mainly used for distribution networks for fast and accurate results [10]. Consider a radial distribution network shown in Fig. 3.1. Buses r & s are connected through a line having a total impedance Z_{rs} .

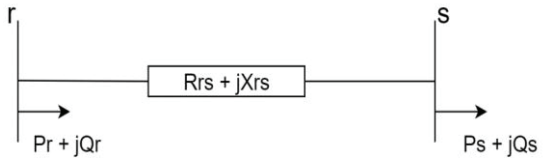

Figure 3.1 Radial distribution network

$$Z_{rs} = R_{rs} + jX_{rs} \tag{3.11}$$

Active power loss for the line between r & s can be written as:

$$APL_{(rs)} = R_{rs}\left(\frac{P_{rs}^2 + Q_{rs}^2}{V_r^2}\right) \tag{3.12}$$

The total active power loss (TAPL) can be computed by:

$$TAPL = \sum_{s=1}^{N_{br}} APL_{(rs)} \tag{3.13}$$

where N_{br} is the total number of branches present in the network, $r = 1{:}\,N_b$ and N_b is the number of buses.

The voltage deviation (VD) determines the weak buses in a network. It is a measure of voltage stability margin in the power system network to maintain voltage within the permissible limits after the occurrence of disturbance. Total voltage deviation (TVD) is given by:

$$TVD = \sum_{r=1}^{N_b} |1 - V_r| \tag{3.14}$$

where, V_r is the voltage at bus r, $r = 1{:}\,N_b$.

In this chapter, two objective functions (F1 and F2) are formulated to minimize active power loss and minimize voltage deviation index. *i.e.,* Minimize $F1 = APF$ and Minimize $F2 =$ TVD.

This multi-objective problem is solved using the weighted sum approach, and the overall objective function (F3) is defined in (3.15).

$$F3 = w_1 * TAPL + w_2 * TVD \tag{3.15}$$

where w_1 and w_2 are the weights of $F1$ and $F2$ respectively. The values considered for w_1 and w_2 are 0.7 and 0.3, respectively. The objective function in (3.15) is minimized with respect to the constraints shown in (3.16-3.20).

- Power Balance Constraints

$$P_{EV} + P_L + P_{Loss} = P_{DERs} + P_G \tag{3.16}$$

where P_g, P_{Loss} and P_{DERs} are the active power of the electrical grid, active losses of the network, and power output of all DERs respectively.

$$Q_L + Q_{Loss} = Q_{DERs} + Q_G \tag{3.17}$$

where Q_g, Q_{Loss} and Q_{DERs} are the reactive power of the electrical grid, reactive losses of the network, and power output of all DERs respectively.

- Voltage limits of the bus

$$V_i^{\acute{m}} < V_i < V_i^{\acute{M}} \quad i = 1,2,\dots,N_b \tag{3.18}$$

where, $V_i^{\acute{m}}$ and $V_i^{\acute{M}}$ are the minimum and maximum bus voltage limits, having values 0.95 and 1.05 respectively. V_i is the voltage magnitude at bus i in pu.

- Power limits of DERs

$$P_{DER,m}^{\acute{m}} < P_{DER,m} < P_{DER,m}^{\acute{M}} \quad m = 1,2,\dots,\mathrm{M} \tag{3.19}$$

$$Q_{DER,m}^{\acute{m}} < Q_{DER,m} < Q_{DER,m}^{\acute{M}} \quad m = 1,2,\dots,\mathrm{M} \tag{3.20}$$

where, $P_{DER,m}^{\acute{m}}$ and $P_{DER,m}^{\acute{M}}$ are the minimum and maximum limits on the active & reactive power output of the m^{th} DER, respectively. M is the total number of DERs.

3.5. Methodology of the proposed algorithm

The flow chart of the proposed method is shown in Fig. 3.2. It has been reported in [11] that among various evolutionary algorithms like Genetic Algorithm, Tabu Search, Teaching Learning Based Optimization, Imperialist Competitive Algorithm, Artificial Bee Colony, Particle Swarm Optimization (PSO) has the best performance for solving energy management problems in less time within the maximum allowable iteration. Therefore, the formulated optimization problem is solved using a well-established meta-heuristic-based approach, PSO, considering population size and iterations as 70 and 200, respectively.

In order to set the lower and upper limits of control parameters for optimization, certain pre-assumptions are made:

- For the scenarios in which DERs are integrated into the test system, the total load of the system is fulfilled only by DERs, which means that the power taken from the grid is zero. Further, the sum of capacities of all DERs present in the network is less than or equal to the total connected load on the system to restrict the over-sizing of DERs.
- DERs are permitted to be located at any bus except the grid-connected bus, i.e., bus number 1.
- A total of four EV charging stations are considered in this system for optimal location. Two charging stations ($RCS\ 1$ & $RCS\ 2$) are assigned to locate for residential buses. However, for a commercial and industrial group of buses, one charging station (CCS & ICS) is allocated to each group.

3.6. Case study & results

The IEEE 33-bus radial distribution system is considered. During the analysis, the base voltage and base MVA considered are 12.66 kV and 100 MVA, respectively. The test system consists of 33 buses and 32 branches, as shown in the single-line diagram depicted in Fig. 3.3. It is assumed that the total real and reactive power loads on the system (with EV charging load) are 3715 kW and 2300 kVAr, respectively. Figure 3.4

shows the daily charging load profile of 160 EVs at residential (RCS), commercial (CCS), and industrial (ICS) charging stations each.

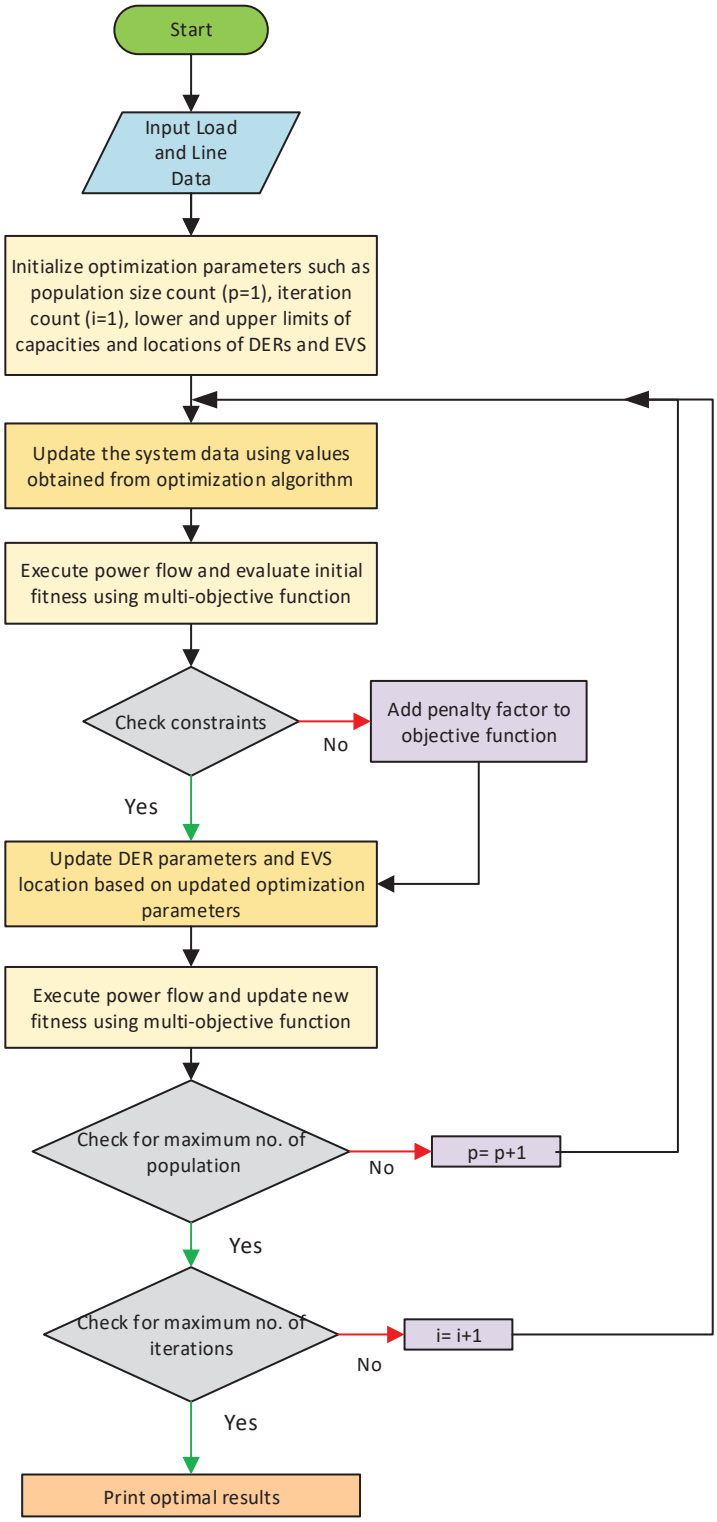

Figure 3.2 Flow chart of the proposed method

Table 3.2 shows the parameters of electric vehicles considered in this work. The peak load of each EV charging load pattern is considered for determining the optimal locations of four EVS.

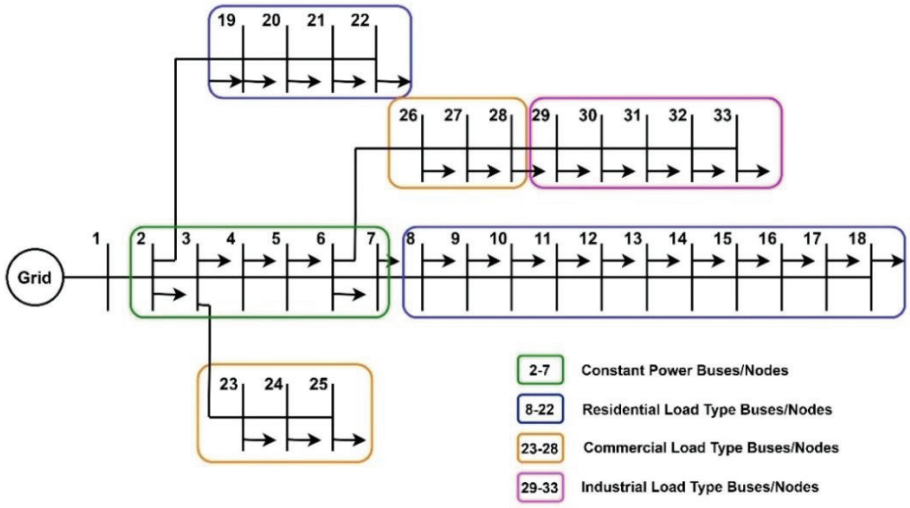

Figure 3.3 IEEE 33 bus modified test system

In this study, five scenarios are considered, i.e., a test system without DER and EVS; without DER but with EVS; with a PV as DER and EVS; with a PV and WTG as DER; and EVS and a test system with all the three DERs, PV, WTG, DEG, and EVS. In scenario 2, optimum allocations of EVS are determined using all three optimization algorithms. Moreover, for scenarios 3,4 and 5, the optimum capacity and allocations of DERs and allocations of EVS are obtained. These results are summarized in Table 3.3.

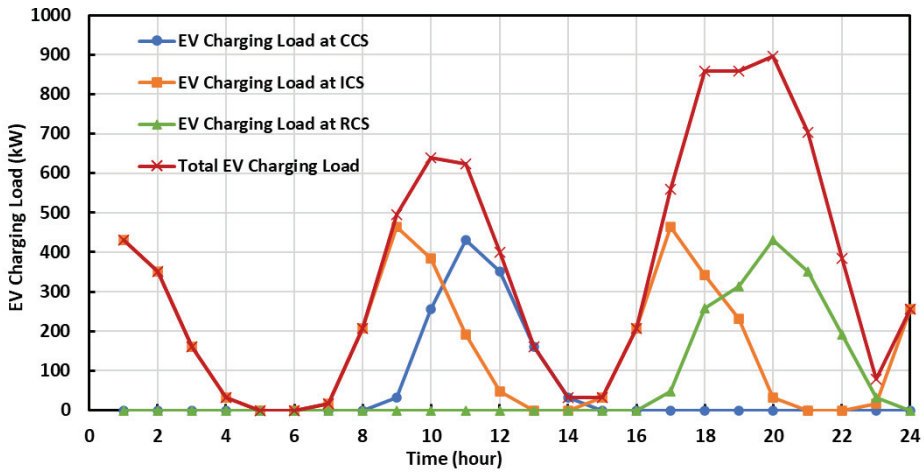

Figure 3.4 Charging load profile of 160 number of EVs at residential (RCS), commercial (CCS) and industrial (ICS) charging station.

Table 3.2 Parameters of EV

PHEV Parameters	Value
S_{EV}^{M} (km/charge)	200
E_{EV}^{R} (kWh)	24
$SOC_{EV}^{m}/SOC_{EV}^{M}$ (%)	20/100
$P_{EV,Ch}$ (kW)	3
$\eta_{EV,Ch}$	85%

In scenario 2, the value of TAPL is higher than base scenario 1 as in this case, EV charging load is also considered. In scenario 3, the optimal location and capacity of DER are 26th bus and 3.9 MW, respectively. It indicates that, in this case, approximately 780 PV arrays are required to fulfill the total load demand. The value of TAPL and maximum VD observed at these optimal solutions is 103.037 kW and 0.0363 on the 18th bus, respectively.

Similarly, in scenario 4, 1.5 MW rated PV allocated on the 24th bus and 2.71 MW rated WTG on the 26th bus are the optimal solutions. It depicts, 300 PV arrays and 18 WTGs are required in this scenario. The TAPL and maximum VD values observed in this case are 74.90 kW and 0.0491 on the 18th bus, respectively.

However, in scenario 5 the optimal locations and rated capacities of PV, WTG, and DEG are 30th bus with 1 MW, 11th bus with 1.65 MW, 24th bus with 1.8 MW, respectively. This implies that the test system requires approximately 200 PV arrays, 11 WTGs and a diesel generator of 1800kW to fulfill the total load demand. The TAPL and maximum VD value in this scenario are the lowest among all scenarios, i.e., 23.76 kW and 0.0212 on the 18th bus. It is evident that as the number of DERs increases in the test system, the value of TAPL decreases.

Fig. 3.5 shows the voltage profile in all the scenarios. It is significant from Fig. 3.5 that the most stable voltage profile is observed for Scenerio 5 with minmum voltage deviation at each bus.

Table 3.3 Results obtained in all the considered scenarios

Different Cases	Optimal Bus No. locations of DER	Capacity of DER	Optimal EVS Bus No. locations	Min value of TAPL (kW)	Maximum Voltage Deviation
Base Scenario 1 – Without DER and EVS	N.A.	N.A.	N.A.	165.72	0.0839 at 18th bus
Scenario 2 – Without DER but with EVS	N.A.	N.A.	$\boldsymbol{RCS_1}$ at 8, $\boldsymbol{RCS_2}$ at 19 $\boldsymbol{CCS}$ at 23, $\boldsymbol{ICS}$ at 29	272.89	0.1013 at 18th bus
Scenario 3 – With PV as DER and EVS	26 (PV)	3.9 kW	$\boldsymbol{RCS_1}$ at 8, $\boldsymbol{RCS_2}$ at 19 $\boldsymbol{CCS}$ at 23, $\boldsymbol{ICS}$ at 29	103.037	0.0363 at 18th bus
Scenario 4 – With PV and WTG as DER and EVS	24 (PV) 26 (WTG)	1.5 MW (PV) 2.71 MW (WTG)	$\boldsymbol{RCS_1}$ at 8, $\boldsymbol{RCS_2}$ at 19 $\boldsymbol{CCS}$ at 23, $\boldsymbol{ICS}$ at 29	74.90	0.0491 at 18th bus
Scenario 5 – With PV, WTG, and DEG as DER and EVS	11 (PV) 30 (WTG) 23 (DEG)	1 MW (PV) 1.65 MW (WTG) 2 MW(DEG)	$\boldsymbol{RCS_1}$ at 11, $\boldsymbol{RCS_2}$ at 19 $\boldsymbol{CCS}$ at 23, $\boldsymbol{ICS}$ at 30	23.76	0.0212 at 18th bus

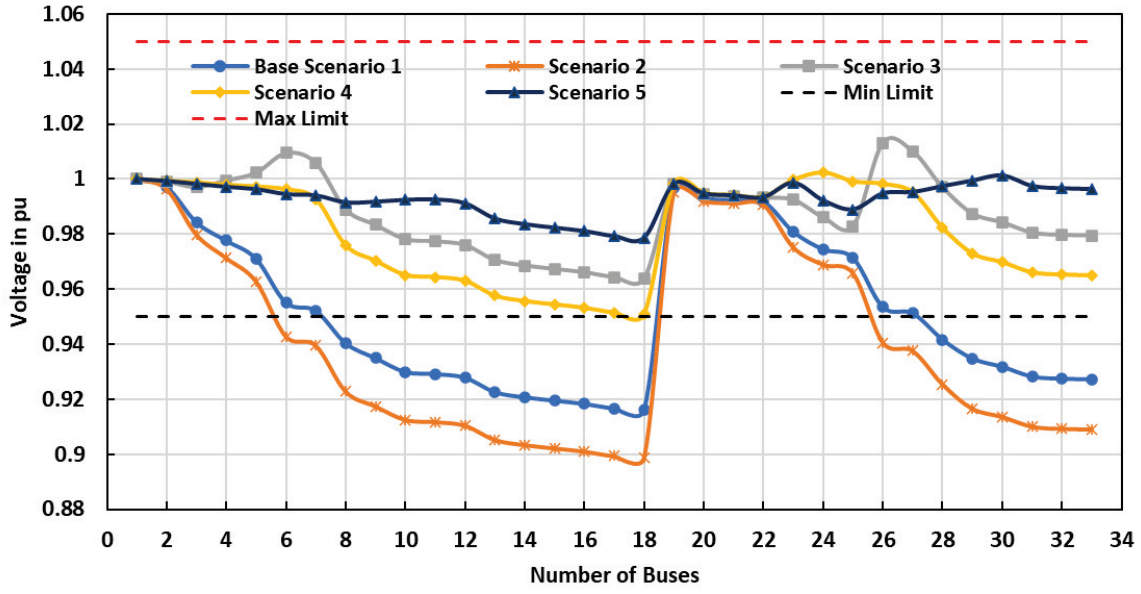

Figure 3.5 Voltage profile in all the considered scenarios

3.7. Conclusion

This chapter proposed a method to estimate the optimal capacity and placement of multiple DERs along with EVS optimal allocation in a radial distribution network. The multi-objective function is employed to minimise the power losses and improve voltage stability. Using the proposed method, a multi-bus community MG having solar PV, WTG, and DEG with voltage-dependent load models such as residential, commercial, and industrial load types is formulated along with EVL. The EVL for various types of charging stations, such as RCS, ICS, and CCS, is modelled using a probabilistic modelling approach. Further, the optimal allocation of these EVS is determined. The results show that as the number of DERs increases in the MG, the total power loss and voltage deviation decreased by 85.66% and 74.73%, respectively, that leads to improved voltage profile which can be observed for Scenario 5.

Further, to achieve the economical, efficient and sustainable operation of the developed community MG, an optimal EMS is formulated in the next chapter 4.

Bibliography

[1] O. Hafez and K. Bhattacharya, "Optimal design of electric vehicle charging stations considering various energy resources," *Renew. Energy*, vol. 107, pp. 576–589, 2017, doi: https://doi.org/10.1016/j.renene.2017.01.066.

[2] I. Diahovchenko, M. Kolcun, Z. Čonka, V. Savkiv, and R. Mykhailyshyn, "Progress and Challenges in Smart Grids: Distributed Generation, Smart Metering, Energy Storage and Smart Loads," *Iran. J. Sci. Technol. - Trans. Electr. Eng.*, vol. 44, no. 4, pp. 1319–1333, 2020, doi: 10.1007/s40998-020-00322-8.

[3] S. M. Moghaddas-Tafreshi and E. Mashhour, "Distributed generation modeling for power flow studies and a three-phase unbalanced power flow solution for radial distribution systems considering distributed generation," *Electr. Power Syst. Res.*, vol. 79, no. 4, pp. 680–686, 2009, doi: 10.1016/j.epsr.2008.10.003.

[4] H. R. Baghaee, M. Mirsalim, G. B. Gharehpetian, and H. A. Talebi, "Reliability/cost-based multi-objective Pareto optimal design of stand-alone wind/PV/FC generation microgrid system," *Energy*, vol. 115, no. October 2017, pp. 1022–1041, 2016, doi: 10.1016/j.energy.2016.09.007.

[5] "124-an-bonus-150-30 @ en.wind-turbine-models.com." [Online]. Available: https://en.wind-turbine-models.com/turbines/124-an-bonus-150-30.

[6] K. Qian, C. Zhou, M. Allan, and Y. Yuan, "Effect of load models on assessment of energy losses in distributed generation planning," *Int. J. Electr. Power Energy Syst.*, vol. 33, no. 6, pp. 1243–1250, 2011, doi: 10.1016/j.ijepes.2011.04.003.

[7] N. Rostami and M. O. Sadegh, "The Effect of Load Modeling on Load Flow Results in Distribution Systems," vol. 6, no. 1, pp. 16–27, 2018, doi: 10.12691/ajeee-6-1-3.

[8] Y. Yao and D. W. Gao, "Charging load from large-scale plug-in hybrid electric vehicles: Impact and optimization," *2013 IEEE PES Innov. Smart Grid Technol. Conf. ISGT 2013*, 2013, doi: 10.1109/ISGT.2013.6497887.

[9] H. Liu, Y. Ji, H. Zhuang, and H. Wu, "Multi-objective dynamic economic dispatch of microgrid systems including vehicle-to-grid," *Energies*, vol. 8, no. 5, pp. 4476–4495, 2015, doi: 10.3390/en8054476.

[10] U. Eminoglu and M. H. Hocaoglu, "Distribution systems forward/backward sweep-based power flow algorithms: A review and comparison study," *Electr. Power Components Syst.*, vol. 37, no. 1, pp. 91–110, 2009, doi: 10.1080/15325000802322046.

[11] V. V. S. N. Murty and A. Kumar, "Multi-objective energy management in microgrids with hybrid energy sources and battery energy storage systems," *Prot. Control Mod. Power Syst.*, vol. 5, no. 1, pp. 1–20, 2020, doi: 10.1186/s41601-019-0147-z.

Chapter 4

Development of an EMS for Economic, Efficient and Sustainable Operation of Community MG

4.1. Introduction

Due to the intermittent generation of various RERs and uncertain charging load patterns of EVs, MGs face numerous challenges regarding their optimal dispatch, reliability, stability, etc., which in turn introduces uncertainty in the system [1], [2]. To eradicate this issue and fulfill the energy demand, the incorporation of BESS plays a prominent role in an islanded MG [3]–[5]. Further, for grid-connected MGs along with BESS, the exchange of power from the utility grid also helps in taking care of uncertainty and fulfilling the electricity demand [6]. In the case of grid-connected MGs, more power is needed to be exchanged from the utility grid to meet the increased electricity demand due to EVs charging load [7][8]. It develops a dependency on the utility grid to accomplish the charging requirement of the EVs and also spikes the power loss and voltage deviation of the power grid because of unanticipated widespread power flow in the system. Consequently, these issues demand an efficient EMS that aims at the stochastic matching of DERs and EVs charging/discharging.

Several literatures have developed EMS for MG considering various aspects like cost optimization, optimal dispatch, power flow management, energy efficiency, energy trading, and stability, which are extensively detailed in Chapter 2. It was found that the EMS proposed in [9], which is termed as basic energy management strategy (BEMS), may fail to perform satisfactorily under various scenarios, including the stability of the MG, due to certain limitations. These limitations are as follows.

1) restriction in the maximum utilization of DERs & energy trading between the MG and utility grid; 2) underutilization of the MG's capability to support the utility grid during contingencies occurring in the system; and 3) inability to minimize APL and VD.

To resolve these shortcomings, an optimal energy management strategy (OEMS) is proposed to meet the non-EV and EV load demand of the MG by maximizing the utilization of DERs. It increases the profit of MG operator (MGO) by promoting energy trading between MG and utility grid, performs peak load management by incorporating governed charging/discharging mode (GCDM) of operation of EVs, aids in the improvement of BESS performance through the developed coordinated charging/ discharging state flow, and diminishes the dependency of MG on the utility grid.

The proposed OEMS formulates an objective function that minimizes the energy drawn from the utility grid required to meet the charging requirement of the EVs, optimizes the surplus energy of DERs supplied to the utility grid, especially during moderate and peak load conditions, and minimizes TAPL and TVD of the MG. It may be noted that the value of APL and VD is directly influenced by power flows in the system. Thus, if the power flow increases or decreases, it may affect the TAPL and TVD of the network, which may cause instability in the network and may alter the operating cost of the system. Therefore, these parameters are also taken into consideration to achieve the optimal energy flow solution.

The performance evaluation of the proposed strategy is analyzed by firstly comparing the simulation results obtained from OEMS with the BEMS secondly by analyzing and comparing the economic aspects of both the strategies through the economic analysis. Further, to improve the performance of OEMS and to perform peak load management in order to increase the efficiency of the system, the GCDM operating mode of EVs is introduced in the system.

The major contributions of this work are summarized below:

- Development of a coordinated charging/discharging scheduling algorithm, which improves the performance of BESS and facilitates its maximum utilization. In order to provide the BESS's schedule, it takes into account certain

operational parameters such as total load demand, SOC of previous interval, and power not fulfilled by RERs and DEG.

- Formulation of an optimal energy management strategy (OEMS) which aims at maximum utilization of DERs, promotes energy trading between MG and utility grid, performs peak load management, and minimizes the dependency of a MG on the utility grid. It is achieved by optimizing the energy exchanged between MG and utility grid considering minimum TAPL and TVD.

4.2. Modeling of energy components of MG

The community MG model designed in Chapter 3 is used in this study. Therefore, the modelling of solar PV systems, WTG, and DEG is similar to that in Chapter 3. However, the BESS is also integrated into it. Furthermore, the EVL modelling is performed for two modes, i.e., Autonomous Charging mode (ACM) and Governed Charging/Discharging mode (GCDM). This section details the modeling of BESS and EVL.

4.2.1. BESS modelling

The BESS is required in the system to surmount the intermittent behaviour of both supply-side i.e., RERs and demand-side. It will improve power controllability and enhance power quality. The attention towards these storage systems is increasing significantly, as proper coordination of BESSs with various generation units can enhance the energy efficiency, reliability, and stability of the MG system [10]. The operation of BESS can be defined using (4.1) and (4.2). In order to have long battery life of BESS, the SOC of BESS should satisfy the below-mentioned constraint:

$$P_{B,Ch}^{t}/P_{B,Dch}^{t} = \begin{cases} P_B^t < 0 \;\; if\; BESS\; is\; charging \\ P_B^t > 0 \; if\; BESS\; is\; discharging \\ P_B^t = 0 \; if\; BESS\; is\; on\; stand-by \end{cases} \quad \forall t \in \mathcal{T} \tag{4.1}$$

$$SOC_B^{t+1} = \begin{cases} SOC_B^t(1-\rho_B) - \left(\frac{P_{B,Ch}^t \cdot \eta_{B,Ch} \cdot \Delta t}{E_B^R}\right) \quad if\; BESS\; is\; charging \\ SOC_B^t(1-\rho_B) - \left(\frac{P_{B,Dch}^t}{\eta_{B,DCh} \cdot E_B^R} . \Delta t\right) if\; BESS\; is\; discharging \end{cases} \quad \forall t \in \mathcal{T} \tag{4.2}$$

where $P_{B,Ch}^t$ and $P_{B,Dch}^t$ are the charging and discharging power of the BESS at time

instant 't', respectively. $P_{B,Ch}^{t}$ is always negative and $P_{B,Dch}^{t}$ is always positive. ρ_B is the self-discharge rate of the BESS. $\eta_{B,Ch}$ and $\eta_{B,DCh}$ are the charging and discharging efficiencies of the BESS. E_B^R is the rated energy capacity of BESS.

Moreover, the BESS operation is subject to the following constraints (4.3-4.5).

$$0 > P_{B,Ch}^{t} > P_{B,Ch}^{\acute{M}} \quad \forall t \in \mathcal{T} \tag{4.3}$$

$$0 < P_{B,Dch}^{t} < P_{B,Dch}^{\acute{M}} \ \forall t \in \mathcal{T} \tag{4.4}$$

$$SOC_B^{\acute{m}} < SOC_B^{t} < SOC_B^{\acute{M}} \quad \forall t \in \mathcal{T} \tag{4.5}$$

where, $P_{B,Ch}^{\acute{M}}$ and $P_{B,Dch}^{\acute{M}}$ are the maximum charging and discharging limit of the BESS. $SoC_B^{\acute{m}}$ and $SoC_B^{\acute{M}}$ are the minimum and maximum limits of the SOC of the BESS, respectively.

4.2.2. Probabilistic modelling of EVL under various modes of EV operation

Like in chapter 3, in this chapter also, the EVL is modelled using parameters such as the number of vehicles, daily distance traveled by an EV, time at which it is plugged in i.e., arrival time and plugged out, i.e., departure time.

It is assumed that all the EVs are assumed to be private vehicles and are charged/ discharged according to three different charging stations/parking nodes i.e., RCS, CCS and ICS. The two modes of EV operation i.e., ACM and GCDM is considered in the simulation studies. In the case of GCDM, for ease of the study, it is assumed that these EVs can be scheduled completely.

4.2.2.1. Autonomous Charging mode (ACM)

In this mode of operation, EV owners start the charging of EVs as soon as they arrive at their residence/workplace till the battery is fully charged. The power flow is completely unidirectional from the distribution network to a vehicle. The modelling of EVL under the ACM is same as that of mentioned in chapter 3.

4.2.2.2. Governed Charging/Discharging mode (GCDM)

This mode deals with the bi-directional power flow between the distribution network and EVs. It coordinates the charging and discharging of EVs in an orderly and centralized way, considering charging at low or moderate load regions while discharging at peak load regions.

The charging time duration (TD_{Ch}^{n}) required to fully charge the EV before undergoing the discharging process can be calculated using (3.7).

The maximum discharging time duration $\left(TD_{Dch}^{\acute{M},n}\right)$ can be calculated from (4.6)[11][12].

$$TD_{Dch}^{\acute{M},n} = \frac{\left(SOC_{EV}^{\acute{M}} - SOC_{EV,Dch}^{th}\right) * E_{EV}^{R}}{P_{EV,Dch}} - \frac{S_{EV}^{n} * E_{EV}^{R}}{P_{EV,Dch} * S_{EV}^{\acute{M}}} \quad \forall n \in \mathcal{N}_{EV} \tag{4.6}$$

where $SOC_{EV}^{\acute{M}}$ refers to the maximum limit of SOC of an EV battery and $SOC_{EV,Dch}^{th}$ refers to the threshold limit of SOC of EV battery till which discharging can be performed. $P_{EV,Dch}$ is the discharging rate of EVs in kW. S_{EV}^{n} is the distance travelled by the EV and $S_{EV}^{\acute{M}}$ is the maximum distance EV can travel in one charge in km.

The plug-in time depends on the type of charging station nodes and arrival time of EVs to their residence/workplace. It is assumed that this plug-in time is the start time of the discharging process. The plug-in time of EVs for RCS, CCS and ICS (both shifts first and second) is obtained from (4.7- 4.10) respectively.

$$T_{RCS,PI}^{n} = \begin{cases} 16, & T_{PI}^{n} < 16 \\ T_{PI}^{n}, & otherwise \end{cases} \quad \forall n \in \mathcal{N}_{EV} \tag{4.7}$$

$$T_{CCS,PI}^{n} = \begin{cases} 8, & T_{PI}^{n} < 8 \\ T_{PI}^{n}, & otherwise \end{cases} \quad \forall n \in \mathcal{N}_{EV} \tag{4.8}$$

$$T_{ICS,1st,PI}^{n} = \begin{cases} 6, & T_{PI}^{n} < 6 \\ T_{PI}^{n}, & otherwise \end{cases} \quad \forall n \in \mathcal{N}_{EV} \tag{4.9}$$

$$T_{ICS,2nd,PI}^{n} = \begin{cases} 14, & T_{PI}^{n} < 14 \\ T_{PI}^{n}, & otherwise \end{cases} \quad \forall n \in \mathcal{N}_{EV} \tag{4.10}$$

where T_{PI}^{n} is the plug-in or arrival time of EV at the charging station.

The time at which discharging ends ($T^{n}_{Dch,end}$) can be calculated as (4.11), which is also assumed to be equal to the time at which charging starts ($T^{n}_{Ch,starts}$).

$$T^{n}_{Dch,end} = T^{n}_{PI} + TD^{\acute{M},n}_{Dch} = T^{n}_{Ch,starts} \tag{4.11}$$

The discharging power ($P^{t,n}_{Dch}$) taken from the EV can be estimated using equation (4.12). The associated time interval to this discharging power can be calculated using (4.11) and T^{n}_{PI} .

$$P^{t,n}_{Dch}\ for\ each\ 't'\ of\ T^{\acute{M},n}_{Dch} = P_{EV,Dch} \quad \forall t \in \mathcal{T}, \forall n \in \mathcal{N}_{EV} \tag{4.12}$$

After the discharging process, the time duration for which EV will be charged ($TD^{n}_{Ch,after\ Dch}$) can be estimated using (4.13).

$$TD^{n}_{Ch,after\ Dch} = TD^{n}_{Ch} + TD^{\acute{M},n}_{Dch} \tag{4.13}$$

The plug-out time of EV (T^{n}_{PO}) which will be the time at which discharging and charging process of EV will end can be estimated as in equation (4.14).

$$T^{n}_{PO} = T^{n}_{PI} + TD^{\acute{M},n}_{Dch} + TD^{n}_{Ch,after\ Dch} \quad \forall n \in \mathcal{N}_{EV} \tag{4.14}$$

Using (3.9) the charging power ($P^{t,n}_{Ch}$) can be estimated.

The daily EVL profile of a large number of EVs for GCDM mode can be calculated using (4.15) as follows:

$$P^{t}_{EV,GCDM} = \sum_{n=1}^{N_{EV}} P^{t,n}_{Dch} + P^{t,n}_{Ch} \quad \forall t \in \mathcal{T}, \forall n \in \mathcal{N}_{EV} \tag{4.15}$$

where $P^{t}_{EV,GCDM}$ is the daily EVL profile of (N_{EV}) EVs in case of GCDM.

4.3. Formulation of proposed Optimal Energy Management Strategy (OEMS)

4.3.1. Problem Statement

The proposed OEMS aims to diminish the dependency of an MG on the utility grid by maximizing the utilization of DERs and minimizing the energy drawn from the utility grid. It also focuses on increasing MGO's profit by optimizing the energy supplied to the

MG and promoting energy trading between the two entities. The active power supplied to or drawn from the utility grid can be expressed by 4.16.

$$P_G^t = P_L^t + P_{EV}^t + P_{Loss}^t - P_{PV}^t - P_{WTG}^t - P_{DEG}^t - P_B^t \;\; \forall t \in \mathcal{T} \tag{4.16}$$

where, P_{EV}^t and P_L^t are the EVs charging/discharging load and the total non-PHEV load the system respectively. P_{PV}^t, P_{WTG}^t, P_{DEG}^t represents the total generated active power of solar PV system, WTG and DEG, respectively. P_B^t shows the charging/ discharging power of BESS. P_{Loss}^t refers to the real power loss in the MG system. If total load i.e., PHEVs charging load and load on the system becomes equal to the total power output of all DERs, then P_G^t is equals to zero and there is no exchange of power between MG and the utility grid. Further when, $P_G^t < 0$ then excess power is supplied to the utility grid by the MG. In contrast, when $P_G^t > 0$ then extra power required to meet the total load is drawn from the utility grid. The total amount of energy supplied to the utility grid (E_S) and energy drawn from the utility grid (E_D) in a whole day (24 hours) can be expressed as:

In the case of $P_G^t < 0$:

$$E_S = \sum_{t=1}^{T} |P_G^t| \;\; \forall t \in \mathcal{T} \tag{4.17}$$

In the case of $P_G^t > 0$:

$$E_D = \sum_{t=1}^{T} P_G^t \;\; \forall t \in \mathcal{T} \tag{4.18}$$

The formulation of TAPL and TVD is discussed in Chapter 3.

The active power levels of DEG and BESS are not pre-determined instead, they are computed by an optimization problem. The optimization problem is formulated in such a way that as a result, it minimizes the total energy drawn from the grid i.e., (E_D) and maximizes the total energy supplied to the utility i.e., (E_S), considering minimum TAPL and TVD. Equation (4.19) represents the objective function (F4) of the proposed strategy.

$$\text{F4} = \; w_1 * P_G^t + w_2 * TAPL + \; w_3 * TVD \tag{4.19}$$

where w_1, w_2 and w_3 are the weights of individual functions and their considered values are 0.6, 0.2, and 0.2 respectively. It may be noted in case of $P_G^t < 0$, F4 is

minimized to maximize the power supplied to the utility grid.

The above-mentioned F4 is minimized subject to the following constraints shown in (4.20-4.23), like power balance, power limits of DERs, voltage constraints, and ramp rate limits of DEG.

- Power Balance of MG system

$$P_L^t + P_{EV}^t + P_{Loss}^t = P_{DERs}^t + P_G^t \;\; \forall t \in \mathcal{T} \tag{4.20}$$

where P_G^t, P_{Loss}^t and P_{DERs}^t are the power output of the utility grid, losses of the MG, and power output of all DERs respectively.

- Bus Voltage limits of MG

$$V_i^{\acute{m}} < V_i < V_i^{\acute{M}} \quad i = 1,2,\dots,N_b \tag{4.21}$$

where, $V_i^{\acute{m}}$ and $V_i^{\acute{M}}$ are the minimum and maximum bus voltage limits, having values 0.95 and 1.05 respectively. V_i and N_b are the voltage magnitude at bus i in pu and number of buses of the MG, respectively.

- Active Power limits of DERs

$$P_{DER,m}^{min} < P_{DER,m,t} < P_{DER,m}^{max} \; \mathrm{m} = 1,2,\dots,M, \forall t \in \mathcal{T} \tag{4.22}$$

where, $P_{DER,m}^{min}$ and $P_{DER,m}^{max}$ are the minimum and maximum limits on the active power output of the m^{th} DER, respectively. M is the total number of DERs.

- Ramp Rate limits of DEG

$$|P_{DEG}^t - P_{DEG}^{t-1}| \leq R_{max} * \Delta t \tag{4.23}$$

where P_{DEG}^t and P_{DEG}^{t-1} is the output of DEG in periods t and $t-1$; R_{max} is the maximum ramp rate of DEG, Δt is the time interval.

4.3.2. Coordinated charging/discharging algorithm for scheduling of BESS

In order to determine the appropriate mode of operation of BESS at a particular instant

't', a coordinated charging/discharging state flow algorithm is proposed. This state flow aims to achieve the maximum utilization of BESS to increase MGO profits. It considers various charge/discharge power levels, SOC ranges of BESS and different load regions, i.e., low load, moderate load, and peak load region. The charging and discharging schedules of BESS have three output ranges, i.e., low, medium, and high, having power output ranges, 100-400kW , 400-700kW, 700-1000kW, respectively. The SOC level of BESS has three levels, i.e., low (L) [15 %, 30%), medium (M) [30%, 60%), and high (H) [60%, 85%). Figure 4.1 shows the state flow diagram of the coordinated charging/discharging algorithm of BESS.

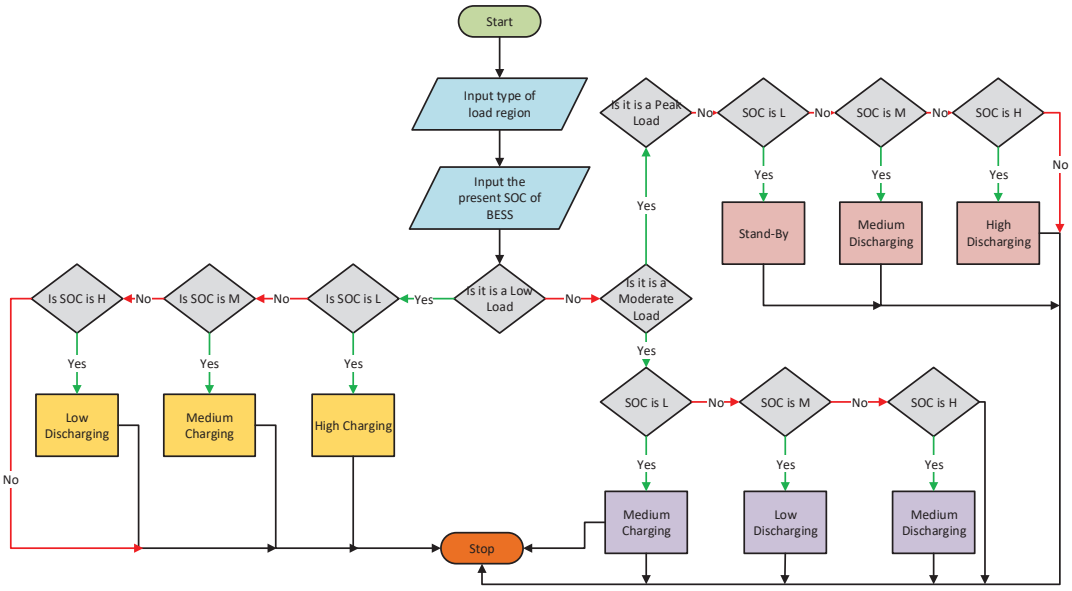

Figure 4.1 State flow diagram of coordinated charging/discharging algorithm of BESS

4.4. Basic Energy Management Strategy (BEMS)

The proposed strategy, OEMS, is compared with the energy management scheme reported in [9]. It aims to minimize total energy drawn from the utility grid i.e., (E_D) as well as extra energy supplied to the utility i.e., (E_S). Basically, it minimizes the summation of E_D and E_S in order to reduce energy exchange between the MG and utility grid. Like in OEMS in this strategy also the active power levels of DEG and BESS are variable and are determined by an optimization algorithm.

4.5. Case study & results

In order to showcase the efficacy of OEMS and GCDM for varying EV penetration level (EVPL), two scenarios are considered, Scenario 1 compares the results of OEMS and BEMS, and Scenario 2 studies the impact of GCDM on OEMS's performance and compares the results with ACM. Moreover, economic analysis is performed for both Scenarios to estimate the MGO's profit. This analysis incorporates the obtained simulation results, energy trading cost, and levelized energy cost of DEG.

4.5.1. Input Data

The community MG designed in Chapter 3 is used in this work. It consists of a 1MW of a solar PV generator, 1.65 MW of wind turbine generator, 2MW of a DEG and additionally a 3.5MWh of BESS that are optimally located at bus numbers 11, 30, 23, and 8 as shown in Fig. 4.2. The variable load profile under this study is estimated based on the IEEE-RTS system [13] and the data associated to load is based on IEEE 33 bus network. The load demand in the peak load region is highest and stands in the range of 94-100% of daily peak load demand and occurs from 4 to 8 pm in a day, whereas the low load region lies between 12 midnight to 6 am, where the load demand ranges from 59-67% of daily peak load. The other time of day is considered as a moderate load region. The solar irradiation and wind speed data for a winter day considered for simulation is taken from the National Research Energy Laboratory [14][15]. The day-ahead hourly energy trading cost from California ISO (CAISO) is considered for the analysis, as shown in Fig. 4.3 [16]. As the DEG considered in this study is a natural gas combined cycle-based generation, therefore its Levelized cost of energy, according to LAZARD ranges from $44/MWh- $73/MWh [17]. Thus, $50/MWh is taken for the analysis.

As buses are segregated based on the nature of the load, i.e., residential, commercial, and industrial, EV stations/parking nodes are also positioned accordingly. Two stations/parking nodes are considered for residential-type load buses located at bus numbers 11 and 19 that are named as RCS. Similarly, one is allotted to industrial-type load buses and one for commercial-type load buses stationed at bus number 30 (ICS) and 23 (CCS), respectively.

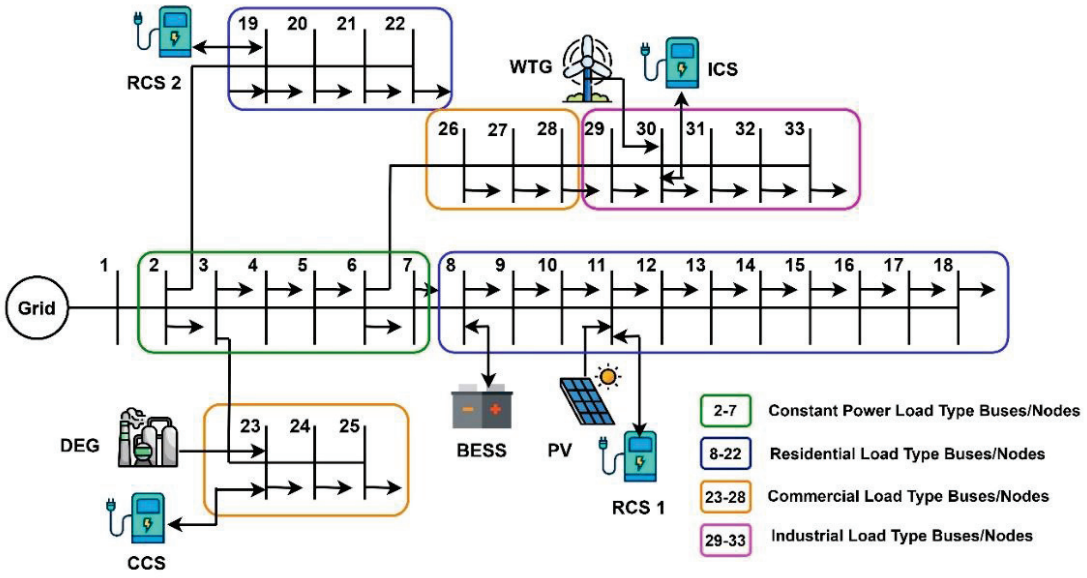

Figure 4.2 Developed microgrid model based on modified IEEE 33 bus

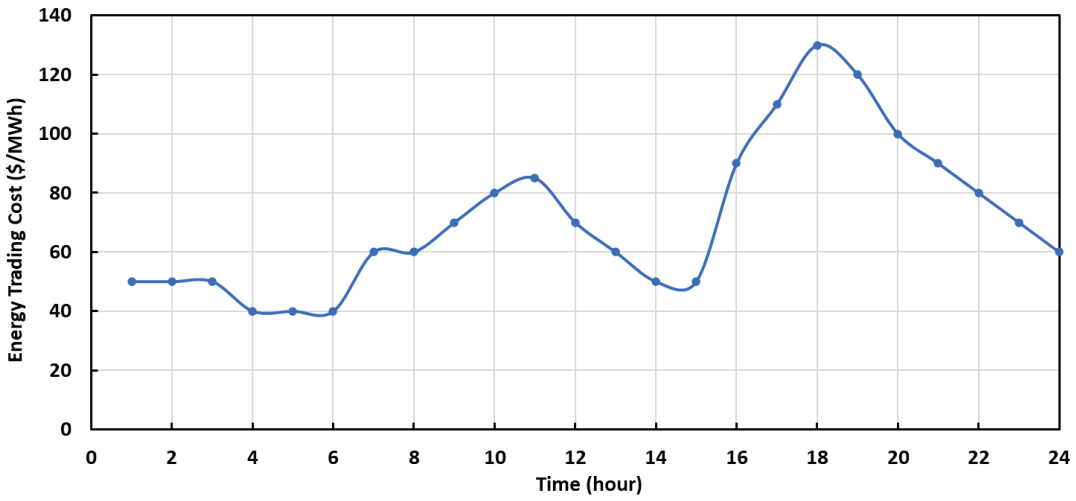

Figure 4.3 Day-ahead energy trading cost from CAISO[16]

The performance of the proposed algorithm is examined at various levels of EVPL. It can be defined as the ratio of the total EV load to the total non-EV load on the MG over 24 hours. Moreover, the generation capacity of DERs that is designed in Chapter 3 is to meet modelled non-EV load in addition to 15% EVPL. The peak active power load (non-EV & EV) on the system is 3715 kW, respectively. Figure 4.4 shows the modelled EV charging load for ACM at different charging stations, considering various EVPL values.

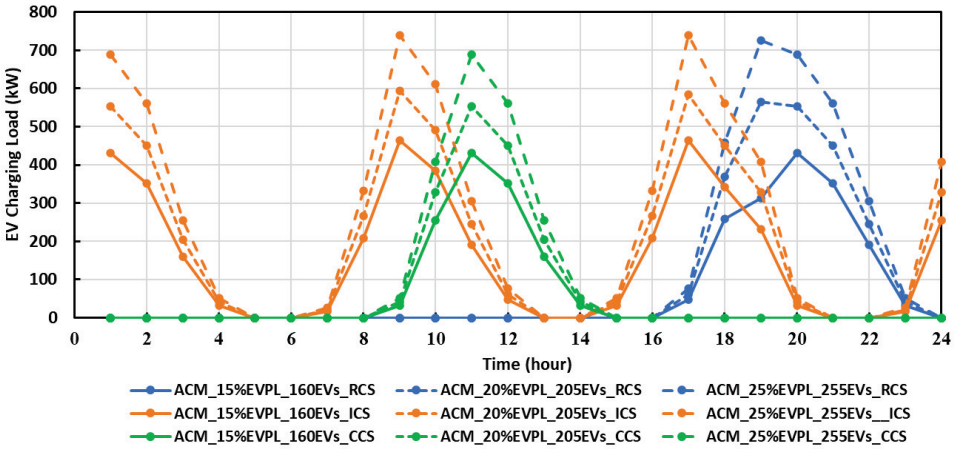

Figure 4.4 EV charging load for ACM case

To have a fair and effective comparison between ACM and GCDM in Scenario 2, they are compared considering an equal number of EVs. Like in the case of ACM, the number of EVs accounting for 15% EVPL, 20% EVPL, and 25% EVPL are 160, 205, and 225 at each charging station. Therefore, under GCDM, the EV load is modelled for 160, 205 and 225 EVs at each charging station. Figure 4.5 shows the modelled EV charging load for ACM and GCDM at different charging stations, considering 160, 205 and 225 EVs at each charging station, respectively.

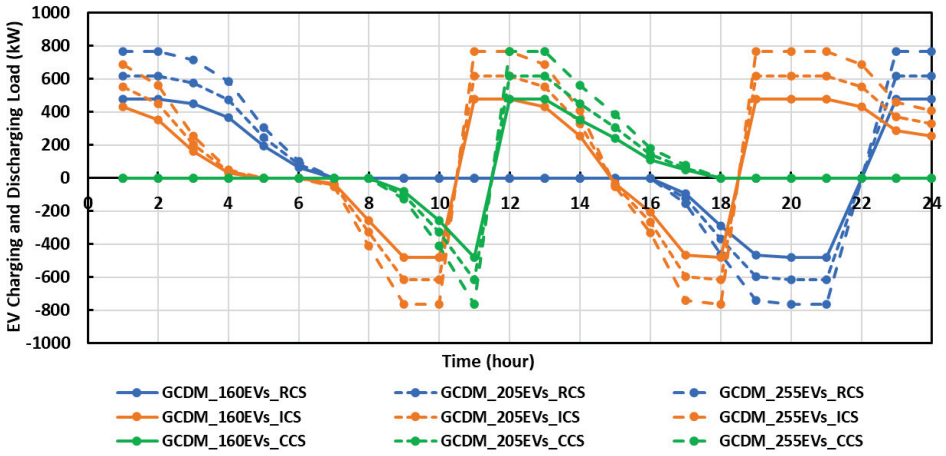

Figure 4.5 EV charging/discharging load for GCDM case

4.5.2. Scenario 1 - Comparison between OEMS and BEMS

This scenario discusses and compares the simulation results obtained from OEMS and BEMS. It is further segregated into three sub-sections. The first sub-section (4.5.2.1)

discusses and compares the simulation results obtained from OEMS and BEMS for the rated system (in which generation capacity is designed according to the total load demand).

The second sub-section (4.5.2.2) analyses the impact of an increase in EVPL values on the performance of OEMS and BEMS. Whereas the third subsection (4.5.2.3) discusses the results of an economic analysis performed for both strategies to estimate the net operation cost of MG.

4.5.2.1. Comparison of OEMS and BEMS for the rated system

This section discusses and compares the simulation results of OEMS and BEMS for the rated system. As mentioned above, the MG system is designed to fulfill the total non-EV load in addition with 15% EVPL. Therefore, 15% EVPL case has been considered as a rated system.

Figure 4.6 shows the obtained schedule, including the total load on the system, PV output, WTG output, the active power exchanged between MG and utility grid, power of DEG and BESS. It can be observed from Fig. 4.6 that in the case of OEMS, utilization of DEG and BESS is increased. As a result, MG optimally feeds power to the utility grid, especially during peak load hours, which benefits the MGO. Moreover, it draws minimum power from the utility grid and reduces its dependency on the utility grid.

Whereas, in the case of BEMS, MG supplies minimum power to the utility grid and draws 10.37 % more power from the utility grid as compared to OEMS. This extra power is drawn to charge the BESS and to compensate for the extra APL that occurred in the system, as the objective function of BEMS does not account for the minimization of TAPL and TVD.

Further Table 4.1 summarizes the comparison between OEMS and BEMS for a day for the rated case, it is evident from Table 4.1 that, OEMS draws 10.37 % less energy as compared to BEMS, and supplies 4195.54 kWh of surplus energy to the utility grid after meeting the total load of MG. It became possible because it maximizes the utilization of DEG and BESS, which is why the total energy supplied/discharged by DEG and BESS in kWh is more for OEMS. It is to be also noted that the total APL and maximum VD

occurred in the system is less for OEMS, which is 690.01 kW and 0.04747, respectively. This is mainly because of the ability of the objective function formulated in OEMS to minimize the APL and VD that occur in the system.

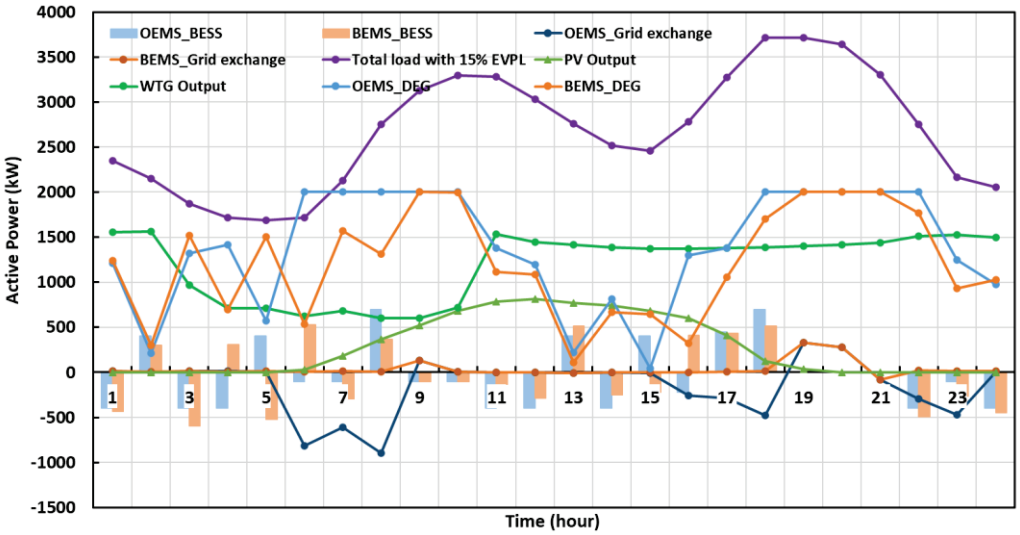

Figure 4.6 Schedule of DERs considering OEMS and BEMS for rated case

Table 4.1 Comparison between OEMS and BEMS for the rated case

Parameters	**OEMS_15%EVPL**	**BEMS_15%EVPL**
Total Energy Supplied to the utility grid ($\boldsymbol{E_s}$) in kWh	4195.54	96.43
Total Energy Drawn from the utility grid ($\boldsymbol{E_D}$) in kWh	813.59	907.73
Total energy generated by DEG in kWh	33281.50	29121.89
Total energy discharged by the BESS in kWh	3405.54	3381.21
Total APL occurred in the system in kW	690.01	710.01
The maximum value of VD occurred in a day	0.04747	0.049392

4.5.2.2. Impact of increase in EVPL on the performance of OEMS and BEMS

To further analyze the performance of OEMS and BEMS with the increase in EVPL, the simulation results are obtained with 20% and 25% EVPL as well. Figures 4.7 and 4.8 represent the active power levels of DEG and BESS, respectively, obtained from OEMS and BEMS considering various values of EVPL. The base active power of ESS is

assumed to be zero. Thus, if BESS's active power is higher than the base load, it is discharging, and if it is lower than the baseload, it indicates that BESS is charging.

It can be observed from Figs. 4.7 and 4.8 that in the case of OEMS, for all the values of EVPL, utilization of DERs (DEG and BESS) reaches a maximum in such a way that MG can meet the total load demand at each instant and optimizes the energy supplied to the utility grid keeping in mind minimum APL and VD. On the other hand, in the case of BEMS, the DERs output varies just to meet MG's load demand.

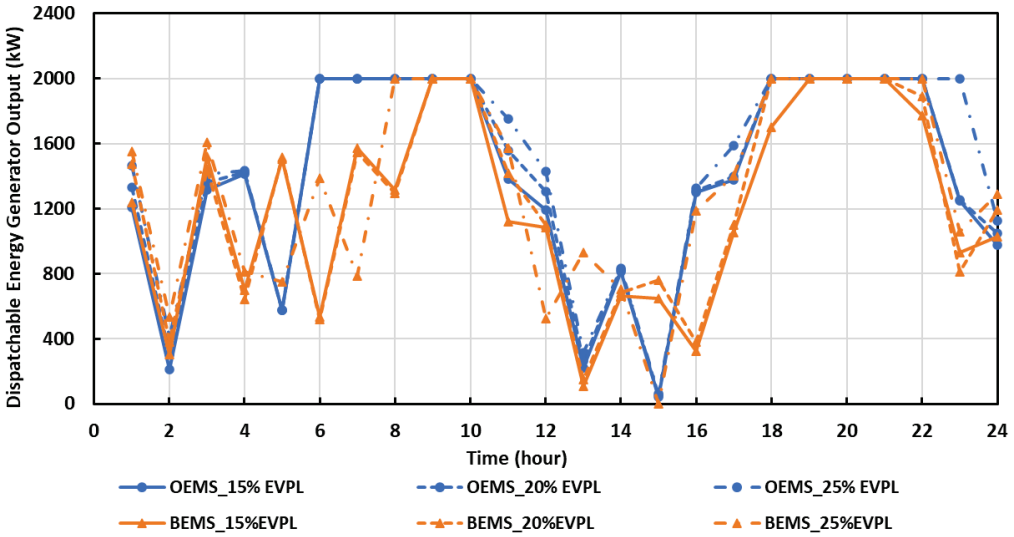

Figure 4.7 Dispatchable energy generator output considering OEMS and BEMS with various EVPL values

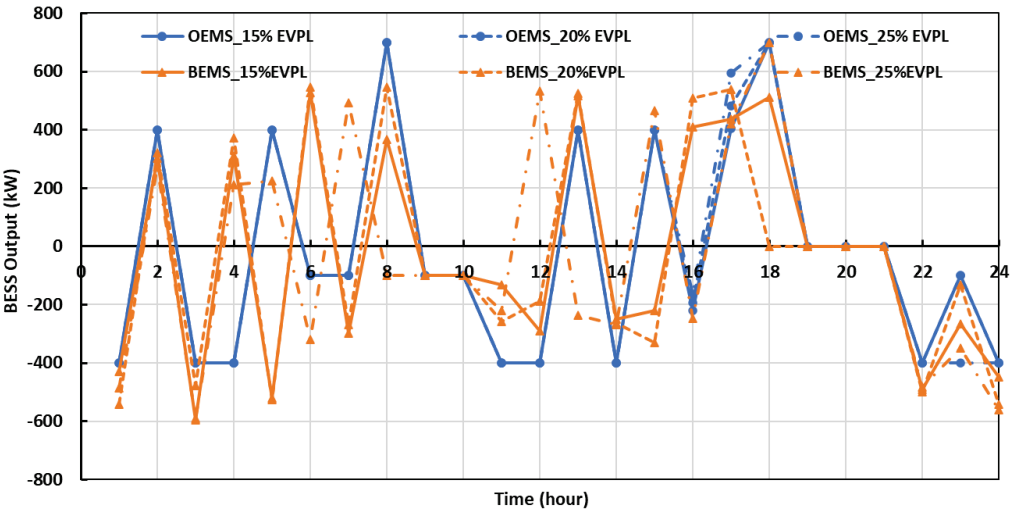

Figure 4.8 Active power output of BESS considering OEMS and BEMS with various EVPL values

The active power exchanged between MG and utility grid considering OEMS & BEMS with various EVPL values is shown in Fig. 4.9. The increase in EVPL in the MG denotes that the total demand on the system is increasing, but the maximum generation capacity of MG is the same. Therefore, it can be observed from Fig. 4.9 that in the case of OEMS, with the increase in EVPL, the total active power supplied to the utility grid decreases.

Further, the total active power drawn from the utility grid is increasing for both strategies with the increase in EVPL. However, it is still more for BEMS than OEMS.

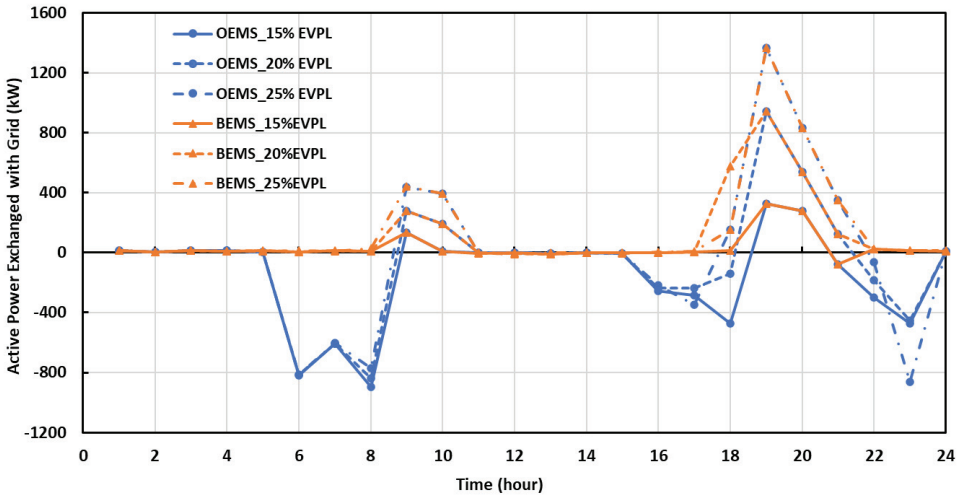

Figure 4.9 Active power exchanged between MG and utility grid considering OEMS and BEMS with various EVPL

Figures 4.10 and 4.11 show the active power losses and maximum voltage deviation that occurred in the system considering OEMS & BEMS with various EVPL values, respectively. It can be noted from Figs. 4.10 and 4.11, for most of the time instant, the TAPL & maximum VD is less for OEMS as compared to BEMS. It is because OEMS considers the minimization of TAPL along with VD in its objective function. Further, due to the increment in EVPL, TAPL and maximum VD increase significantly during peak load for both strategies. Also, it is observed from Fig. 4.11 that in the case of OEMS, the maximum VD remains under/closer to the limit for all the EVPL.

Figure 4.12 shows the SOC level of BESS for OEMS and BEMS with various EVPL values. The initially assumed SOC is 50%. It is clear from Fig. 4.12 that in the case of OEMS, BESS is getting charged during off-peak hours and discharging more, especially

during peak hours, which facilitates its maximum utilization and helps in the efficient operation of MG.

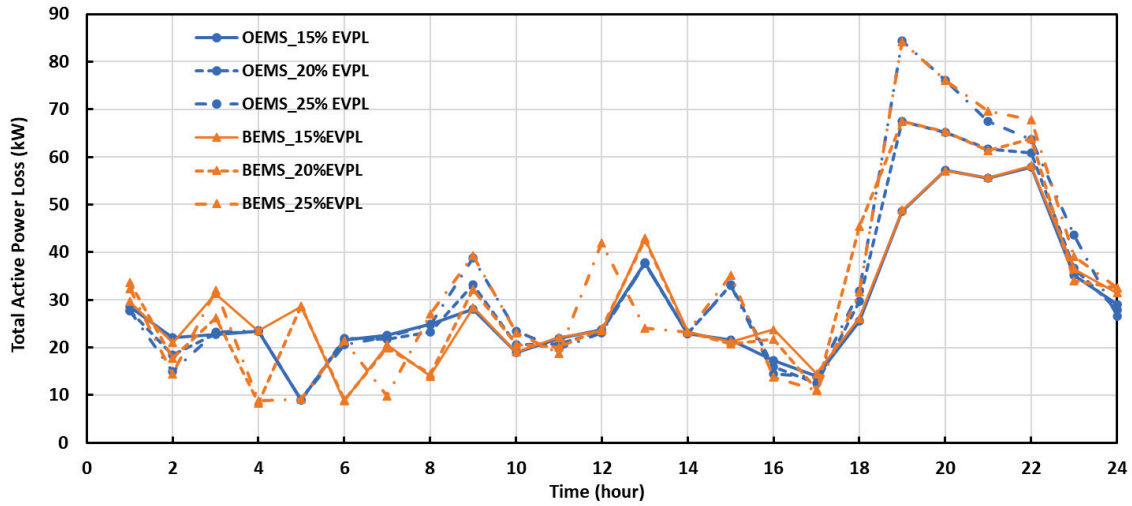

Figure 4.10 Total active power losses of MG considering OEMS and BEMS with different EVPL

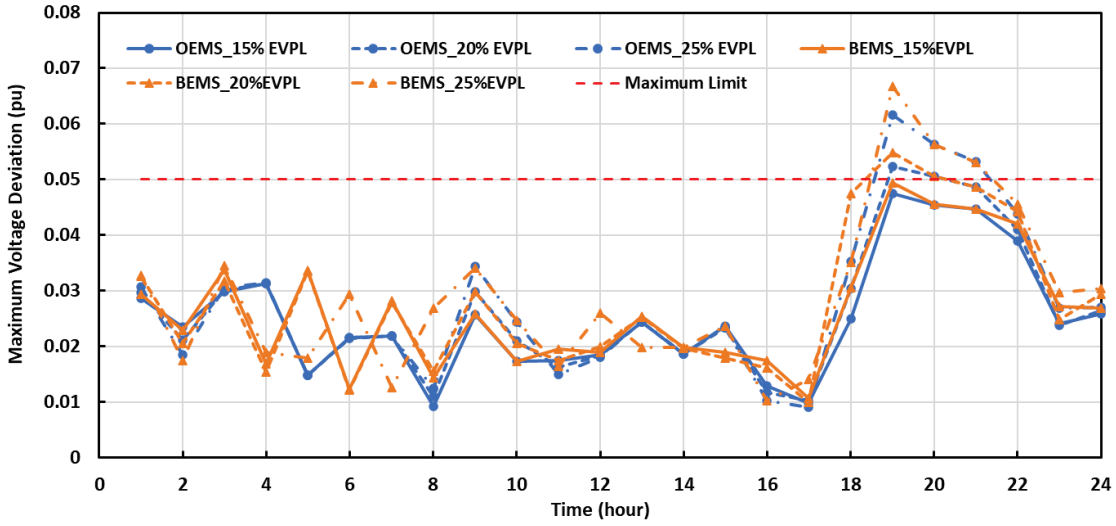

Figure 4.11 Maximum voltage deviation considering OEMS and BEMS with different EVPL

Table 4.2 shows the comparison of OEMS and BEMS with the increasing EVPL. It can be observed from Table 4.2 that as EVPL increases, the energy supplied to the utility grid decreases and energy drawn from the grid increases for both strategies. Also, the energy generated/ discharged by the DEG & BESS, total APL and maximum value of VD is increased.

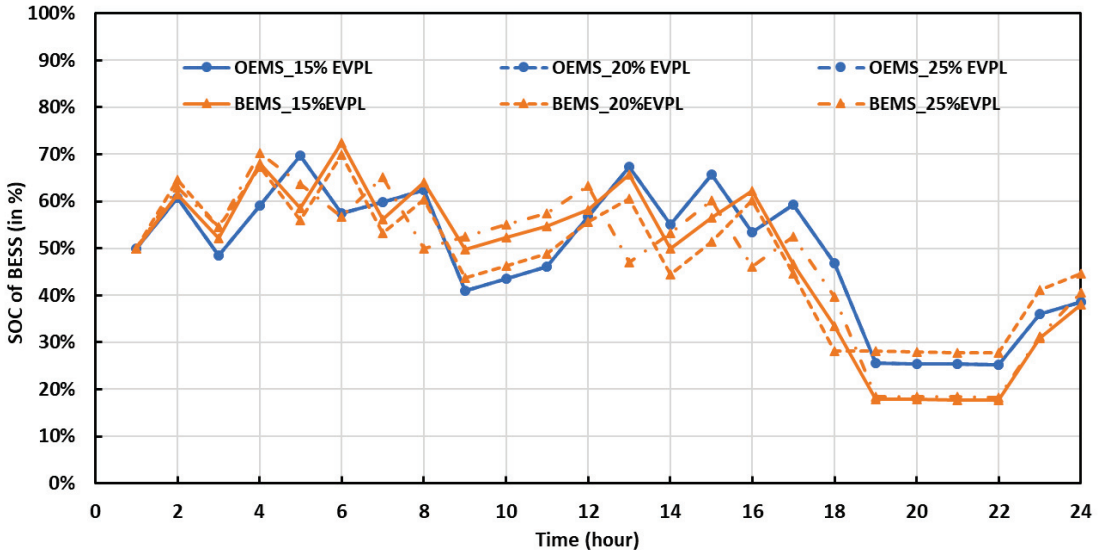

Figure 4.12 SOC level of BESS considering OEMS and BEMS with various EVPL

Table 4.2 Comparison of OEMS and BEMS with the increasing EVPL

Parameters	**OEMS_ 15% EVPL**	**OEMS_ 20% EVPL**	**OEMS_ 25% EVPL**	**BEMS_ 15% EVPL**	**BEMS_ 20% EVPL**	**BEMS_ 25% EVPL**
Total Energy Supplied to the utility grid ($\boldsymbol{E_S}$) in kWh	4195.54	3528.10	3489.82	96.43	20.98	15.77
Total Energy Drawn from the utility grid ($\boldsymbol{E_D}$) in kWh	813.59	2143.17	3601.16	907.73	2795.70	3707.97
Total energy generated by DEG in kWh	33281.5	34011.7	35728.3	29121.9	30309.9	32107.5
Total energy discharged by the BESS in kWh	3405.54	3482.46	3594.27	3381.21	3358.55	3319.16
Total APL occurred in the system in kW	690.01	738.32	786.6	710.01	744.26	792.55
The maximum value of VD occurred in a day	0.04747	0.05227	0.06167	0.04939	0.05487	0.06673

4.5.2.3. Economic analysis of OEMS and BEMS

To further examine the performance of OEMS and BEMS, economic analysis is performed using obtained simulation results, energy trading cost of grid, and Levelized cost of energy of considered DEG. This analysis estimates the net operating cost of MG, and by comparing these costs, a more profitable strategy for MGO can be determined.

Table 4.3 presents the estimated net operating cost of OEMS and BEMS, along with the increase in MGO's profit due to OEMS. It can be noted from Table 4.3, (a) for all the considered EVPL values, net operating cost is less in the case of OEMS as compared to BEMS, (b) with the increment of EVPL, the percentage increase in MGO's profit is reducing. It is mainly due to the reduction in total energy supplied to the utility grid with the increase in EV load on the MG.

Lastly, from the comparison Tables 4.1, 4.2 and 4.3, it can be concluded that OEMS is superior to BEMS, as it facilitates the efficient & stable operation of MG and simultaneously provides a cost-benefit to the MGO.

Table 4.3 Estimated net operating cost and increase in MGO's profit due to OEMS

Cases	**15% EVPL**	**20% EVPL**	**25% EVPL**
Net operating cost with OEMS	\$1441	\$1685	\$1912
Net operating cost with BEMS	\$1536	\$1787	\$1976
Percentage increase in MGO's profit due to OEMS w.r.t BEMS	6.15%	5.71%	3.23%

4.5.3. Scenario 2 – Impact of GCDM on OEMS performance

In order to improve the efficiency of OEMS and to perform peak load management, GCDM operation of PHEVs is introduced in the system. This section analyses and compares the simulation results obtained from OEMS with ACM and GCDM. The impact of GCDM on MG's total demand is visible from Fig. 4.13. It shifts the peak load to the off-peak load region as a result, peak load management in MG can be achieved.

Figure 4.14 shows the active power exchanged between MG and utility grid considering ACM & GCDM with various EVPL. It is observed from Fig. 4.14 that due to GCDM, the energy supplied to the utility grid is increased mainly during peak load hours, and energy drawn from the utility grid is shifted to the low load period.

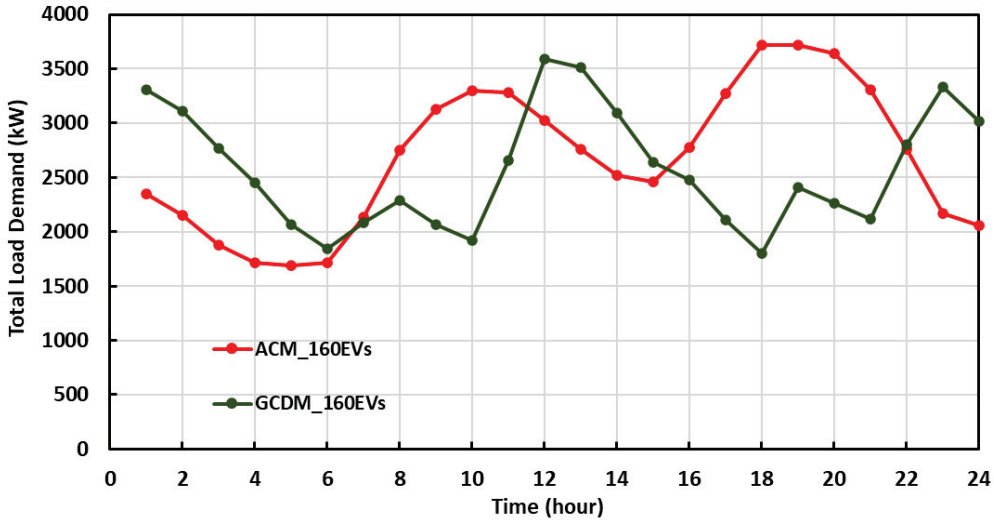

Figure 4.13 Impact of GCDM on MG's total load demand

This is beneficial for MG as it is performing peak load management. Moreover, it seems to be a profitable solution for the grid operator as well because it improves the ancillary service support of MG to the grid.

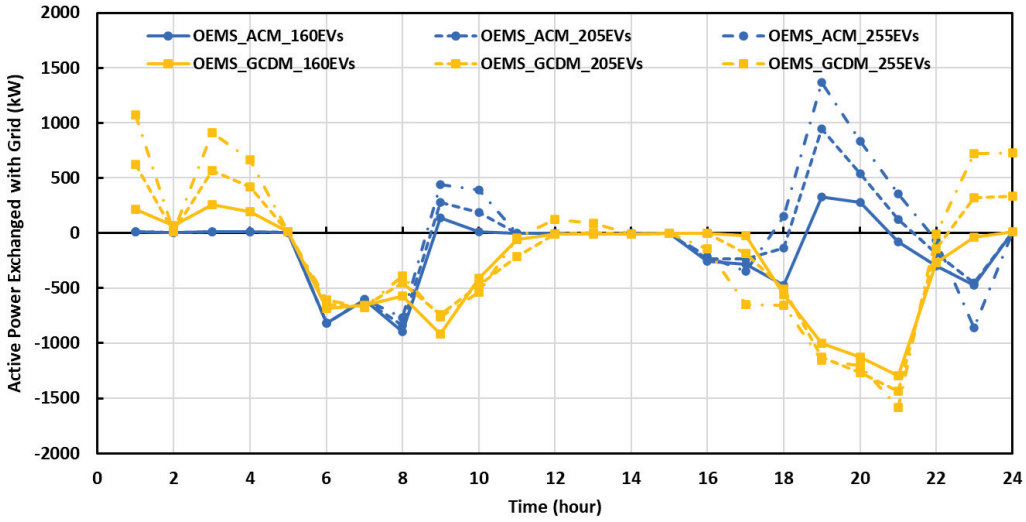

Figure 4.14 Active power exchanged between MG and utility grid considering ACM & GCDM with various EVPL

To investigate and estimate the increased performance of OEMS due to the incorporation of GCDM, economic analysis has been performed in a similar way as discussed in Section 4.5.2.3. Table 4.4 shows the estimated net operating cost of MG and the percentage increase in MGO's profit from OEMS with GCDM.

Table 4.4 Estimated net operating cost and increase in MGO's profit due to GCDM

Cases	15% EVPL	20% EVPL	25% EVPL
Net operating cost with OEMS_ACM	$1441	$1685	$1912
Net operating cost with OEMS_GCDM	$1103	$1173	$1236
Percentage increase in MGO's profit due to GCDM	23.44%	30.37%	35.34%

It is evident from Table 4.4 that 1) MGO's profit has been increased due to the incorporation of GCDM in OEMS for all the EVPLs, and 2) an increase in EVPL leads to an increase in MGO's profit. This is because of the increase in total energy supplied to the utility grid (mainly during peak load hours) with the increased EVPL.

4.6. Conclusion

This chapter proposed an OEMS for a grid-connected community MG that maximizes the utilization of DERs, increases the MGO profit by promoting energy trading between MG and the utility grid, and reduces the dependency of MG on the utility grid. The formulated objective function aims at minimization of energy drawn from the utility grid and optimize the energy supplied to the utility grid in such a way that TAPL and TVD of MG are minimal. In order to achieve maximum utilization of BESS, a coordinated charging/ discharging algorithm has been developed and incorporated in the OEMS. Further, to evaluate the effectiveness of the proposed algorithm the obtained simulation results are compared with the previously reported strategy. The results obtained from the simulation and economic analysis reveal that the OEMS is superior to the previous reported strategy, as it facilitates the efficient & stable operation of MG and simultaneously provides cost-benefit to the MGO. It has decreased the energy drawn from the grid by 10.37% and increased MGO's profit in the range of 3.23-6.15% (depending on EVPL) in comparison with the previously reported strategy.

The efficacy of OEMS is further improved, and peak load management for MG is achieved by incorporating a GCDM of EV. The superiority of GCDM over ACM is explained by the obtained results. It shows that in the case of OEMS with GCDM, the MGO's profit is increased to 23.44%, 30.37 %, and 35.34% for 15% EVPL, 20% EVPL,

and 25% EVPL, respectively, in comparison from OEMS with ACM. Lastly, OEMS with GCDM can be considered the most profitable solution for MG as well as the utility grid in terms of economical, stable, and efficient operation.

Further, in the next chapter 5 discusses the design and deployment of the other type of MG, i.e., building MG. Moreover, using the data from the developed system, an improved EMS is formulated to achieve optimal and efficient operation.

Bibliography

[1] M. R. Sandgani and S. Sirouspour, "Coordinated Optimal Dispatch of Energy Storage in a Network of Grid-Connected Microgrids," *IEEE Trans. Sustain. Energy*, vol. 8, no. 3, pp. 1166–1176, 2017, doi: 10.1109/TSTE.2017.2664666.

[2] M. O. Badawy and Y. Sozer, "Power Flow Management of a Grid Tied PV-Battery System for Electric Vehicles Charging," *IEEE Trans. Ind. Appl.*, vol. 53, no. 2, pp. 1347–1357, 2017, doi: 10.1109/TIA.2016.2633526.

[3] M. S. ElNozahy, T. K. Abdel-Galil, and M. M. A. Salama, "Probabilistic ESS sizing and scheduling for improved integration of PHEVs and PV systems in residential distribution systems," *Electr. Power Syst. Res.*, vol. 125, no. May 2019, pp. 55–66, 2015, doi: 10.1016/j.epsr.2015.03.029.

[4] A. S. A. Awad, T. H. M. El-Fouly, and M. M. A. Salama, "Optimal distributed generation allocation and load shedding for improving distribution system reliability," *Electr. Power Components Syst.*, vol. 42, no. 6, pp. 576–584, 2014, doi: 10.1080/15325008.2014.880962.

[5] S. J. Hossain, B. D. Biswas, R. Bhattarai, M. Ahmed, S. Abdelrazek, and S. Kamalasadan, "Operational Value-Based Energy Storage Management for Photovoltaic (PV) Integrated Active Power Distribution Systems," *IEEE Trans. Ind. Appl.*, vol. 55, no. 5, pp. 5320–5330, 2019, doi: 10.1109/TIA.2019.2920229.

[6] H. R. Baghaee, M. Mirsalim, G. B. Gharehpetian, and H. A. Talebi, "Unbalanced harmonic power sharing and voltage compensation of microgrids using radial basis function neural network-based harmonic power-flow calculations for distributed and decentralised control structures," *IET Gener. Transm. Distrib.*, vol. 12, no. 7, pp. 1518–1530, 2018, doi: 10.1049/iet-gtd.2016.1277.

[7] N. Saxena, I. Hussain, B. Singh, and A. L. Vyas, "Implementation of a Grid-Integrated PV-Battery System for Residential and Electrical Vehicle Applications," *IEEE Trans. Ind. Electron.*, vol. 65, no. 8, pp. 6592–6601, 2018, doi: 10.1109/TIE.2017.2739712.

[8] M. van der Kam and W. van Sark, "Smart charging of electric vehicles with photovoltaic power and vehicle-to-grid technology in a microgrid; a case study," *Appl. Energy*, vol. 152, pp. 20–30, 2015, doi: 10.1016/j.apenergy.2015.04.092.

[9] G. R. Chandra Mouli, P. Bauer, and M. Zeman, "System design for a solar powered electric vehicle charging station for workplaces," *Appl. Energy*, vol. 168, no. 2016, pp. 434–443, 2016, doi: 10.1016/j.apenergy.2016.01.110.

[10] V. V. S. N. Murty and A. Kumar, "Multi-objective energy management in microgrids with hybrid energy sources and battery energy storage systems," *Prot. Control Mod. Power Syst.*, vol. 5, no. 1, pp. 1–20, 2020, doi: 10.1186/s41601-019-0147-z.

[11] T. Rawat and K. R. Niazi, "Impact of EV charging/discharging strategies on the optimal operation of islanded microgrid," *J. Eng.*, vol. 2019, no. 18, pp. 4819–4823, 2019, doi: 10.1049/joe.2018.9335.

[12] H. Liu, Y. Ji, H. Zhuang, and H. Wu, "Multi-objective dynamic economic dispatch of microgrid systems including vehicle-to-grid," *Energies*, vol. 8, no. 5, pp. 4476–4495, 2015, doi: 10.3390/en8054476.

[13] C. Grigg *et al.*, "The IEEE Reliability Test System-1996. A report prepared by the Reliability Test System Task Force of the Application of Probability Methods Subcommittee," *IEEE Trans. Power Syst.*, vol. 14, no. 3, pp. 1010–1020, 1999, doi: 10.1109/59.780914.

[14] National Renewable Energy Laboratory (NREL), "RE Data Explorer Colombia," no. Philibert 2011, pp. 1–6, 2020.

[15] "Index @ Www.Nrel.Gov." [Online]. Available: https://www.nrel.gov/.

[16] "191013825ea760bdd31f35a7d402c44e1c1a742d @ www.eia.gov." [Online]. Available: https://www.eia.gov/electricity/monthly/.

[17] "lcoe2020 @ www.lazard.com." [Online]. Available: https://www.lazard.com/perspective/lcoe2020.

Chapter 5

Designing of a Prosumer Building MG and Achieving its Optimal Operation by Considering BESS Degradation Model

5.1. Introduction

Due to the increased large-scale RERs installation, the need for energy storage technology has significantly increased [1][2]. Therefore, energy storage systems are becoming critical technological components of today's power grid infrastructure. Recently, BESSs have been deployed for a variety of grid applications, ranging from their installation at the generation site to the end-user site [3]. Their abilities, such as fast response, storage and provision of energy when needed (time shifting), and adaptable installation capabilities due to the modularization of their cell structure, have made them more popular and advantageous [4][5]. Because of the mentioned features, BESSs can have a wide range of power and energy capabilities. Hence, they balance the uncertain nature of renewable energy sources, especially in MG scenarios.

The lifespan of BESS is mainly determined by various components, such as depth of discharge, charge-discharge cycles, and environmental conditions [6]. For any of the BESS applications, maximizing the depth of discharge reduces the energy storage capacity and thus increases the number of cycles. Further, the degradation factor of BESS mainly depends on its energy exchange, which in turn diminishes battery capacity and is termed as capacity fading [7]. Although the ageing mechanism of batteries is complex, for optimal scheduling, parameters like the DOD and charge/discharge cycles have the

most significant influence on degradation. The number of cycles of BESS is defined as the maximum number of charge/discharge cycles allowed to a BESS. The BESS is considered thoroughly degraded when its number of cycles reaches its maximum value or its energy capacity is reduced to a predetermined level (for example, 80% of rated capacity). The maximum number of cycles for a particular battery type is determined from the experimental data [8]. Therefore, it varies depending on its manufacturer.

Aside from applications of BESSs in large and interconnected power systems, many small-scale systems, including households, buildings, localities, or even factories, have recently employed their BESSs [9]–[11]. These buildings are major electricity consumers and are incentivized to incorporate renewable energy generation and BESSs into their energy system to create a new class of flexible and effective prosumers. Moreover, building prosumers can attain substantial economic profit if they optimally manage their energy production, consumption, and the energy they exchange with the utility grid. However, because of the high capital investment of the BESS and the limited amount of available energy due to its SOC, there is a need for an effective energy management strategy for prosumer buildings that aim at economical and efficient operation of MGs. The economic operation leads to the minimization of the operating cost of MG, and efficient operation deals with improving the active life span of BESS.

After a through literature review presented in Chapter 2, it is noted that previous studies, either do not focus on reducing battery degradation (termed as conventional energy management strategy (CEMS)) or use piece-wise linear approximation to linearise the life cycle function of BESS, and ignore calendar ageing (termed existing energy management strategy (EEMS)). Therefore, these studies fail to depict the practical degradation and estimation of the life span of BESS.

In this regard, there is a need to design an EMS for an MG that incorporates a realistic BESS life span estimation model based on static and dynamic degradation, and is independent of linear approximation of life cycle function. Further, it should also consider the generation and load uncertainties, and results in lower operation cost of MG and improved the operating life span of BESS.

In view of the limitations of previously reported EMSs and identified research limitations, an attempt has been made through this work to address these shortcomings. The major contributions of this chapter are as follows:

- A non-linear battery degradation model considering calendar and cyclic ageing in terms of static and dynamic degradation factors, respectively, is used to estimate the practical operating life span of BESS.
- An improved energy management strategy (IEMS) is developed to increase the profit of a prosumer building and improve the operating life span of BESS. It is achieved by minimizing the formulated cost objective function of MG as per the proposed rule-based algorithm (RBA). The proposed RBA effectively utilizes the BESS and power grid based on solar PV power, load demand power, type of load demand (off-peak load/peak load), and SOC of the BESS.

5.2. Designing of a building MG

This section details the design methodology of a prosumer building. This design methodology includes selected site location analysis as per the availability of the irradiance, calculation of required solar power capacity to meet the load demand of the system, selection of solar PV panels and their number on the basis of calculated solar power capacity and available area, selection of inverter capacity, determination of BESS capacity. A detailed description of this design methodology is as follows.

5.2.1. Selection of site

A building located at BITS, Pilani campus is selected to install solar PV and BESS based grid connected MG and build a prosumer building. It is selected on several bases, such as available irradiance, ambient temperature, wind speed, dust on the module, and humidity. The building is located in Pilani which is situated in the northern part of India in the Jhunjhunu district of Rajasthan, which is a semi-arid region. Its latitude is 28.3802^{o} N and has a longitude of 75.6092^{o} E. After a thorough study of its weather pattern, it was found that Pilani receives sufficient solar irradiance (around 600W/m^2) for more than 300 days and has an average sunshine of 6 hours/day [12]. This signifies that this building's

location has a high potential for solar PV electricity generation and is suitable to install solar PV based MG.

5.2.2. Calculation of required solar power capacity

In order to calculate required solar PV capacity, firstly, the maximum load demand and daily average energy consumption of a building should be known, which is found out to be 25 kW and 150 kWh, respectively, from the previous year's data (2015-2021). Further, it is necessary to know the operating factor of that location, inverter, and BESS efficiency. These factors are crucial for designing a MG as they significantly affect the energy output of the solar PV system. The operating factor of any location mainly depends upon temperature, wind speed, humidity, dust on the module, solar irradiance, and sunshine hours of the day. It ranges between 0.60 to 0.90, implying that the output power is 60 to 90% of the rated output power. In this study, the operating factor, inverter efficiency, and BESS efficiency, DC link voltage are considered as 0.75, 0.9, 0.9, and 360V, respectively. The equations (5.1-5.5) show the calculation of the required solar power capacity.

Let's assume the total solar power capacity be 'P' kW

The actual power output of PV panel = Total solar power capacity $*$ Operating factor

$$= P * 0.75 \tag{5.1}$$

The combined efficiency of the inverter and BESS will be calculated as:

$$\text{combined efficiency} = \text{Inverter efficiency} * \text{BESS efficiency}$$

$$\text{combined efficiency} = 0.9 * 0.9 = 0.81 = 81\% \tag{5.2}$$

Power available for load (When both inverter and BESS are operating) =

$$P * 0.75 * 0.81 \tag{5.3}$$

$$\text{Maximum load demand of the building} = 25 \text{ kW} \tag{5.4}$$

Now, the power available for load should be equal to the maximum load demand of the building.

$$P = \frac{25}{0.75*0.81} = 41.152 \text{ kW} \quad (5.5)$$

The total solar power capacity should be 41.152 kW to meet the maximum load demand of the building.

5.2.3. Selection of solar PV panels and estimation of their number

The building has a limited rooftop area of 234.9 m^2. Therefore, to produce maximum PV power with this limited area, a maximum rated power panel of 535Wp (available in the market) has been selected for designing the MG. A detailed market survey of available 535Wp-rated solar PV panels was conducted. From the thorough comparative study of various PV panel manufacturers, it was found that Longi Green Energy Technology Co. Ltd. is providing the economical solar PV panel (rated 535Wp) with almost similar efficiency and panel dimensions. Thus, the solar PV panel of model number LR5-72HPH-535M (rated capacity 535Wp) of Longi Green Energy Technology Co. Ltd. has been selected. The details of the selected PV panel are discussed in Table 5.1. The number of PV panels mainly depends on two factors, i.e., total solar power capacity and available rooftop area. Hence, keeping these two constraints in mind, an optimized number of PV panels is determined, i.e., 77.

Table 5.1 Details of selected solar PV panel

Parameter	**Value**
Maximum power	535 W
Open circuit voltage	49.35 V
Short circuit current	13.78 A
Voltage at maximum power	41.5 V
Current at maximum power	12.9 A
Module efficiency	20.9 %
Temperature coefficient of short circuit current	+0.048%/^{o}C
Temperature coefficient of open circuit voltage	-0.270%/^{o}C
Temperature coefficient of maximum power	-0.350%/^{o}C
Dimensions	2256*1133*35 mm
Area	2.55m^2

Figure 5.1 shows the optimized arrangement of these 77 solar PV panels on the rooftop of a building. Among these, nine panels are placed horizontally in a row; likewise, eight rows are formed, and at the end, five panels are placed separately to form a 9th row. A solar panel covers a length of 3.19 m distance by considering its own shadow. The shadow distance is 1.011 m. The total covered area by solar PV panels is 267.98 m^2, which is more than the available rooftop area; therefore, it can be stated that the PV panels are placed optimally to cover the rooftop area of building to its maximum limit.

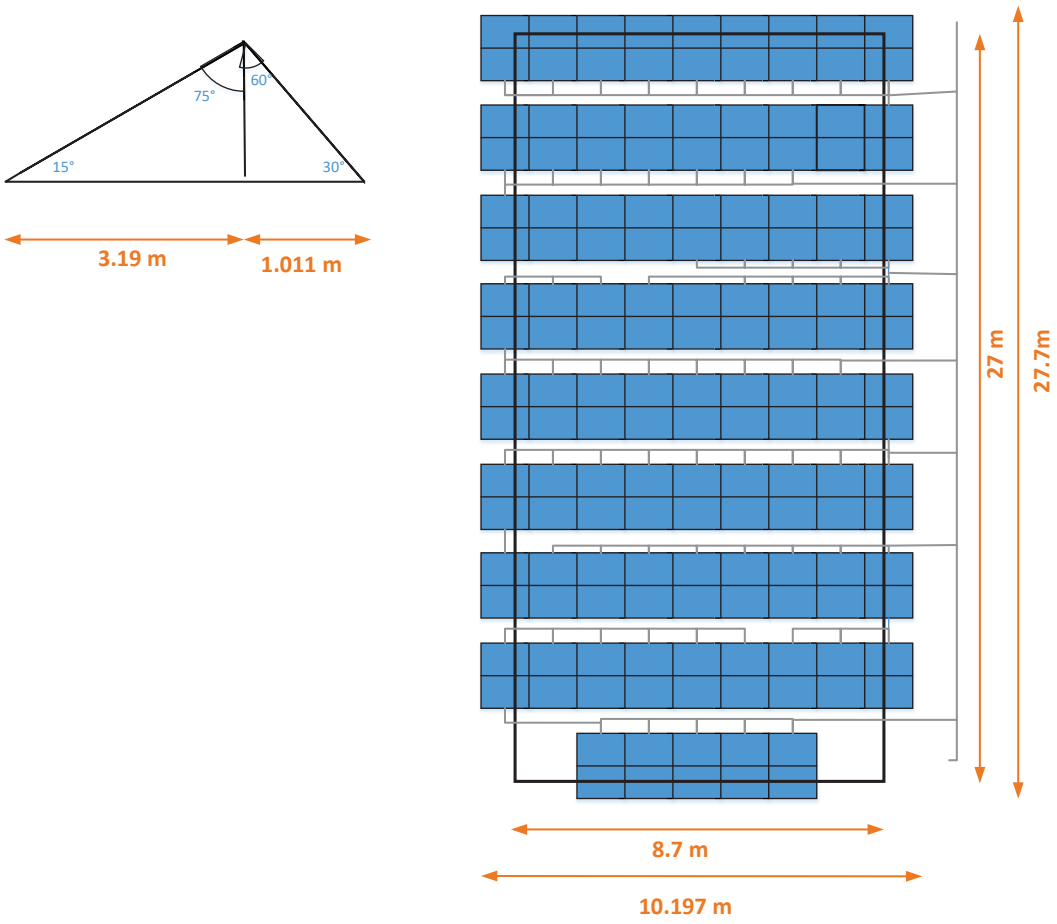

Figure 5.1 Building rooftop with layout of solar PV panels

5.2.4. Selection of inverter capacity

The inverter's capacity is decided based on the maximum connected load of the building, which is approximately 30 kW. In order to compensate for the losses of the

inverter, its rating must be chosen 1.25-1.3 times the maximum connected load of the building. The rating of the inverter is calculated using (5.6-5.7).

$$\text{Rating of inverter} = \text{maximum connected load} * 1.3 \tag{5.6}$$

$$\text{Rating of inverter} = 30 * 1.3 = 39\ \text{kVA} \tag{5.7}$$

A 40 kVA inverter is used, considering the availability of inverters in the market. The inverter is a multi-mode hybrid inverter. Table 5.2 represents the parameters of the inverter.

Table 5.2 Details of selected hybrid inverter

Parameter	**Value**
DC input voltage range	360 to 460 V
Self-consumption	<4%
Output voltage (Inverter mode)	415V AC ± 2%
Voltage regulation	± 2%
Total harmonic distortion (THD)	≤ 3% at linear load
Inverter efficiency (%)	≥ 90%
Modes available	Hybrid, Grid export, Standalone

5.2.5. PV array connections

An array is formed from the 77 solar PV panels. In order to meet up the inverter's input DC link voltage, 11 panels are connected horizontally and vertically to make a series string. Likewise, such seven-series strings are formed. Further, these seven series strings are connected in parallel in order to keep the current below the rated value at the input side of the inverter.

5.2.6. Determination of BESS capacity

The BESS is designed only to meet essential loads of the building. The essential loads include lighting loads, fans, and computer systems. They account for almost 7 kW of load, and their energy consumption is approximately 56 kWh in a day. The lead acid battery is selected as it is more economical than other batteries.

In order to integrate BESS with the inverter, the BESS must be designed and configured to match the input voltage range of the inverter. It is necessary to regulate the charging and discharging of the batteries according to the system requirements. The battery efficiency has been considered to be 90%.

The battery ampere-hour (Ah) is calculated by (5.8-5.9).

$$\text{Battery Ah} = \frac{\text{selected energy consumption by battery}}{\text{Efficiency}*\text{DOD}*\text{voltage}} \tag{5.8}$$

$$\text{Battery Ah} = \frac{56000}{0.9*0.8*360} = 216.04\ Ah \tag{5.9}$$

A detailed market survey of available batteries was conducted. Thus, the lead acid battery of model STT22500 (rated capacity 12V, 225 Ah) of Solance industries has been selected for designing the BESS. Such 30 batteries are connected in series to meet the input voltage of the inverter. Hence, the rating of the BESS becomes 360V, 225Ah.

5.3. Line diagram and glimpses of the developed and deployed MG

Figure 5.2 shows the schematic of prosumer building with AC-DC hybrid MG structure. Further pictures of solar PV and BESS-based AC-DC hybrid MG installed at a building is shown in Fig. 5.3.

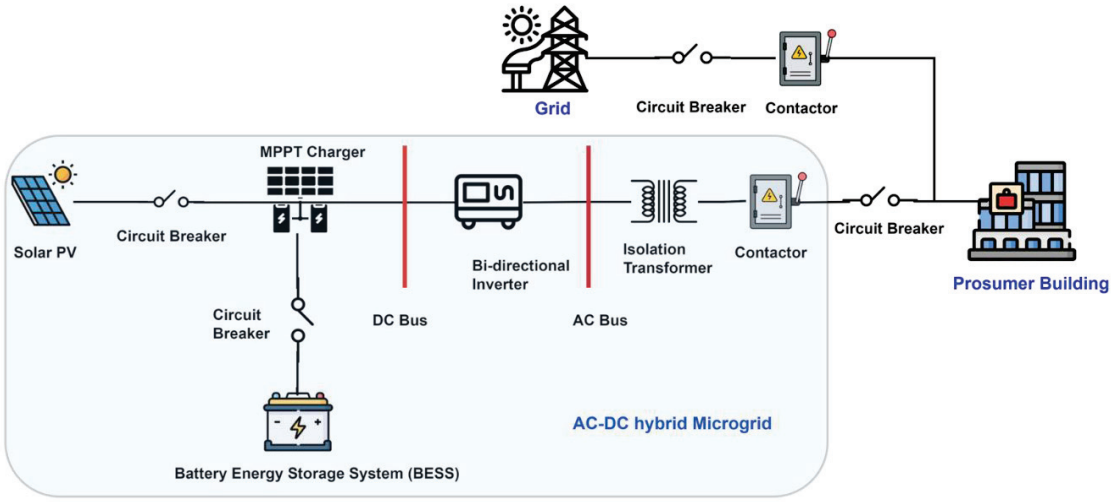

Figure 5.2 Schematic of prosumer building with AC-DC hybrid MG structure

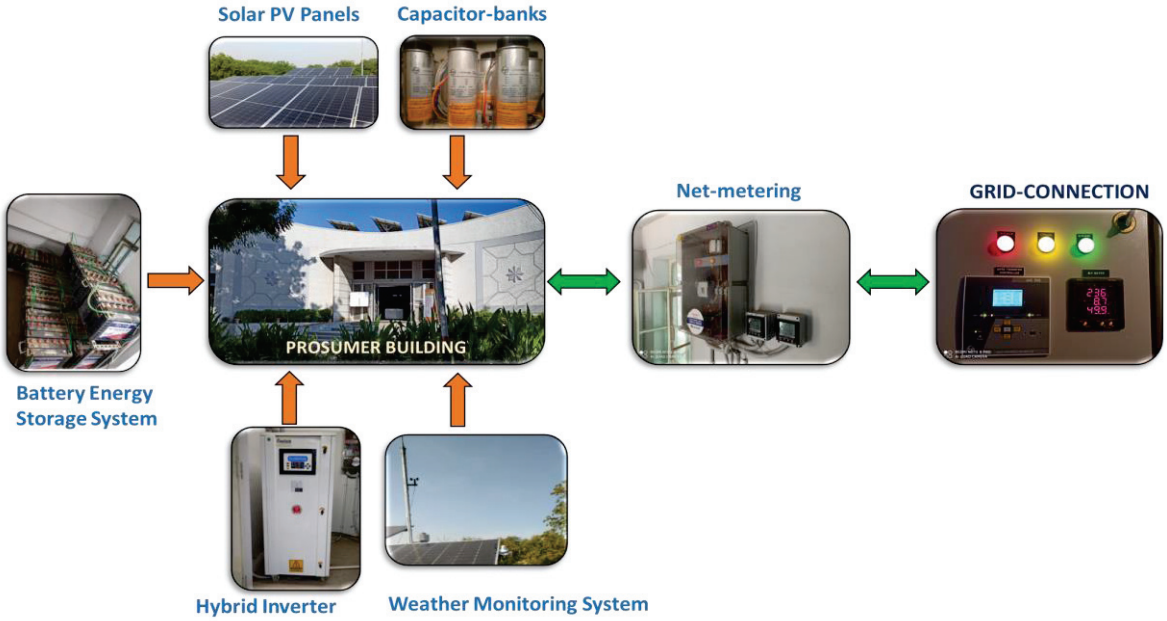

Figure 5.3 Solar PV and BESS-based AC-DC hybrid MG installed at a building

5.4. Mathematical modelling of MG components

The mathematical modelling of solar PV system and BESS is similar as discussed in Chapter 3 and 4, respectively. Further, the modeling of electrical load demand and grid connection is discussed below.

5.4.1. Load demand of the prosumer building

The load demand of the building is composed of two components, i.e., flexible and non-flexible load. The flexible load demand can be shifted to any time slot. The load demand can be represented by (5.10).

$$P_L^t = P_{FL}^t + P_{NFL}^t \quad \forall t \in \mathcal{T} \tag{5.10}$$

Where P_L^t is the load demand power of the prosumer building. P_{FL}^t and P_{NFL}^t are the flexible and non-flexible load power. The load demand of the building varies as per the constraint in (5.11).

$$P_L^{\acute{m}} \leq P_L^t \leq P_L^{\acute{M}} \tag{5.11}$$

Where $P_L^{\acute{m}}$ and $P_L^{\acute{M}}$ are the minimum and maximum limits of load demand.

5.4.2. Grid power modeling

The grid power (P_G^t) flow is bidirectional and is expressed by (5.12). The grid power acts as a source for the MG to satisfy the load power and as a sink when there is excess renewable generation.

$$P_G^t = \begin{cases} > 0 \;\; Grid\ is\ exporting\ to\ MG \\ < 0 \;\; Grid\ is\ importing\ from\ MG \end{cases} \quad \forall t \in \mathcal{T} \tag{5.12}$$

The grid operation is restricted by the constraints discussed in (5.13-5.14).

$$0 < P_G^t < P_{G,Ex}^{\acute{M}} \;\; \forall t \in \mathcal{T} \tag{5.13}$$

$$P_{G,Im}^{\acute{M}} < P_G^t < 0 \;\; \forall t \in \mathcal{T} \tag{5.14}$$

where, P_G^t is positive when the grid is exporting to MG and becomes negative when the grid is importing from MG. $P_{G,Ex}^{\acute{M}}$ and $P_{G,Im}^{\acute{M}}$ are the maximum limits of power export and import with grid.

5.5. Formulation of non-linear life estimation model of a battery

The battery life model has two aspects, i.e., calendar life and cycle life. The calendar life reflects the capacity decline over time (due to the passage of time) without taking into account the battery's cycles. It is affected by the factors surrounding the battery installation location and is therefore considered a non-operational factor. However, cycle life is determined by the maximum possible charge and discharge cycles of a battery. It is primarily determined by operational approaches, such as how often and how deeply the battery charges and discharges.

The degradation of battery life refers to the loss of life induced by the degradation of battery functional qualities and changes in operating conditions. In other words, battery degradation is stated as a percentage decrease in battery lifetime. There are several factors that contribute to battery life degradation, such as battery cycle time, charge-discharge status, temperature, and its way of operation. The battery degradation factor is segregated into two components, static and dynamic degradation, and can be expressed by (5.15).

$$BDf = BDf_S + BDf_D \tag{5.15}$$

The static degradation (BDf_S) is mainly caused by the deterioration of functional qualities of the battery, such as the growth of a passivation layer on the negative electrodes, thickening of the electrolyte interface film, electrode active material loss, and electrolyte oxidation.

As a result of this functional feature degradation, the storage battery's internal resistance will rise, which will reduce its capacity. It is considered linear with battery shelf life because it is independent of operating conditions. The annual static depreciation is expressed in (5.16) [7].

$$BDf_S = \frac{1}{T_S} \tag{5.16}$$

where T_S stands for the battery calendar/shelf life. For instance, if the calendar/shelf life of the battery is 12 years, then one year's static degradation is 1/12 = 8.33%.

The dynamic degradation (BDf_D) is completely associated with the operating conditions of the battery. Operating factors include the depth of discharge and the charge-discharge rate, which correspond to the battery's charge-discharge procedure. Because practical charge-discharge cycles are aperiodic, the dynamic deterioration becomes non-linear. Therefore, it is crucial to consider practical operating circumstances while calculating the dynamic degradation, as indicated by (5.17) [7].

$$BDf_D = \sum_{i=1}^{N} {1}\Big/{\acute{\varsigma}_{i(kl)}} \quad \mathrm{i} = 1,2,\dots,\mathrm{N} \tag{5.17}$$

where i denotes the i^{th} charge-discharge cycle, k and l denote the beginning and end of the charge-discharge process between SOC values, SOC_k and SOC_l. N represents the total number of charge-discharge intervals. $\acute{\varsigma}_{i(kl)}$ is the number of cycles of the battery when it is charged and discharged between k and l, until its capacity falls to 60% of its nominal capacity, and it is calculated using (5.18).

$$\frac{1}{\acute{\varsigma}_{i(kl)}} = \frac{1}{2}\left(\frac{1}{\acute{\varsigma}_{i(k)}} - \frac{1}{\acute{\varsigma}_{i(l)}}\right) \quad \mathrm{i} = 1,2,\dots,\mathrm{N} \tag{5.18}$$

where, in regard to i^{th} charge-discharge cycle, $\acute{\varsigma}_{i(k)}$ and $\acute{\varsigma}_{i(l)}$ are the cycle numbers when the SOC charges and discharges from SOC_k and SOC_l to 100%, respectively.

Further, $\frac{1}{\acute{C}_{i(k)}}$, $\frac{1}{\acute{C}_{i(l)}}$ and $\frac{1}{\acute{C}_{i(kl)}}$ is the dynamic degradation when battery charges and discharges from SOC_k to $SOC_{100\%}$, SOC_l to $SOC_{100\%}$, and SOC_k to SOC_l respectively.

The dynamic degradation of battery (BDf_D^T) can be expressed using (5.19) [7].

$$BDf_D^T = \sum_{t=1}^{T} BDf_D^t = \sum_{t=1}^{T} \left\{ \sum_{i=1}^{N} \left| \frac{1}{2} \left(\frac{1}{\acute{C}_{i(k)}} - \frac{1}{\acute{C}_{i(l)}} \right) \right| \right\} \; \mathrm{i} = 1,2 \ldots, \mathrm{N}, \forall \mathrm{t} \in \mathcal{T} \tag{5.19}$$

where N represents the total number of charge-discharge intervals in a time interval 't'. BDf_D^t is the dynamic degradation for time interval 't'.

Using (5.15-5.19), if $T = 8760h = Y$, then the annual battery degradation factor (BDf^Y) becomes,

$$BDf^Y = \frac{1}{T_S} + \sum_{t=1}^{T} BDf_D^t \quad \forall \mathrm{t} \in \mathcal{T} \tag{5.20}$$

In order to estimate the accurate BDf for any battery, only the relationship between the number of cycles and its SOC or DOD needs to be examined. Thus, it is possible to compute battery degradation of any charge-discharge interval for practical operating conditions and estimate the total operating life (T_{OL}) of any battery energy storage.

When the battery life degradation process reaches 100%, i.e., the battery degradation factor becomes unity as shown in (5.21), the estimated total operating life (T_{OL}) can be determined.

$$\sum_{Y=1}^{Y=T_{OL}} BDf^Y = 100\% \quad \forall \mathrm{Y} \tag{5.21}$$

Figure 5.4 shows the flowchart for calculating T_{OL} of a battery.

5.6. Development of a proposed Improved Energy Management Strategy (IEMS)

In order to compensate for the limitations of the CEMS and EEMS of MG, this chapter develops an IEMS. The major objective of IEMS is to minimize the operating cost of the MG for the prosumer building and increase the lifespan of the BESS. The salient features of IEMS are as follows –

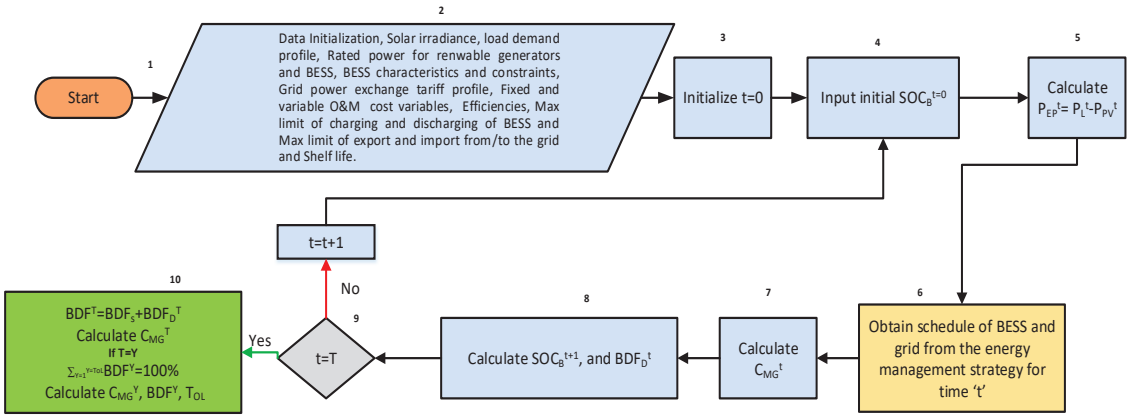

Figure 5.4 Flowchart for calculating T_{OL} of a battery

- It aims to maximize the profit of the prosumer building by optimizing the operating cost associated with MG.
- It focuses on improving the total operating lifetime of BESS by reducing its degradation factor and optimally utilizing solar PV generation.
- It consists of a rule-based algorithm (RBA) that governs the operation of MG depending on four factors: solar PV power, load demand power, type of load demand (off-peak/peak), and the current status of the BESS.
- The formulated RBA decides the contribution of BESS and grid, which depends on rules considering the above four factors as input.

To minimize the total operating cost ($\mathbb{C}_{MG}^T$) of the MG, a cost optimization model is formulated that considers the O&M cost of solar PV system, complete BESS's O&M cost model with variable and fixed cost terms, and cost associated with the grid power exchange. The formulated cost optimization model is shown in (5.22). The mathematical expressions of the components of the formulated model are presented in (5.23-5.25).

$$\min \mathbb{C}_{MG}^T = \sum_{t=1}^{T} \mathbb{C}_{MG}^t = \sum_{t=1}^{T} \zeta_{PV}^{O\&M} + \left\{\left(\left| P_{B,\frac{Ch}{Dch}}^t * \Delta t \right| * \Phi_B^{O\&M}\right) + \Psi_B^{O\&M}\right\} + \{(P_G^t * \Delta t) * \lambda_G^t\} \quad \forall t \in \mathcal{T} \quad (5.22)$$

$$\mathbb{C}_{PV} = \zeta_{PV}^{O\&M} \quad (5.23)$$

$$\mathbb{C}_B^t = \left(\left| P_{B,Ch/Dch}^t * \Delta t \right| * \Phi_B^{O\&M}\right) + \Psi_B^{O\&M} \quad \forall t \in \mathcal{T} \quad (5.24)$$

$$\mathbb{C}_G^t = (P_G^t * \Delta t) * \lambda_G^t \quad \forall t \in \mathcal{T} \tag{5.25}$$

where, $\mathbb{C}_{MG}^T$ is the total operation cost of MG, $\mathbb{C}_{PV}$ is the hourly O&M cost of solar PV systems, $\mathbb{C}_B^t$ is the hourly O&M cost of BESS and $\mathbb{C}_G^t$ is the hourly cost of energy exchanged with the grid at a time 't'. $\zeta_{PV}^{O\&M}$ is the operation and maintenance coefficient for the installed PV system in \$/h. $P_{B,Ch/Dch}^t$ is BESS's charging or discharging power at time instant 't'. $\Phi_B^{O\&M}$ and $\Psi_B^{O\&M}$ are the variable and fixed O&M cost coefficients of BESS in \$/kWh and \$/h, respectively, where $\Phi_B^{O\&M}$ depends on the $P_{B,Ch/Dch}^t$. P_G^t is the power exchanged with the grid at a time 't'. λ_G^t is the energy trading price of the grid at a time 't' in \$/kWh.

The formulated cost objective function is minimized subject to the constraints presented in (4.3-4.5), (5.11), (5.13-5.14), and (5.26):

$$P_L^t - P_{PV}^t - P_{B,Ch/Dch}^t - P_G^t = 0 \quad \forall t \in \mathcal{T} \tag{5.26}$$

where P_L^t , P_{PV}^t and P_G^t are the load demand on the microgrid, power generated by solar PV, and power exported/imported to/from the grid at time instant 't'.

Figure 5.5 shows the proposed IEMS flow chart. In this scheme, the variable BESS's discharging power ($P_{B,Dch}^t$) has two bounds for optimization, i.e., Low and High. For the low bound, the variable ($P_{B,Dch}^t$) will remain between the limits 0 to $P_{B,Dch}^{\acute{M}} * \beta$, whereas, for the high bound, it will vary between 0 to $P_{B,Dch}^{\acute{M}}$. Here, β is the constant that decides the contribution of BESS, which is taken as 0.85 after multiple simulations. Further, the SOC of BESS also has a threshold level, i.e., $SOC_{B,th}$. The decision for every time instant 't' is taken based on the equivalent power at a time 't' (P_{EP}^t) calculated using (5.27) average off-peak load demand ($P_L^{Off-peak}$), and SOC of BESS at a time 't' (SOC_B^t).

$$P_{EP}^t = P_L^t - P_{PV}^t \quad \forall t \in \mathcal{T} \tag{5.27}$$

5.7. Case Study & Results

5.7.1. Input Data

In order to show the efficacy of IEMS, two-time scales are considered. In Case 1, the performance analysis of IEMS over CEMS and EEMS is compared considering real-time yearly data of the prosumer building for a year time scale. Figures 5.6(a) and 5.6(b) show real-time yearly data (365 days) of solar PV generation and load demand with a 1-h time step. The result for this scenario is analyzed and compared with different DOD levels, i.e., 30%, 50%, and 70%.

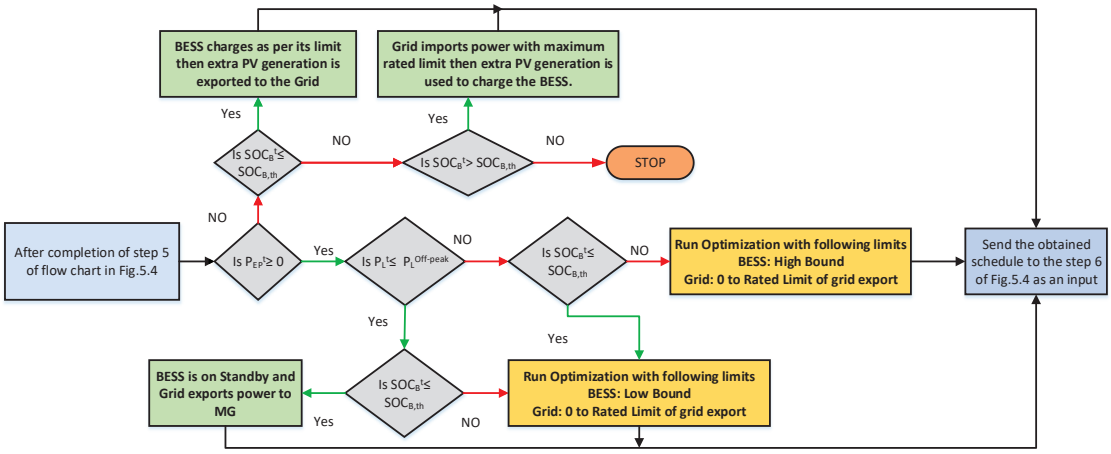

Figure 5.5 Flow chart of the proposed IEMS

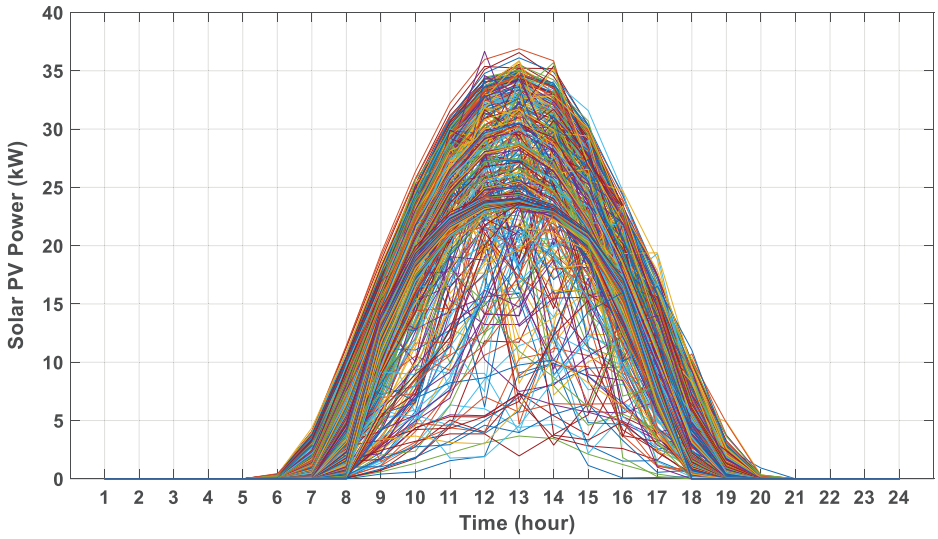

(a)

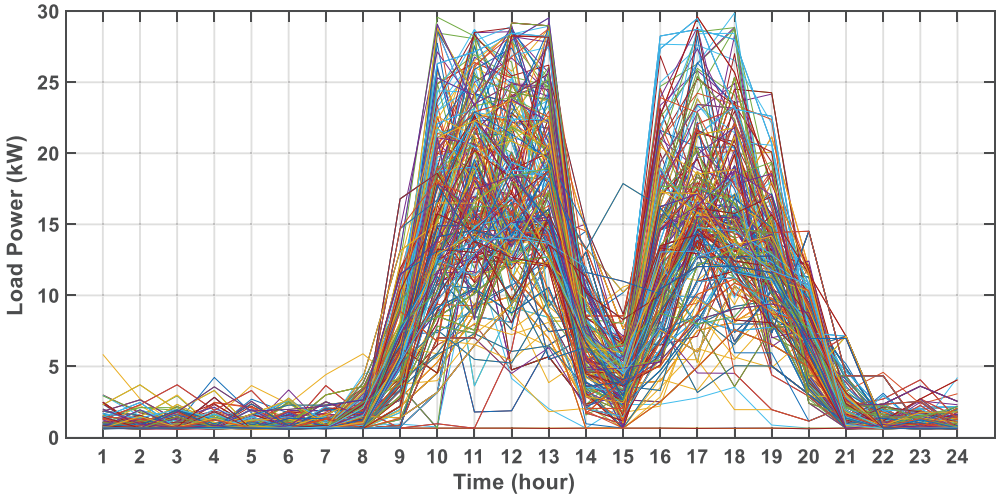

(b)

Figure 5.6 Real-time data based 365 scenarios (a) solar PV generation and (b) load demand.

Further, in order to handle the uncertainty associated with solar PV generation and load demand and reduce the computational burden, the real-time yearly data is reduced to 10 scenarios using the Scenario reduction technique [13][14]. Thus, in Case 2, the performance of IEMS over CEMS and EEMS is compared considering these scenarios, and further day-ahead scheduling is obtained. The result for this case is analyzed for 70% DOD level. Figures 5.7(a) and 5.7(b) show the 10 solar PV generation and load demand scenarios obtained using the scenario reduction technique. Figure 5.8 shows the day-ahead grid exchange prices. The solar PV generation and load demand for case 2 are expressed by (5.28) and (5.29).

$$P_{PV}^{t} = \sum_{s=1}^{S} \pi_{PV}^{t,s} * P_{PV}^{t,s} \quad \text{s} = 1,2,3,\dots,\text{S} \tag{5.28}$$

$$P_{L}^{t} = \sum_{s=1}^{S} \pi_{L}^{t,s} * P_{L,s}^{t,s} \quad \text{s} = 1,2,3,\dots,\text{S} \tag{5.29}$$

where, S is the total number of scenarios and s is the index of a scenario. $P_{PV}^{t,s}$ and $P_{L,s}^{t,s}$ are the solar PV and load power of scenario 's' at time instant 't'. $\pi_{PV}^{t,s}$ and $\pi_{L}^{t,s}$ represents the probabilities of each scenario 's' for time instant 't'.

As discussed, the estimation of BDf for a battery depends on the relationship between the number of cycles and its SOC or DOD. Figure 5.9 shows the curve of the number of cycles (until battery capacity falls to 60% of its nominal capacity) vs. DOD of a battery of rating 12V, 225Ah @C20 [16].

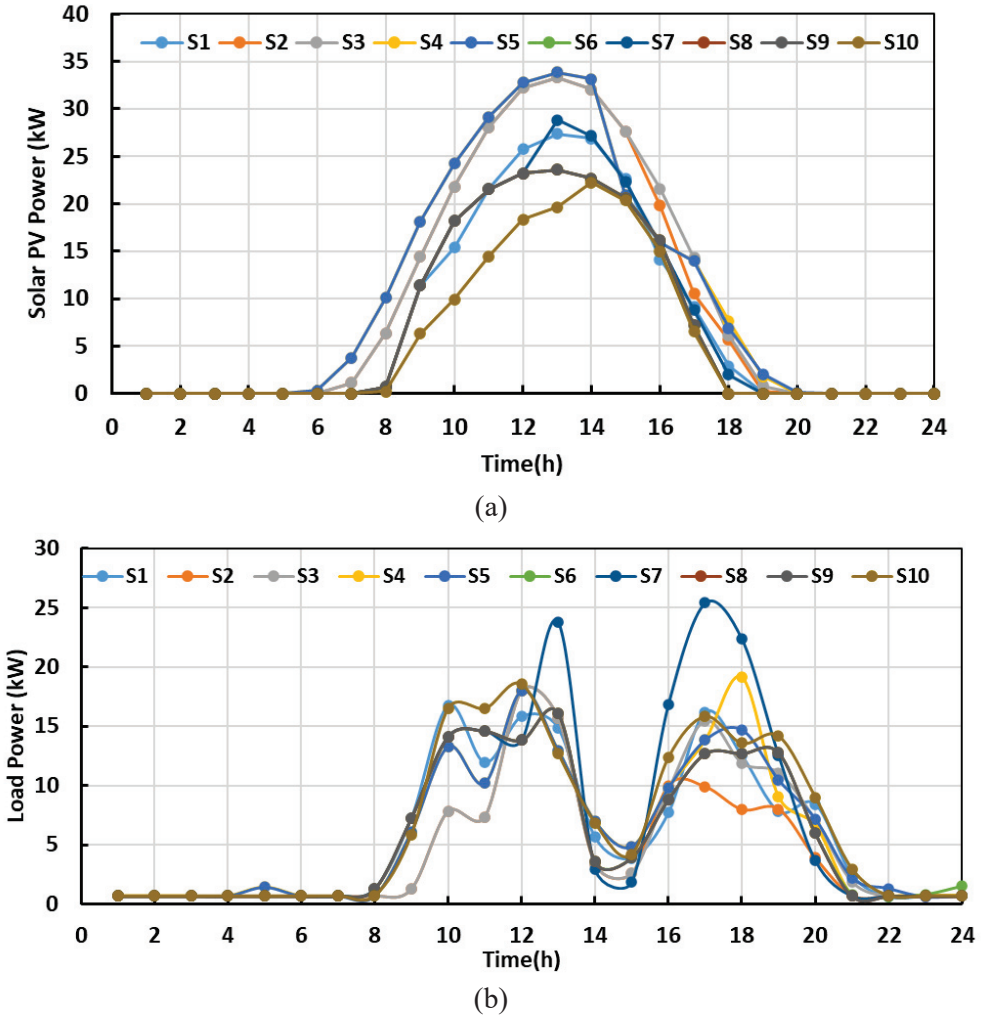

Figure 5.7 Reduced scenarios of (a) solar PV generation and (b) load demand obtained using Scenario reduction technique.

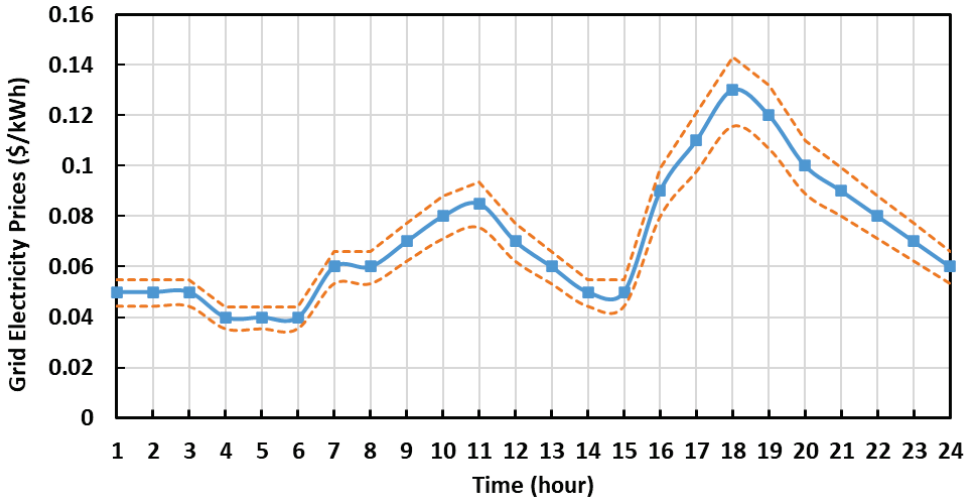

Figure 5.8 Day-ahead grid exchange prices [15]

Using the curve fitting technique, a mathematical relationship between the number of cycles and DOD for LA BESS of C20 rate is estimated, which is shown by (5.30).

$$\acute{C}_i^{LA\_C20} = 5278.8 * e^{(-3.02*DOD_i)} + 5.894 * e^{(4.701*DOD_i)} \quad (5.30)$$

where $\acute{C}_i$ is the number of cycles at a depth of discharge (DOD_i) as defined in (5.31).

$$DOD_i = 1 - SOC_i \quad (5.31)$$

where DOD_i means that the battery charges and discharges repeatedly between SOC_i

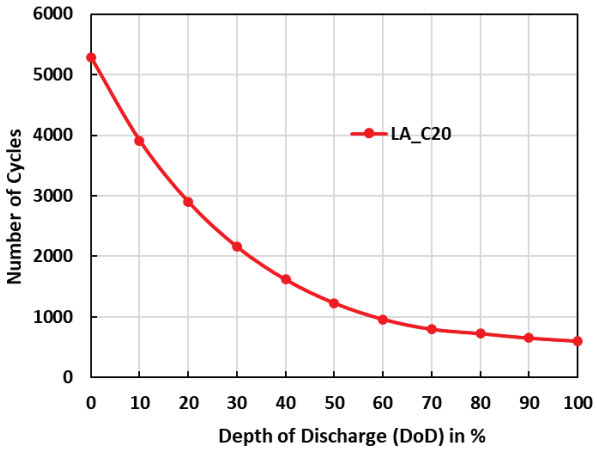

Figure 5.9 Number of cycles (until battery capacity falls to 60% of its nominal capacity) vs. DOD of LA BESS [16]

and $SOC_{100\%}$. Therefore, using (5.31), the mathematical relationship between the number of cycles and SOC_i can be shown by (5.32).

$$\acute{C}_i^{LA\_C20} = 5278.8 * e^{(-3.02*(1-SOC_i))} + 5.894 * e^{(4.701*(1-SOC_i))} \quad (5.32)$$

Table 5.3 presents the parameters used in the simulation studies that are obtained from the real-time MG installed at prosumer building [16]. Table 5.4 shows the cost coefficients of batteries and solar PV [17]–[19].

5.7.2. Case 1 – Performance analysis of CEMS, EEMS, and IEMS for a year time scale

This section presents the performance analysis of CEMS, EEMS, and IEMS based on three major factors, i.e., the annual degradation factor, the total operating life of BESS,

and the annual operating cost of MG. The impact of change in DOD on MG operation is also analyzed.

Figures 5.10, 5.11, and 5.12 show the annual operating cost of MG, the annual dynamic degradation factor, and the estimated total operating life of BESS for CEMS, EEMS, and IEMS, respectively. The annual static degradation (BDf_S) of BESS only depends on the shelf

Table 5.3 Parameters used in the simulation studies.

S.No.	Parameter	Value
1.	$\boldsymbol{SOC_B^{\acute{M}}}$	100%
2.	$\boldsymbol{SOC_B^{\acute{m}}}$ (Depending on DOD)	70%, 50%, 30%
3.	$\boldsymbol{E_B^R}$	81kWh
4.	$\boldsymbol{P_{G,Ex}^{\acute{M}}}$	35kW
5.	$\boldsymbol{P_{G,Im}^{\acute{M}}}$	-14kW
6.	$\boldsymbol{P_{B,\mathrm{Ch}/Dch}^{\acute{M}}}$	-4.05kW/4.05kW
7.	$\boldsymbol{\rho_B}$	5% per month
8.	$\boldsymbol{\eta_{B,Ch}/\eta_{B,Dch}}$	0.85
9.	$\boldsymbol{T_S}$	6 years
10.	$\boldsymbol{BDf_S}$	0.1666 per year

Table 5.4 Cost coefficients of batteries and solar PV system

$\boldsymbol{\Phi_B^{O\&M}}$(\$/kWh)	$\boldsymbol{\Psi_B^{O\&M}}$ (\$/h)	$\boldsymbol{\zeta_{PV}^{O\&M}}$(\$/h)
0.0005125	0.02854	0.057 \$/h

life of the BESS and is 0.166 for all the cases. Therefore, it is independent of the operational mode of MG and DOD levels of the BESS. The lower value of the degradation factor results in a higher total operating life of BESS.

Figures 5.10 and 5.11 show that IEMS has significantly reduced the operating cost of the MG and dynamic degradation factor of BESS compared to CEMS and EEMS. Thus, BESS's estimated total operating life is higher for IEMS than for CEMS and EEMS, as shown in Fig. 5.12. Moreover, it is also noted that, as DOD increases, the dynamic degradation factor increases irrespective of the scheme, thereby decreasing BESS's

operating life. It is because of the decrease in the number of cycles, and the estimated operating life of BESS decreases.

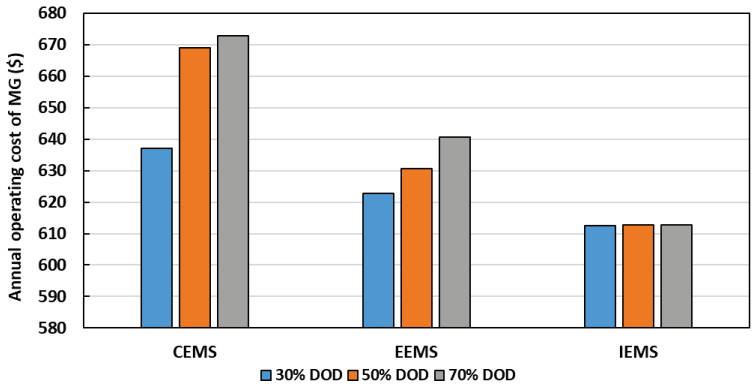

Figure 5.10 Annual operating cost of MG for CEMS, EEMS, IEMS considering various DOD levels

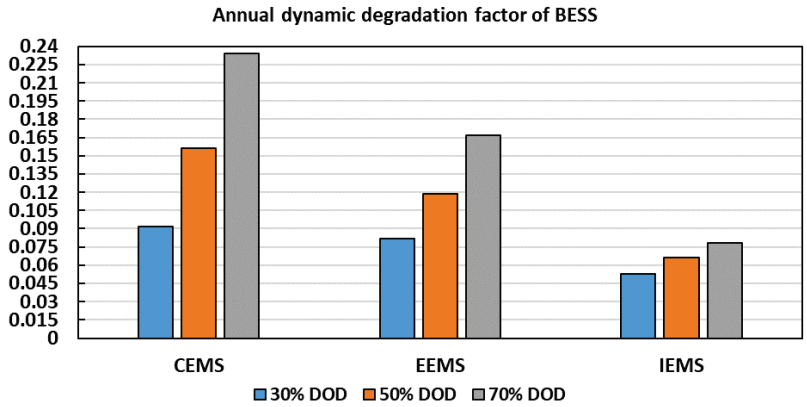

Figure 5.11 Annual dynamic degradation factor of BESS for CEMS, EEMS, IEMS considering various DOD levels

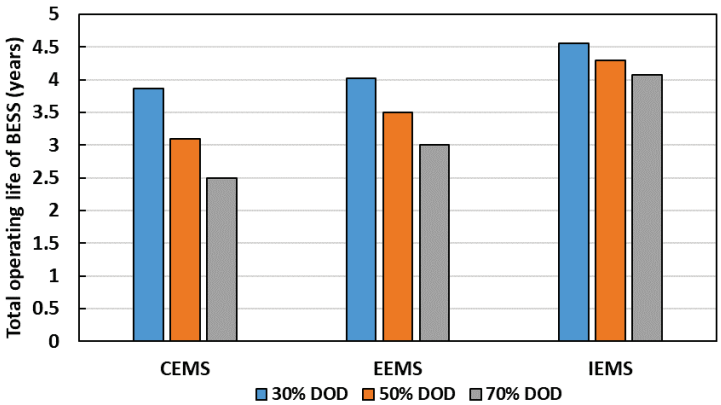

Figure 5.12 Total operating life of BESS for CEMS, EEMS, IEMS considering various DOD levels

5.7.2.1. Impact of IEMS on various factors with respect to CEMS

The percentage change in the annual operating cost of MG, annual dynamic degradation factor and estimated total operating life of BESS from IEMS with respect to CEMS is tabulated in Table 5.5. The negative sign shows the decrement, and the positive sign shows the increment in the factor.

Table 5.5 shows that for the scenario of 70% DOD, there is an 8.93% and 66.55% reduction in the operating cost of MG and degradation factor, respectively, and there is a 63.67% increment in the total operating life of BESS. Thus, profit earned by the prosumer building owner is significant in the case of IEMS in terms of cost and life of BESS.

Table 5.5 Percentage change in operating cost of MG, dynamic degradation factor, and estimated total operating life of BESS from IEMS with respect to CEMS

DOD Levels	Percentage change in $\mathbb{C}_{MG}^{Y}$	Percentage change in BDf_{D}^{Y}	Percentage change in T_{OL}
30%	-3.87	-42.62	17.83
50%	-8.42	-57.60	38.60
70%	-8.93	-66.55	63.67

5.7.2.2. Impact of IEMS on various factors with respect to EEMS

Table 5.6 shows the percentage change in the annual operating cost of MG, annual dynamic degradation factor and estimated total operating life of BESS from IEMS with respect to EEMS. It can be observed that, for 70% of DOD, IEMS has decreased the operating cost and degradation of BESS by 4.37% and 52.99%, respectively, which is the highest among all DODs. Further, it improved the operating life of BESS by 36.06% with respect to EEMS.

Table 5.6 Percentage change in operating cost of MG, dynamic degradation factor, and estimated total operating life of BESS from IEMS with respect to EEMS

DOD Levels	Percentage change in $\mathbb{C}_{MG}^{Y}$	Percentage change in BDf_{D}^{Y}	Percentage change in T_{OL}
30%	-1.68	-35.71	13.34
50%	-2.82	-44.17	22.48
70%	-4.37	-52.99	36.06

Therefore, it can be concluded from Tables 5.5 and 5.6 that IEMS is superior to CEMS and EEMS in terms of enhancing the MGO's profit and improving the operating life of BESS.

5.7.3. Case 2 – Performance analysis of CEMS, EEMS, and IEMS for day-ahead scheduling

The performance analysis of CEMS, EEMS, and IEMS considering reduced scenarios is discussed in this section. This study is performed for 70% of DOD levels, as the higher DOD level is the most critical one. Figure 5.13 shows the day-ahead optimal schedule of BESS and grid considering CEMS, EEMS, and proposed IEMS. Figure 5.14 shows the SOC profile of BESS from CEMS, EEMS, and IEMS.

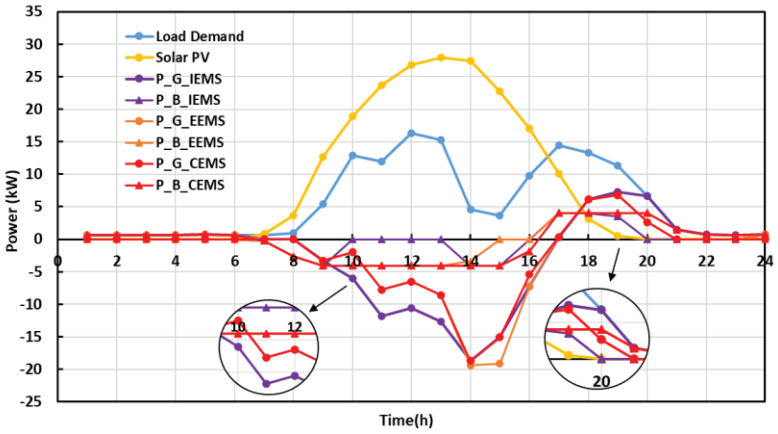

Figure 5.13 Optimal day-ahead schedule of BESS for CEMS, EEMS and IEMS

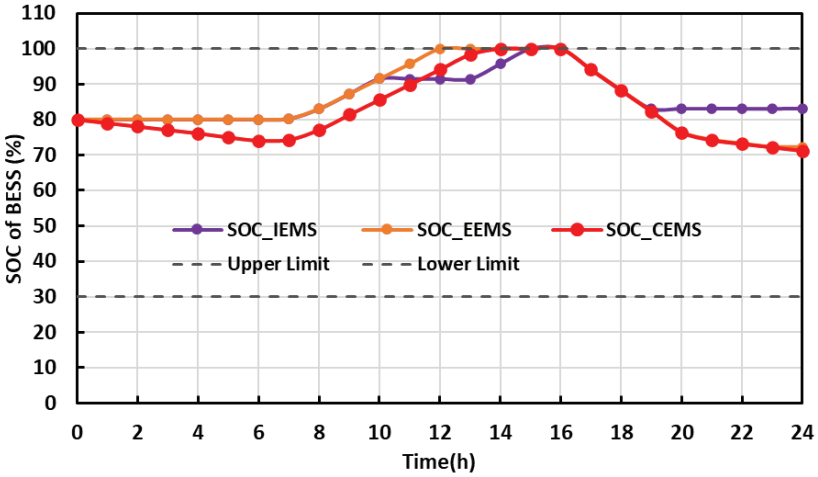

Figure 5.14 SOC of BESS for CEMS, EEMS and IEMS.

It can be observed that as the IEMS aims at optimal utilization of BESS, for time instants 10 and 11, when the BESS reaches to 90% SOC, it is not getting charged, due to which surplus generation is supplied to the grid and finally ends up reducing the operating cost of the MG. When the equivalent power is positive, for time instant 20, after the peak hours, the BESS either discharges at a slightly lower discharge rate than that of CEMS and EEMS or comes to a standby mode to decrease its degradation.

The daily operating cost of MG ($\mathbb{C}_{MG}^{T}$), and the dynamic degradation factor from CEMS, EEMS, and IEMS is tabulated in Table 5.7. The negative sign in the daily operating cost of MG shows the profit earned by the prosumer building owner.

Table 5.7 Daily operating cost of MG and dynamic degradation factor of BESS from CEMS, EEMS, and IEMS

Parameters	**CEMS**	**EEMS**	**IEMS**
Daily operating cost of MG ($\mathbb{C}_{MG}^{T}$) in $	-0.2	-0.38	-0.64
Dynamic degradation factor (BDf_{D}^{T})	33.92E-5	24.73E-5	12.50E-5

It can be noted from Table 5.7 that the daily operating cost of MG ($\mathbb{C}_{MG}^{T}$) and the dynamic degradation factor of BESS is lowest for IEMS. Therefore, the proposed IEMS can maximize the profit of the prosumer building owner and improve the operating life of BESS compared to CEMS and EEMS.

5.8. Conclusion

This chapter develops an IEMS for a prosumer building consisting of a solar PV and BESS-powered grid-tied AC-DC hybrid MG. The proposed scheme aims to maximize the building owner's profit by optimizing the operating cost associated with the MG while simultaneously improving the total operating lifetime of BESS by reducing its degradation factor. It consists of a RBA, as per which the formulated objective function of MG is minimized. The proposed RBA decides the contribution of BESS and grid based on solar PV power, load demand power, type of load demand (off-peak load/peak load) and condition of the BESS. Moreover, this study considers a non-linear battery degradation model that includes static and dynamic degradation factors to estimate BESS's practical operating life span.

In case 1, the proposed IEMS is tested for the yearly 1-h time step, data obtained from grid-connected real-time MG consisting of a solar PV system and a BESS installed at a building of a university, BITS, Pilani. Further, to handle the uncertainty associated with solar PV generation and load demand and to reduce the computational burden, the Scenario reduction technique is used to reduce these 365 scenarios to 10 scenarios. In Case 2, a day ahead of the optimal schedule is obtained using these reduced scenarios. The performance of the proposed IEMS is validated by comparing the results of the IEMS with the CEMS and EEMS of the MG. In order to showcase the effectiveness of IEMS, different levels of DOD of BESS are considered, i.e., 30%, 50% and 70%.

The results conclude that, for the critical DOD such as 70% and the yearly analysis, IEMS has reduced the operating cost of MG and dynamic degradation of BESS by 4.37% and 52.99%, respectively and increased the operating life span of BESS by 36.06% in comparison to EEMS. Thus, the proposed method can be regarded as a superior EMS for prosumer building in terms of improved economic profit and system efficiency by increasing the operating life of BESS.

Further to increase the sustainability of the developed building MG and improve the performance of IEMS, chapter 6 presents the formulation of the FLS scheme. Moreover, in order to account for more practical EVL, its advanced probabilistic modelling is developed. Finally, the performance assessment of IEMS integrated with FLS and EVL is discussed.

Bibliography

[1] D. Zhang, H. Zhu, H. Zhang, H. H. Goh, H. Liu, and T. Wu, "Multi-Objective Optimization for Smart Integrated Energy System Considering Demand Responses and Dynamic Prices," *IEEE Trans. Smart Grid*, vol. 13, no. 2, pp. 1100–1112, 2022, doi: 10.1109/TSG.2021.3128547.

[2] Y. Qiu *et al.*, "Two-stage distributionally robust optimization-based coordinated scheduling of integrated energy system with electricity-hydrogen hybrid energy storage," *Prot. Control Mod. Power Syst.*, vol. 8, no. 1, p. 33, 2023, doi: 10.1186/s41601-023-00308-8.

[3] P. Sharma, D. Bhattacharjee, H. D. Mathur, P. Mishra, and H. Siguerdidjane, "Novel optimal energy management with demand response for a real-time community microgrid," *Proc. - 2023 IEEE Int. Conf. Environ. Electr. Eng. 2023 IEEE Ind. Commer. Power Syst. Eur. EEEIC / I CPS Eur. 2023*, pp. 1–6, 2023, doi: 10.1109/EEEIC/ICPSEurope57605.2023.10194855.

[4] J. F. Manwell and J. G. McGowan, "Lead acid battery storage model for hybrid energy systems," *Sol. Energy*, vol. 50, no. 5, pp. 399–405, 1993, doi: https://doi.org/10.1016/0038-092X(93)90060-2.

[5] C. Goebel, H. Hesse, M. Schimpe, A. Jossen, and H.-A. Jacobsen, "Model-Based Dispatch Strategies for Lithium-Ion Battery Energy Storage Applied to Pay-as-Bid Markets for Secondary Reserve," *IEEE Trans. Power Syst.*, vol. 32, no. 4, pp. 2724–2734, 2017, doi: 10.1109/TPWRS.2016.2626392.

[6] P. Sharma, P. Mishra, and H. D. Mathur, "Optimal energy management in microgrid including stationary and mobile storages based on minimum power loss and voltage deviation," *Int. Trans. Electr. Energy Syst.*, vol. 31, no. 12, p. e13182, 2021, doi: https://doi.org/10.1002/2050-7038.13182.

[7] G. Yan, D. Liu, J. Li, and G. Mu, "A cost accounting method of the Li-ion battery energy storage system for frequency regulation considering the effect of life degradation," *Prot. Control Mod. Power Syst.*, vol. 3, no. 1, pp. 1–9, 2018, doi: 10.1186/s41601-018-0076-2.

[8] J. O. Lee and Y. S. Kim, "Novel battery degradation cost formulation for optimal scheduling of battery energy storage systems," *Int. J. Electr. Power Energy Syst.*, vol. 137, no. October 2021, p. 107795, 2022, doi: 10.1016/j.ijepes.2021.107795.

[9] M. Rouholamini *et al.*, "A Review of Modeling, Management, and Applications of Grid-Connected Li-Ion Battery Storage Systems," *IEEE Trans. Smart Grid*, vol. 13, no. 6, pp. 4505–4524, 2022, doi: 10.1109/TSG.2022.3188598.

[10] X. Li and S. Wang, "Energy management and operational control methods for grid battery energy storage systems," *CSEE J. Power Energy Syst.*, vol. 7, no. 5, pp. 1026–1040, 2021, doi: 10.17775/CSEEJPES.2019.00160.

[11] S. Liu *et al.*, "Operational optimization of a building-level integrated energy system considering additional potential benefits of energy storage," *Prot. Control Mod. Power Syst.*, vol. 6, no. 1, p. 4, 2021, doi: 10.1186/s41601-021-00184-0.

[12] K. S. Sangwan *et al.*, "Comparative Analysis for Solar Energy Based Learning Factory: Case Study for TU Braunschweig and BITS Pilani," *Procedia CIRP*, vol. 69, no. May, pp. 407–411, 2018, doi: 10.1016/j.procir.2017.11.018.

[13] N. Gröwe-Kuska, H. Heitsch, and W. Römisch, "Scenario reduction and scenario tree construction

for power management problems," *2003 IEEE Bol. PowerTech - Conf. Proc.*, vol. 3, pp. 152–158, 2003, doi: 10.1109/PTC.2003.1304379.

[14] V. Singh, T. Moger, and D. Jena, "Uncertainty handling techniques in power systems: A critical review," *Electr. Power Syst. Res.*, vol. 203, no. February 2021, p. 107633, 2022, doi: 10.1016/j.epsr.2021.107633.

[15] "prices @ www.eia.gov." [Online]. Available: https://www.eia.gov/todayinenergy/prices.php.

[16] D. Sheet, "MODEL J185P-AC with Bayonet Cap MOTIVE J185P-AC," no. mm.

[17] A. Walker *et al.*, "Model of Operation-and-Maintenance Costs for Photovoltaic Systems," *NREL Tech. Rep.*, no. June 2020, [Online]. Available: https://www.nrel.gov/docs/fy20osti/74840.pdf.

[18] A. Jäger-Waldau, *PV Status Report 2019*. 2019.

[19] K. Mongird, V. Viswanathan, J. Alam, C. Vartanian, V. Sprenkle, and R. Baxter, "2020 Grid Energy Storage Technology Cost and Performance Assessment," *Energy Storage Gd. Chall. Cost Perform. Assess. 2020*, no. December, pp. 1–20, 2020, [Online]. Available: https://www.pnnl.gov/sites/default/files/media/file/PSH_Methodology_0.pdf.

Chapter 6

Enhancing the Performance of IEMS with an Advanced Probabilistic EV Load Model and Flexible Load Shifting

6.1. Introduction

The DR programs enhance the performance of EMS because they allow the load to contribute in energy management operations [1]. Therefore, many researchers have presented EMS that considers DR programs, as discussed in Chapter 2. However, these DR strategies may not improve the reliability of the prosumer building because, in these methods, the load is shifted/controlled as per the grid energy prices without considering the RER utilization. In this regard, this chapter formulates an FLS scheme that aims to shift the flexible loads from the time slot where the equivalent power (solar PV generation subtracted from the load power) is the maximum to the time slot where it is the minimum. The proposed FLS scheme is integrated into the developed IEMS to improve its effectiveness in further reducing the operating cost of MG, reducing the degradation of BESS, and achieving sustainable operation of the system.

Further, as EVs have gained great attention as a green energy transportation method in the past few years [2], it is necessary to examine their effect on the system. These EVs can also play a crucial role in the energy management of MG by optimally managing their charging time as a DR program and by discharging energy stored in their batteries as V2G services. By enabling the V2G power transfer technology, the MG owner and EV owner not only can obtain financial benefits, but this technology can also provide the

necessary energy resources during islanded operation [3][4]. However, the efficient modeling of EV load also with V2G technology becomes complicated due to the uncertain EV owner's charging and discharging patterns. Further, it was found from the literature review presented in Chapter 2 that most of the studies have modelled EV load considering assumptions that as the EV arrives at the station, it starts charging instantly irrespective of the available number of EV plug points and the EV will leave the station only after it is fully charged. In other words, they have not taken into account the availability of EV plug-points and the random leave time duration for the EV. These limitations restrict the practical modelling of the EVL profile.

Therefore, this work presents the advanced probabilistic modelling of EVL by considering–

- A practical situation where the number of EVs arriving at the station may be more than the available EV plug-points at the station.
- An uncertain behavior of EV owner regarding their leave time from the EVS is modelled by considering a variable "leave time duration", i.e., the time duration after which EV may leave the EVS, which is random in nature.

Further, a governed charging/discharging with demand response mode (GCD_DRM) of EV operation is introduced that combines the concept of V2G power transfer services and vehicle demand response strategy to minimize the peak load on the prosumer building.

6.2. Formulation of Flexible load shifting (FLS) scheme

The load shifting is a part of the load management technique in which the flexible loads are shifted to the off-peak hours from the peak hours of the day. The flexible loads can operate at any time of the day. Therefore, these loads are usually shifted as per the grid tariff or peak/off-peak load hours. However, in this study, a flexible load shifting (FLS) scheme is developed that performs the load shifting mechanism of flexible loads based on the equivalent power (P_{EP}^{t}) as it can give information on excess renewable generation and load unmet by renewable sources. Therefore, the FLS mechanism focuses

on shifting this unmet flexible load to the time instant where excess generation is available. It can minimize the burden on BESS and reduce the grid export to MG, thereby decreasing the dynamic degradation of BESS and the operating cost of MG. After a thorough study of the prosumer building discussed in Chapter 5, it is observed that most shiftable types of equipment are operated from 16:00 to 20:00. Also, the peak of load unmet by MG occurs during this duration as the solar PV generation is low. Therefore, shifting these flexible types of equipment to the time slot where excess solar generation is available is desirable. Further, the flexible and non-flexible load power ratio is approximately 30-35%. The FLS scheme is governed using the following steps:

- Identifying the time intervals with the minimum value (negative peak) of equivalent power and calculating the total excess solar PV power generation and its size.
- Identifying the time slots with the maximum value (positive peak) of equivalent power and estimating the total flexible load power that can be shifted.
- Selecting the time slots of the same size of flexible load power as that of excess solar generation. Calculate the total flexible load power to be shifted as per the excess solar generation power.
- Move the flexible load on the selected time slot.

Implementing FLS will change the daily load profile of the building, but the total load remains the same. To restrict the overpower at any time instant, the constraint (6.1) must hold true, such as

$$P_L^{\acute{m}} \leq P_L^{\hat{t}} \leq P_L^{\acute{M}} \quad \forall t \in \mathcal{T} \tag{6.1}$$

where $P_L^{\hat{t}}$ is the load demand of the building obtained after the implementation of FLS.

6.3. Advanced probabilistic modelling of EVL

This section details the probabilistic modelling of EVL for clusters of various types of EVs. In this study, the EVL is obtained for two user modes, i.e., ACM and governed charging/discharging with demand response mode (GCD_DRM). The daily distance travelled by an EV and the arrival time (time at which the EV arrives at the EV station)

is extracted by using Monte Carlo simulation from the log-normal and normal probability density functions, respectively, as discussed in previous Chapters 3 and 4. This work takes into account the two most essential conditions in the probabilistic modelling of EVL, which are as follows:

- If the number of available EV plug-points is less than the number of EVs arriving at the station, in that case the arrival time of the EV and the plug-in time (time at which EV is plugged-in) may not be equal.
- The expected time at which the EV may leave the EV station, i.e., leave time, is highly uncertain and is governed by human behavior. Therefore, it may not be equal to the estimated plug-out time (the time at which EV is fully charged).

Hence, in order to accurately model the EVL these above conditions are important. As the leave time duration of EV and type of EV, which are input by the EV owners, are uncertain parameters, therefore, they are modelled as a random variable.

Four different types of EVs are considered in this study. The EV owners are segregated into three categories: employees of the buildings, visitors coming to the buildings, and residential public coming to charge their EVs.

Let the total number of EVs coming to the station be N_{EV}. Further, the number of EVs of employees (N_{EV}^{E}), visitors (N_{EV}^{V}), and residential people (N_{EV}^{R}) can be calculated using (6.2-6.5).

$$N_{EV}^{E} = \alpha_E N_{EV} \tag{6.2}$$

$$N_{EV}^{V} = \alpha_C N_{EV} \tag{6.3}$$

$$N_{EV}^{R} = \alpha_R N_{EV} \tag{6.4}$$

$$\alpha_E + \alpha_V + \alpha_R = 1 \tag{6.5}$$

where α_E, α_V and α_R are the ratios of employees, visitors, and residential EV owners with respect to total number of EVs.

The mean and standard deviation used to generate the arrival time of EV (T_{AT}^{n}) for employees, visitors, and residential EV owners are shown in Table 6.1.

Table 6.1 Mean and standard deviation of arrival time of EV for employees, visitors, and residential EV owners

Type of EV owner	Mean of T_{AT}^{n}	Standard deviation of T_{AT}^{n} in hour
Employees	9:00	0.25
Visitors	11:00 and 18:00	1
Residential	20:00	1

6.3.1. Autonomous charging mode (ACM) considering advanced probabilistic model

This mode focuses on unidirectional power flow, i.e., only charging the EVs. As the EV reaches the station, the EV aggregator takes the specific input from the EV owner, such as the present SOC of the EV and the leave time, i.e., the expected time at which the EV may leave the station, irrespective of its SOC. Using these inputs, the EV aggregator will calculate the estimated plug-out time (the time at which the EV will be fully charged) and will display it to the EV owner. If the leave time is less than the estimated plug-out time, then a notification will be sent to the EV owner regarding this difference in this time, after depending on the owner's input, represented by ξ_{ACM}^{n}, aggregator takes the decision.

The plug-in time of EV (T_{PI}^{n}) can be calculated by (6.6). It is assumed that the plug-in time of the EV is the start time of charging of the EV.

$$T_{PI}^{n} = \begin{cases} T_{AT}^{n} & if\ N_{EV\_P} \geq N_{EV} \\ T_{PO}^{n-1} & if\ N_{EV\_P} < N_{EV} \end{cases} \qquad \forall n \in \mathcal{N}_{EV} \tag{6.6}$$

Where T_{PO}^{n-1} is the plug-out time of the previous EV. N_{EV_P} is the number of EV plug-points.

The SOC of EV for each n^{th} number EV having d^{th} type at the time of arrival can be calculated using (6.7). $\mathcal{D}_{EV}$ is a subset of $\mathbb{N}$, represents type of EV and is defined as $\mathcal{D}_{EV} = [1,2,3 \dots, D_{EV}]$. D_{EV} represents the total types of EVs.

$$SOC_{EV,PI}^{n,d} = 1 - \left(\frac{S_{EV}^{n,d}}{S_{EV}^{\acute{M},d}}\right) \quad \forall n \in \mathcal{N}_{EV} \ \forall d \in \mathcal{D}_{EV} \tag{6.7}$$

$S_{EV}^{n,d}$ and $S_{EV}^{\acute{M},d}$ are the distance travelled by the n^{th} number EV having d^{th} type and maximum distance d^{th} type EV can travel in one charge.

The charging duration (TD_{Ch}^{n}) of each EV can be obtained from (6.8).

$$TD_{Ch}^{n} = \frac{\left(1-SOC_{EV,PI}^{n,d}\right)*E_{EV}^{R,d}}{\eta_{EV,Ch}*P_{EV,Ch}^{d}} \quad n \in \mathcal{N}_{EV} \;\; \forall d \in \mathcal{D}_{EV} \tag{6.8}$$

$SOC_{EV,PI}^{n,d}$ is the SOC of n^{th} EV having d^{th} type, at the time of plug-in; $E_{EV}^{R,d}$ represents the rated energy capacity of EV in kWh, $P_{EV,Ch}^{d}$ is the charging rate of EV in kW/h; $\eta_{EV,Ch}$is the charging efficiency of EVs.

The estimated plug-out time of EV (T_{EPO}^{n}) can be further calculated using (6.9).

$$T_{EPO}^{n} = T_{PI}^{n} + TD_{Ch}^{n} \quad \forall n \in \mathcal{N}_{EV} \tag{6.9}$$

The actual plug-out time of EV (T_{PO}^{n}) totally depends on the leave time duration of EV (TD_{L}^{n}) and the decision input (ξ_{ACM}^{n}) given by the EV owner and can be calculated by (6.10).

$$T_{PO}^{n} = \begin{cases} T_{EPO}^{n} & if\ TD_{L}^{n} \geq TD_{Ch}^{n} \\ T_{EPO}^{n} & if\ TD_{L}^{n} < TD_{Ch}^{n}\ and\ \xi_{ACM}^{n} = 1 \\ T_{L}^{n} & if\ TD_{L}^{n} < TD_{Ch}^{n}\ and\ \xi_{ACM}^{n} = 0 \end{cases} \quad \forall n \in \mathcal{N}_{EV} \tag{6.10}$$

The charging power ($P_{Ch}^{t,n}$) required to charge the EV can be estimated using equation (6.11). The associated time interval to this charging power can be calculated using equation (6.6) and (6.9).

$$P_{Ch}^{t,n}\ for\ each\ 't'\ interval\ of\ TD_{Ch}^{n} = P_{EV,Ch}^{d} \quad \forall t \in \mathcal{T}, \forall n \in \mathcal{N}_{EV}, \forall d \in \mathcal{D}_{EV} \tag{6.11}$$

As EVs charging time intervals are independent of each other, therefore they can be accumulated. The daily EVL profile of a large number of EVs for ACM mode can be calculated using (6.12) as follows:

$$P_{EV,ACM}^{t} = \sum_{n=1}^{N_{EV}} P_{Ch}^{t,n} \quad \forall t \in \mathcal{T}, \forall n \in \mathcal{N}_{EV} \tag{6.12}$$

where $P_{EV,ACM}^{t}$ is the daily EVL of (N_{EV}) EVs in case of ACM.

6.3.2. Governed charging/discharging with demand response mode (GCD_DRM)

This mode is a combination of V2G and governed grid to vehicle, i.e., DR mode of EVs. It provides flexibility to the EV owner in discharging their EV batteries and earning financial incentives from it. The V2G deals with the bi-directional power flow between the EVs and MG, and the DR mode governs the G2V operation. In the GCD_DRM mode, the EV aggregator plays two vital roles. It allows the EVs to discharge during dynamic peak price hours and charge them during low price hours. The amount of power to be discharged from the EVs is dynamic and depends on the leave time of the EV. Hence, the EV aggregator calculates it and makes sure that EV is fully charged (after participating in V2G) before the leave time duration of EV. Further, it motivates the EV owners to participate in the DRS by shifting their charging load from peak load hour to off-peak load hour.

The plug-in time of EV (T_{PI}^{n}) and the charging duration (TD_{Ch}^{n}) of each EV can be obtained from (6.6) and (6.8), respectively.

The desired plug-out time of EV (T_{DPO}^{n}) can be calculated using (6.13).

$$T_{DPO}^{n} = T_{PI}^{n} + TD_{L}^{n} \quad \forall n \in \mathcal{N}_{EV} \tag{6.13}$$

where TD_{L}^{n} is the leave time duration of nth EV.

The EV aggregator takes the decision ($K_{GCD\_DRM}^{n}$) of performing V2G/DR/G2V(ACM) depending on the following conditions as shown by (6.14).

$$K_{GCD\_DRM}^{n} = \begin{cases} if\ T_{PP}^{start} \le T_{PI}^{n} \le T_{PP}^{end}\ and\ TD_{L}^{n} \ge TD_{L}^{\acute{m}}\ and\ T_{DPO}^{n} > (T_{PP}^{end} + TD_{Ch}^{n}) \\ Send\ request\ to\ the\ EV\ owner\ to\ perform\ V2G \\ if\ T_{PP}^{start} \le T_{PI}^{n} \le T_{PP}^{end} \\ Send\ request\ to\ the\ EV\ owner\ to\ participate\ in\ DR \\ otherwise \\ Allow\ the\ EV\ owner\ to\ perform\ G2V\ (ACM)\ mode\ of\ operation \end{cases} \tag{6.14}$$

where T_{PP}^{start} and T_{PP}^{end} are the start and end of the peak price time interval. $TD_{L}^{\acute{m}}$ is the minimum value of leave time duration of EV required for the V2G.

6.3.2.1. Decision of the EV aggregator: Allowing the EV owner to perform V2G

The plug-in time of EV is assumed to be the start of the discharging time of the EV. The maximum discharging duration ($TD_{Dch}^{\acute{M},n}$) of EV until it reaches the threshold SOC (set by the EV aggregator) can be calculated from (6.15).

$$TD_{Dch}^{\acute{M},n} = \frac{(SOC_{EV}^{\acute{M}} - SOC_{EV,Dch}^{th})*E_{EV}^{R,d}}{P_{EV,Dch}^{d}} - \frac{S_{EV}^{n,d}*E_{EV}^{R,d}}{P_{EV,Dch}^{d}*S_{EV}^{\acute{M},d}} \quad \forall n \in \mathcal{N}_{EV}, \forall d \in \mathcal{D}_{EV} \tag{6.15}$$

where $SOC_{EV}^{\acute{M}}$ refers to a maximum limit of SOC of an EV battery and $SOC_{EV,Dch}^{th}$ refers to threshold limit of SOC of EV battery till which discharging can be performed. $P_{EV,Dch}^{d}$ is the discharging rate of EVs in kW/h. $S_{EV}^{n,d}$ is the distance travelled by the EV and $S_{EV}^{\acute{M},d}$ is the maximum distance EV can travel in one charge in km.

The estimated plug-out time of EV (T_{EPO}^{n}) where EV starts charging after the end of peak price (T_{PP}^{end}) can be calculated using (6.16).

$$T_{EPO}^{n} = T_{PP}^{end} + TD_{Ch}^{n} \quad \forall n \in \mathcal{N}_{EV} \tag{6.16}$$

Using above equations, the discharging duration (TD_{Dch}^{n}) of EV can be obtained using (6.17).

$$TD_{Dch}^{n} = \begin{cases} (T_{DPO}^{n} - T_{EPO}^{n}) & if\ T_{DPO}^{n} > T_{EPO}^{n}\ and\ T_{DPO}^{n} - T_{EPO}^{n} < TD_{Dch}^{\acute{M}\,n} \\ T_{Dch}^{\acute{M}\,n} & if T_{DPO}^{n} > T_{EPO}^{n}\ and\ T_{DPO}^{n} - T_{EPO}^{n} > TD_{Dch}^{\acute{M}\,n} \end{cases} \forall n \in \mathcal{N}_{EV} \tag{6.17}$$

The time at which discharging of EV ends ($T_{Dch,end}^{n}$) can be calculated using (6.18).

$$T_{Dch,end}^{n} = T_{PI}^{n} + TD_{Dch}^{n} \tag{6.18}$$

The discharging power ($P_{Dch}^{t,n}$) taken from the EV can be estimated using (6.19). The associated time interval to this discharging power can be calculated using (6.6) and (6.18).

$$P_{Dch}^{t,n}\ for\ each\ 't'\ of\ TD_{Dch}^{n} = P_{EV,Dch}^{d} \quad \forall t \in \mathcal{T}, \forall n \in \mathcal{N}_{EV}, \forall d \in \mathcal{D}_{EV} \tag{6.19}$$

The time at which charging of EV starts ($T_{Ch,starts}^{n}$) after discharging is calculated from (6.20).

$$T^{n}_{Ch,starts} = \begin{cases} T^{n}_{Dch,end} \; if \; T^{n}_{Dch,end} \geq T^{end}_{PP} \\ T^{end}_{PP} \quad if \; T^{n}_{Dch,end} < T^{end}_{PP} \end{cases} \quad \forall n \in \mathcal{N}_{EV} \tag{6.20}$$

The actual plug-out time of EV (T^{n}_{PO}) which will be the time at which discharging and charging process of EV will end can be estimated by (6.21).

$$T^{n}_{PO} = T^{n}_{Ch,starts} + TD^{n}_{Ch} + TD^{n}_{Dch} \quad \forall n \in \mathcal{N}_{EV} \tag{6.21}$$

The charging power of EV can be estimated using (6.11). As EVs discharging and charging time intervals are independent of each other, therefore they can be accumulated.

By combining all the cases above, the daily EVL profile of a large number of EVs for V2G operation can be calculated using (6.22) as follows:

$$P^{t}_{EV,V2G} = \sum_{n=1}^{N_{EV}} P^{t,n}_{Dch} + P^{t,n}_{Ch} \quad \forall t \in \mathcal{T}, \forall n \in \mathcal{N}_{EV} \tag{6.22}$$

where $P^{t}_{EV,V2G}$ is the daily EVL of (N_{EV}) EVs in case of V2G user operation.

6.3.2.2. Decision of the EV aggregator: To send the request to the EV owner to participate in DR

In this case also the plug-in time of EV (T^{n}_{PI}) and the charging duration (T^{n}_{Ch}) of each EV can be obtained from (6.6) and (6.8), respectively. Further, depending on the EV owner's input (ξ^{n}_{DRS}) towards the sent DR request, the EV aggregator takes the decision. The actual plug-out time of EV (T^{n}_{PO}) can be calculated using (6.23).

$$T^{n}_{PO} = \begin{cases} T^{end}_{PP} + TD^{n}_{Ch} \quad if \; EV \; owner \; accepts \; the \; DR \; request \; (\xi^{n}_{DRS} = 1) \\ T^{n}_{PI} + TD^{n}_{Ch} \; if \; EV \; owner \; denies \; the \; DR \; request (\xi^{n}_{DRS} = 0) \end{cases} \forall n \in \mathcal{N}_{EV} \tag{6.23}$$

Moreover, the charging power calculation of EV is similar as in (6.11). The daily EVL of a large number of EVs for DR operation can be calculated using (6.24) as follows:

$$P^{t}_{EV,DR} = \sum_{n=1}^{N_{EV}} P^{t,n}_{Ch} \quad \forall t \in \mathcal{T} \tag{6.24}$$

The total EV load (P^{t}_{EV,GCD_DRM}) for GCD_DRM can be defined as

$$P^{t}_{EV,GCD\_DRM} = P^{t}_{EV,ACM} + P^{t}_{EV,V2G} + P^{t}_{EV,DR} \quad \forall t \in \mathcal{T} \tag{6.25}$$

where $P^t_{EV,ACM}$, $P^t_{EV,V2G}$ and $P^t_{EV,DR}$ are the modelled EV load for ACM, V2G and DR operations.

6.4. Case study and results

This section discusses the impact of the proposed FLS and modelled EVL on the developed IEMS (in Chapter 5). The model specifications and parameters are similar to those in Chapter 5. Figure 6.1 shows the schematic of the system with a prosumer building, EV aggregator and grid. Further, the simulation parameters associated to EV load modelling are shown in Table 6.2. Moreover, the details of the types of EVs, along with their specifications, are discussed in Table 6.3.

It is assumed that the EVs will charge at a price of 0.07 $/kWh and the EVs participating in V2G will be charged (after discharging) with an electricity rate of 0.04 $/kWh. Based on these values, the cost paid by EV aggregator ($\mathbb{C}^T_{EVAG}$) to MG is estimated. In this study, the modeling of EVL is performed for 10, 20, and 30 EVs and for each level and both modes, 365 EV load scenarios are generated using the developed probabilistic model. The modelled EVL for ACM and GCD_DRM considering 20 EVs are shown in Fig. 6.2(a) and Fig. 6.2(b), respectively.

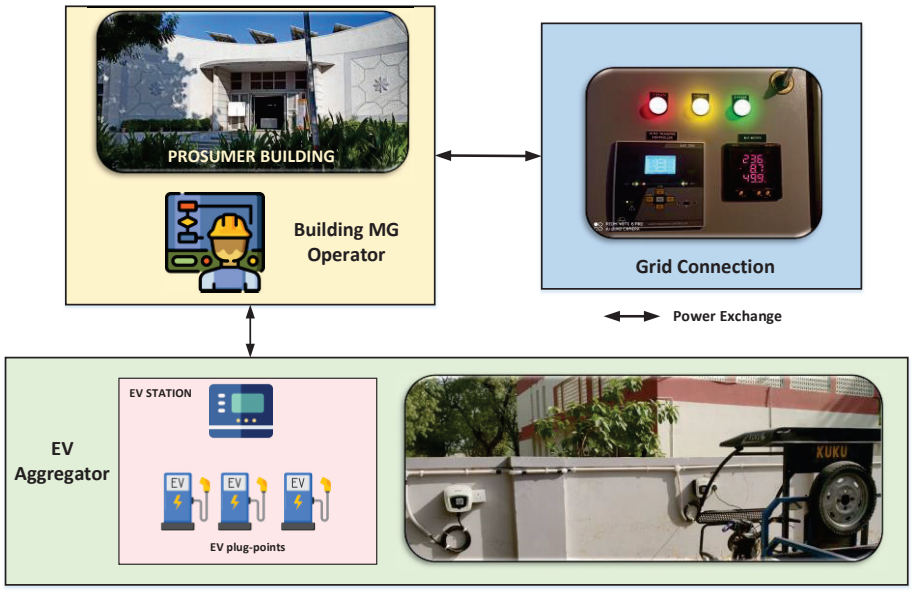

Figure 6.1 Schematic of the system with prosumer building, EV aggregator and grid

Table 6.2 Values of different simulation parameters

S.No.	Parameter	Value
1.	N_{EV}	10,20,30
2.	$\alpha_E, \alpha_V, \alpha_R$	30%, 50%, 20%
3.	N_{EV_P}	3
4.	$\eta_{EV,Ch}/\eta_{EV,Dch}$	90%
5.	D_{EV}	4
6.	$TD_L^{ń}$	3 hours
7.	T_{PP}^{start}	18:00
8.	T_{PP}^{end}	20:00
9.	$SOC_{EV}^{Ḿ}$	100%
10.	$SOC_{EV,Dch}^{th}$	60%

Table 6.3 Details of the types of EVs along with their specifications

Type of EV	Wheeler Type	$E_{EV}^{R,d}$ in kWh	$P_{EV,Ch/Dch}^{d}$ in kW/h	$S_{EV}^{Ḿ,d}$ in km	Time required for full charge in hours
Type 1	2-wheeler	3	0.6	128	5
Type 2	2-wheeler	4.56	1.14	145	4
Type 3	3-wheeler	7.4	1.85	125	4
Type 4	3-wheeler	5.76	1.65	60	4

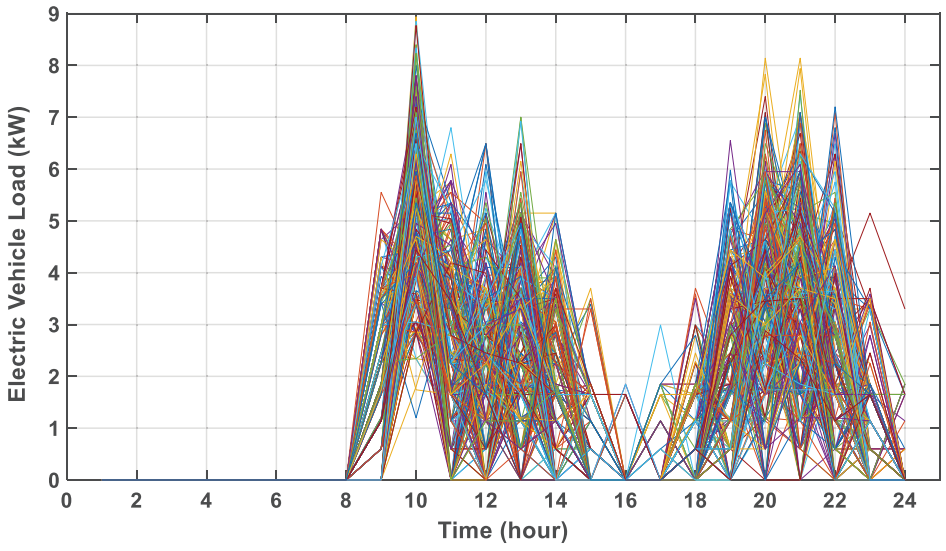

(a)

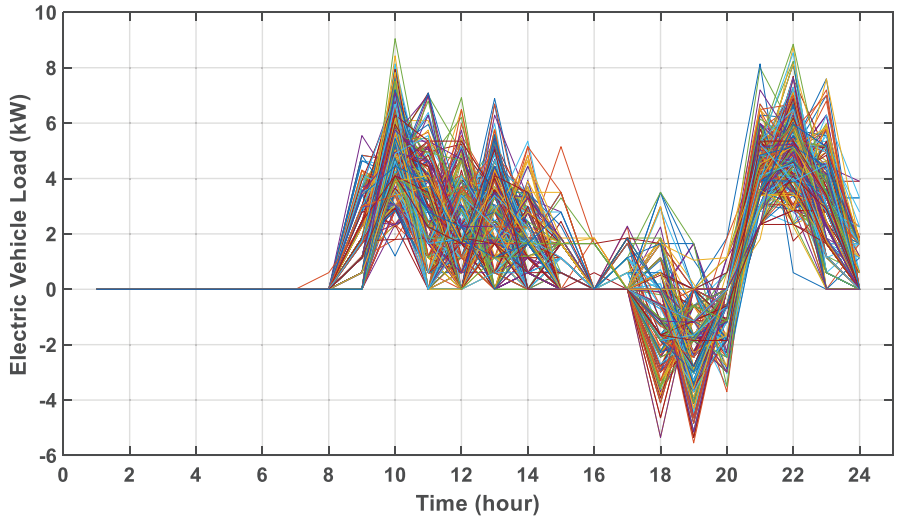

(b)

Figure 6.2 EVL modelled for (a) ACM and (b) GCD_DRM considering 20 EVs

6.4.1. Performance assessment of IEMS with FLS

Figures 6.3, 6.4, and 6.5 show the annual operating cost of MG, the annual dynamic degradation factor, and the estimated total operating life of BESS for IEMS and IEMS+FLS, respectively.

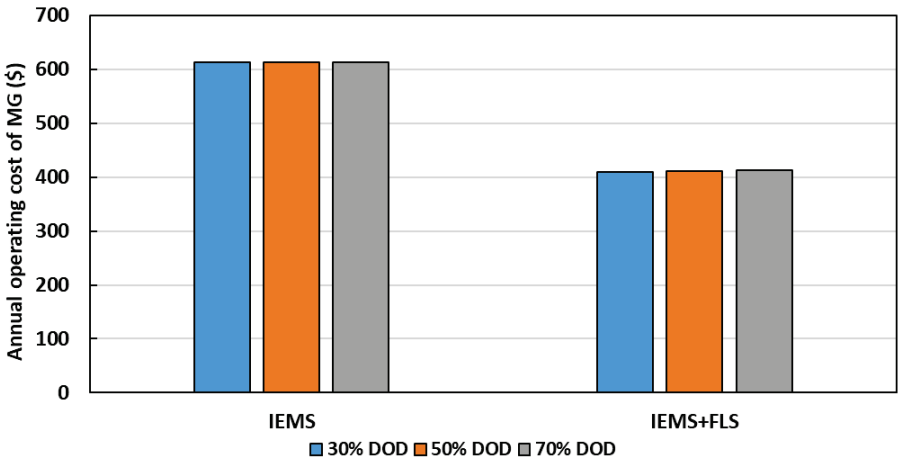

Figure 6.3 Annual operating cost of MG for IEMS and IEMS+FLS considering various DOD levels

It can be observed from Figs. 6.3, 6.4 and 6.5, and the FLS scheme improves the performance of IEMS by further reducing the operating cost of the MG and dynamic degradation factor and improving the total operating life of BESS. By integrating FLS,

the burden on BESS has been reduced, thereby decreasing its dynamic degradation factor and its operating & maintenance (O&M) cost. Due to this, the total operating cost of MG reduces. Additionally, as the power exported by the grid also decreases, the operating cost of MG is further reduced.

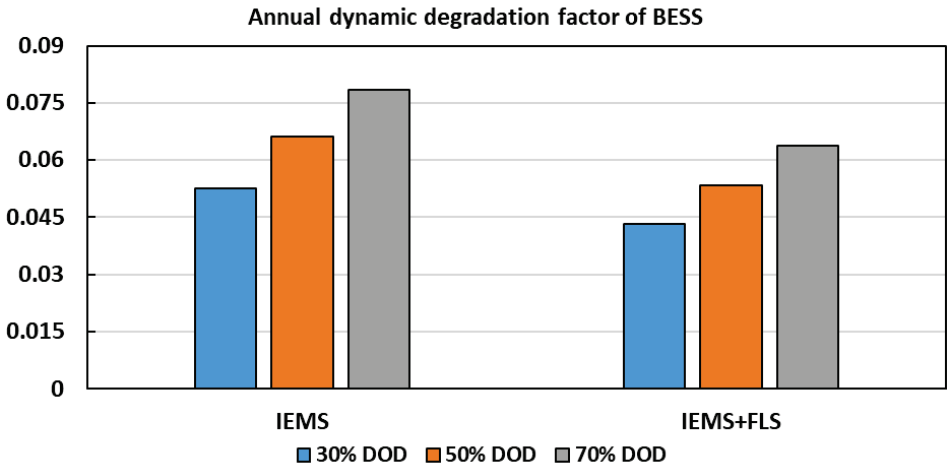

Figure 6.4 Annual dynamic degradation factor of BESS for IEMS and IEMS+FLS considering various DOD levels

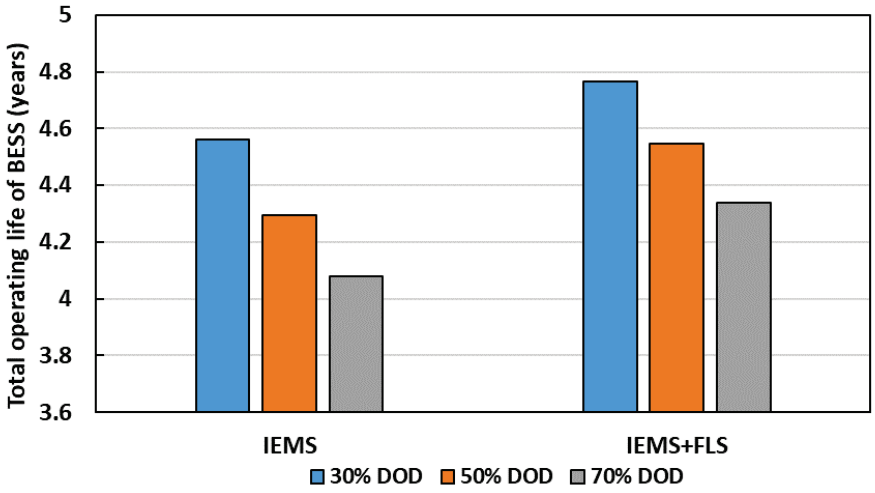

Figure 6.5 Total operating life of BESS for IEMS and IEMS+FLS considering various DOD levels

Table 6.4 shows the impact of FLS on IEMS in terms of the percentage change in the annual operating cost of MG, annual dynamic degradation factor and estimated total operating life of BESS from IEMS+FLS with respect to IEMS.

Table 6.4 Percentage change in operating cost of MG, dynamic degradation factor, and estimated total operating life of BESS from IEMS+FLS with respect to IEMS

DOD Levels	Percentage change in $\mathbb{C}_{MG}^{Y}$	Percentage change in BDf_{D}^{Y}	Percentage change in T_{OL}
30%	-33.06	-17.87	4.48
50%	-33.01	-18.39	5.83
70%	-32.70	-18.64	6.34

Table 6.4 shows a considerable improvement in all the key factors by integrating IEMS and FLS. For 70% DOD, the decrease in operating costs and degradation factor is 32.70% and 18.64% from IEMS+FLS with respect to IEMS. Further, there is a 6.34% increment in the total operating life of BESS. It can be concluded that IEMS+FLS provides the maximum benefit to the prosumer building in terms of economic and efficiency perspective.

To further assess the operation of BESS and grid with IEMS and IEMS+FLS daily is performed. Figure 6.6 shows the day-ahead optimal schedule of BESS and grid considering IEMS+FLS and IEMS with 70% DOD. Moreover, Fig. 6.7 shows the SOC profile of BESS from IEMS+FLS and IEMS.

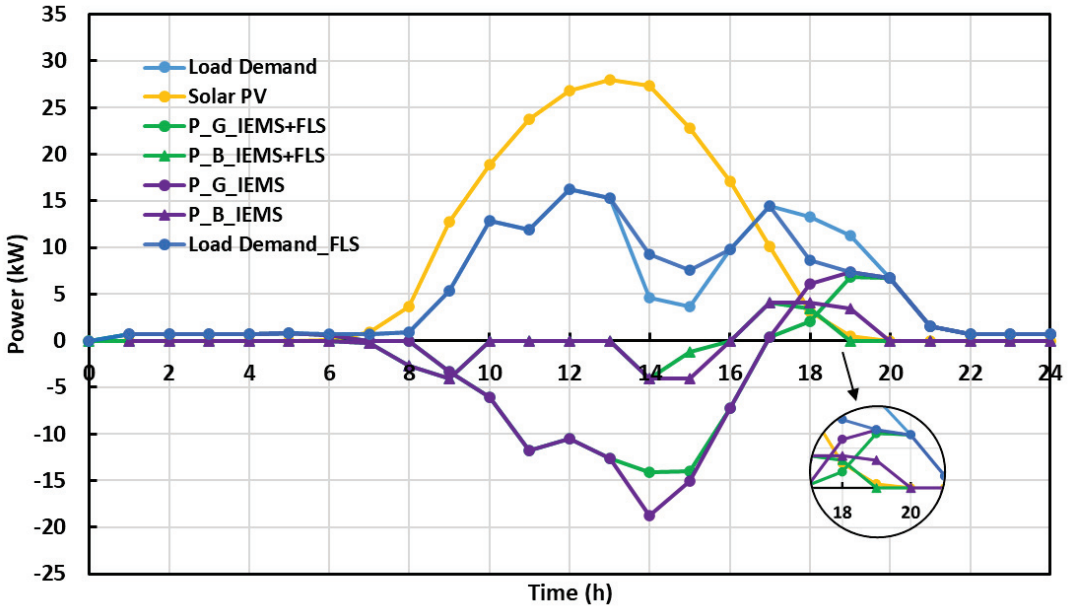

Figure 6.6 Optimal day-ahead schedule of BESS for IEMS and IEMS+FLS

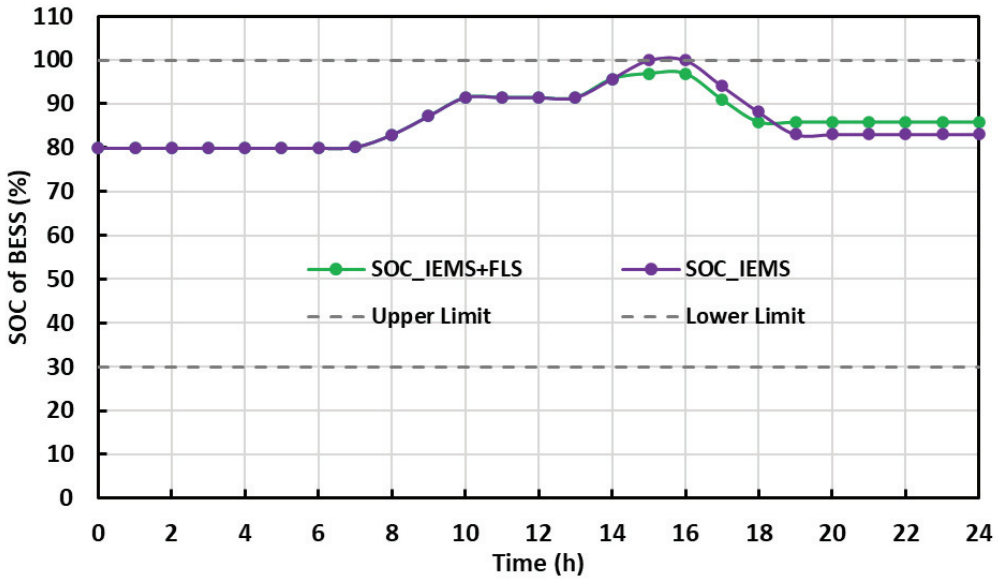

Figure 6.7 SOC of BESS for IEMS and IEMS+FLS

It can be observed from Figs. 6.6 and 6.7 that with the FLS scheme, the flexible load demand is shifted from the time slot where generation is less than the load, to the time slot where excess generation is available. Further, due to this, the burden on BESS and grid especially during peak hours has been significantly reduced. Therefore, for time instants 18 and 19, the BESS discharges and grid exports with lesser value than in IEMS as shown in Fig. 6.6.

The daily operating cost of MG ($\mathbb{C}_{MG}^{T}$), and the dynamic degradation factor from IEMS, and IEMS+FLS is tabulated in Table 6.5.

Table 6.5 Daily operating cost of MG and dynamic degradation factor of BESS from IEMS and IEMS+FLS

Parameters	**IEMS**	**IEMS+FLS**
Daily operating cost of MG ($\mathbb{C}_{\mathbf{MG}}^{\mathbf{T}}$) in $	-0.64	-0.95
Dynamic degradation factor ($\mathbf{BDf}_{\mathbf{D}}^{\mathbf{T}}$)	12.50E-5	8.53E-5

It can be noted that FLS has considerably improved the performance of IEMS, therefore IEMS+FLS leads to optimal operation of MG in terms of profit of building owner as well as life of BESS.

6.4.2. Performance assessment of IEMS with EVL

Figures 6.8 and 6.9 show the annual operating cost of MG and annual cost paid by EV aggregator, respectively, with IEMS, IEMS+ACM and IEMS+GCD_DRM considering 10, 20 and 30 EVs.

It can be observed from Fig. 6.8 that, as the EV penetration increases, the operating cost of MG decreases irrespective of EV operating mode. It is mainly because as the EV load is increased, the MG starts using surplus power to charge the EVs rather than exporting it to the grid. However, GCD_DRM leads to a lowering of the operating cost of MG as compared to ACM, as in this mode, EV starts discharging at peak hours and also tries to shift the load from peak hours to off-peak hours, due to which the burden on BESS and grid is reduced.

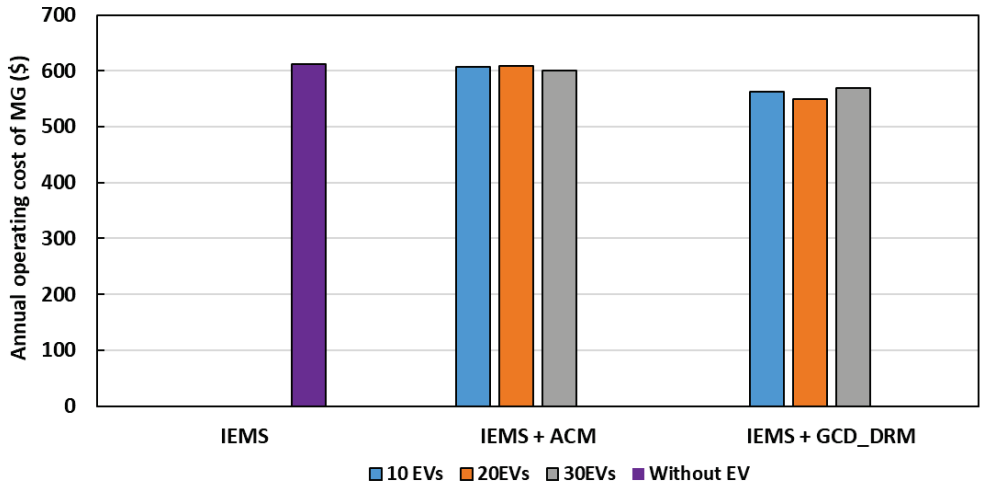

Figure 6.8 Annual operating cost of MG with IEMS, IEMS+ACM and IEMS+GCD_DRM considering 10, 20 and 30 EVs

From Fig. 6.9 it is clearly observed that, as the EV penetration level increases, the annual cost paid by the EV aggregator also increases irrespective of mode of EV operation. Further, it can be noted that, GCD_DRM mode of EV operation reduces the cost paid by EV aggregator as compared to ACM.

Figures 6.10 and 6.11 show the annual dynamic degradation factor and total operating life of BESS, respectively, with IEMS, IEMS+ACM and IEMS+GCD_DRM considering 10, 20 and 30 EVs.

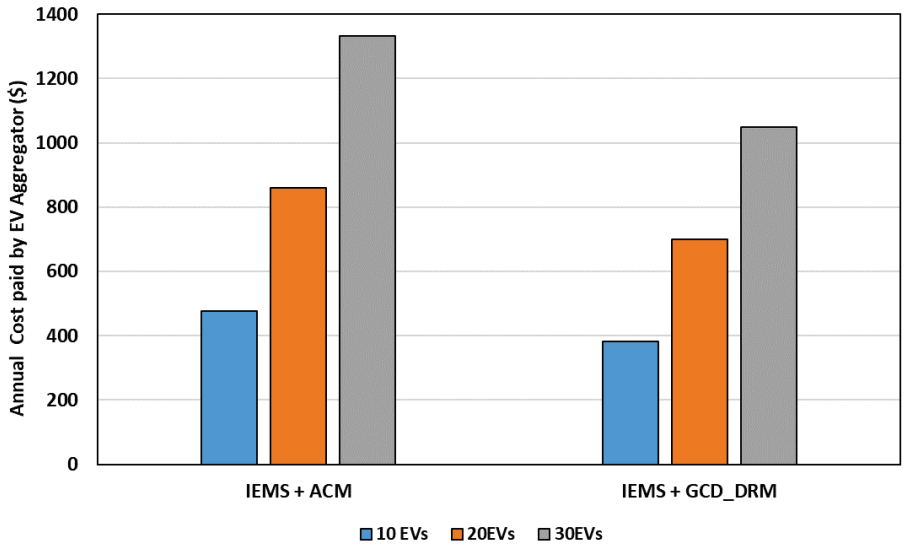

Figure 6.9 Annual cost paid by EV aggregator with IEMS+ACM and IEMS+GCD_DRM considering various number of EV levels

It can be noticed from Figs. 6.10 and 6.11 that, as the EV penetration increases, the annual dynamic degradation factor of BESS also increases, thus resulting in reduction of the total operating life of BESS. However, the GCD_DRM lowers this effect on BESS operation.

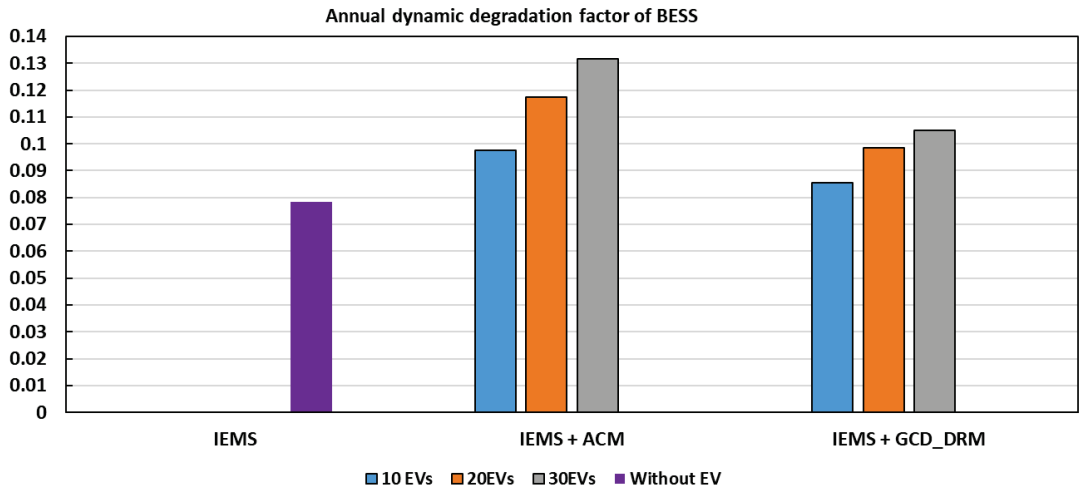

Figure 6.10 Annual dynamic degradation factor of BESS with IEMS, IEMS+ACM and IEMS+GCD_DRM considering 10, 20 and 30 EVs

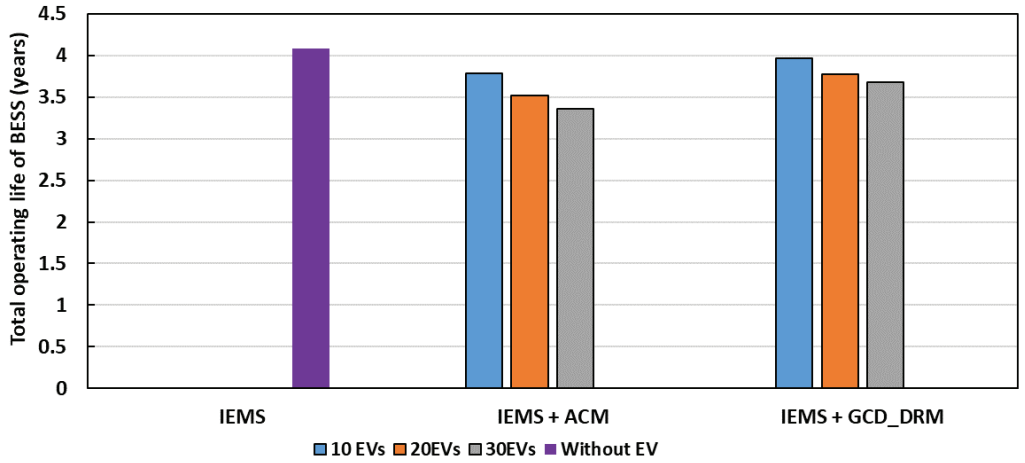

Figure 6.11 Total operating life of BESS with IEMS, IEMS+ACM and IEMS+GCD_DRM considering various number of EV levels

Table 6.6 shows the percentage change in operating cost of MG, dynamic degradation factor, and estimated total operating life of BESS from IEMS+ACM with respect to IEMS.

It can be concluded from Table 6.6 that, for the highest EV penetration level i.e., 30 EVs, the IEMS+ACM, decreases the operating cost of MG by 2.06%. However, the degradation factor increases by 67.69%, thereby the operating life of BESS has reduced by 17.80%.

Table 6.6 Percentage change in operating cost of MG, dynamic degradation factor, and estimated total operating life of BESS from IEMS+ACM with respect to IEMS

EV Levels	Percentage change in $\mathbb{C}_{MG}^{Y}$	Percentage change in BDf_{D}^{Y}	% Percentage change in T_{OL}
10	-0.92	24.46	-7.26
20	-0.52	49.71	-13.72
30	-2.06	67.69	-17.80

Table 6.7 shows the percentage change in operating cost of MG, cost paid by EV aggregator, dynamic degradation factor, and estimated total operating life of BESS from IEMS+GCD_DRM with respect to IEMS+ACM.

Table 6.7 Percentage change in operating cost of MG, cost paid by EV aggregator, dynamic degradation factor, and estimated total operating life of BESS from IEMS+GCD_DRM with respect to IEMS+ACM

EV Levels	Percentage change in $\mathbb{C}_{MG}^{Y}$	Percentage change in $\mathbb{C}_{EVAG}^{Y}$	Percentage change in BDf_{D}^{Y}	Percentage change in T_{OL}
10	-7.33	-19.63	-12.30	4.76
20	-6.97	-20.57	-16.10	7.13
30	-5.18	-21.24	-20.08	9.71

From Table 6.7 it is noted that, for 30 EVs load, the GCD_DRM, decreases the $\mathbb{C}_{MG}^{Y}$ and $\mathbb{C}_{EVAG}^{Y}$ by 5.18% and 21.24%, respectively as compared to ACM. Moreover, it also decreases the BDf_{D}^{Y} by 20.08% and thus increases the operating life of BESS by 9.71%.

It can be concluded that, IEMS+GCD_DRM helps in optimizing the operation of MG as well as EV aggregator by increasing their profit as compared to IEMS+ACM.

6.4.3. Performance assessment of IEMS with FLS and EVL

To estimate the performance of IEMS with the integration of FLS and EVL, critical values such as 70% DOD and 30 EVs are considered. Figures 6.12 and 6.13 show the annual operating cost of MG and the annual cost paid by EV aggregator with IEMS, IEMS+FLS, IEMS+ACM, IEMS+GCD_DRM, IEMS+ACM+FLS and IEMS+GCD_DRM+FLS.

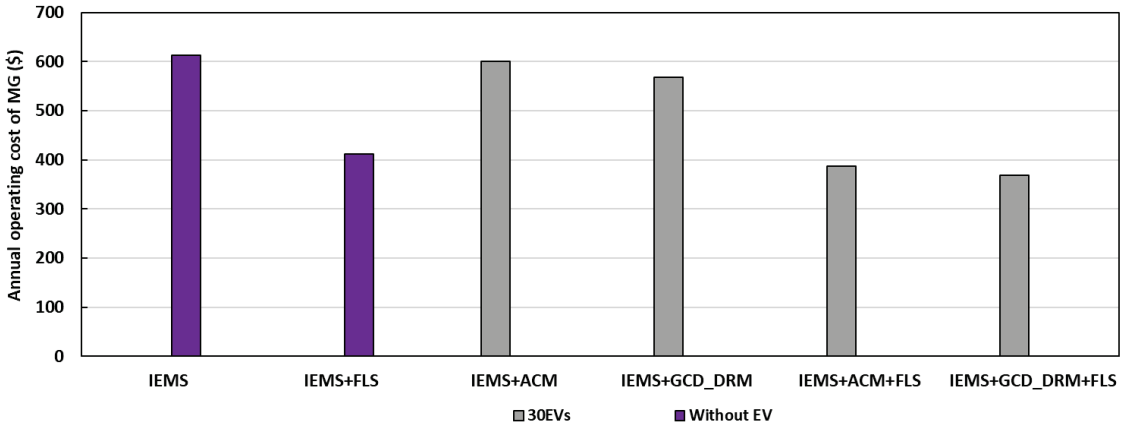

Figure 6.12 Annual operating cost of MG for all the considered cases considering 30 EVs

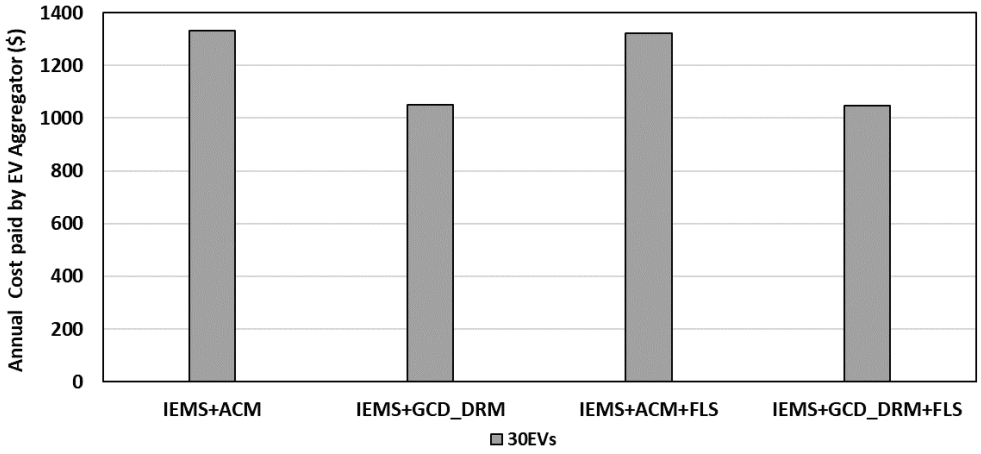

Figure 6.13 Annual cost paid by EV aggregator for all the considered cases considering 30 EVs

It is observed from Figs. 6.12 and 6.13 that IEMS+GCD_DRM+FLS results in minimum annual operating cost of MG and cost paid by EV aggregator as compared to other cases.

The annual dynamic degradation factor and total operating life of BESS with IEMS, IEMS+FLS, IEMS+ACM, IEMS+GCD_DRM, IEMS+ACM+FLS and IEMS+GCD_DRM+FLS are shown in Figs. 6.14 and 6.15, respectively.

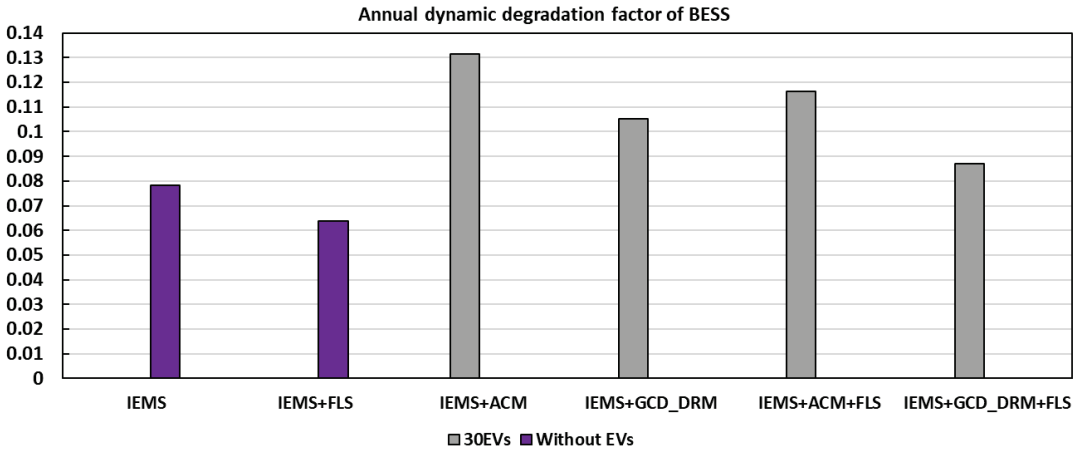

Figure 6.14 Annual dynamic degradation factor of BESS with each case considering 30 EVs

From Figs. 6.14 and 6.15, it is noticed that, without EV penetration, IEMS+FLS results in minimum annual dynamic degradation of BESS and thus ends up with maximum value of total operating life of BESS. However, with the EV penetration,

IEMS+GCD_DRM+FLS has the lowest annual dynamic degradation of BESS and, therefore, achieves the highest value of the total operating life of BESS.

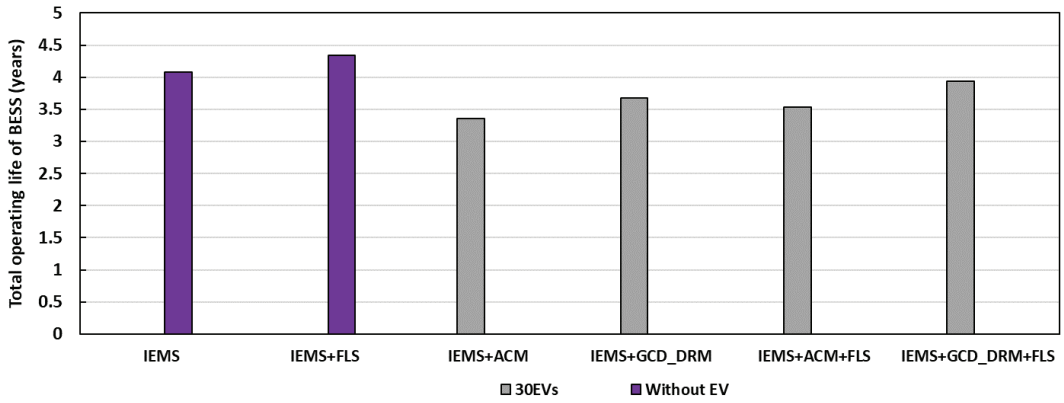

Figure 6.15 Total operating life of BESS for each case considering 30 EVs

It can be concluded from Figs. 6.12 to 6.15, that integration of FLS and GCD_DRM significantly improves the performance of the developed IEMS by maximizing the financial profit of the MGO & EV aggregator and improving the reliability, life and efficiency of the MG.

6.5. Conclusion

This chapter formulates an FLS scheme to improve the efficacy of the proposed IEMS and achieve sustainable and more efficient operation of the prosumer building. It effectively utilizes solar PV generation and shifts the loads of the building as per the equivalent power. The integration of IEMS with FLS further reduces the operating cost of MG from 32.7% to 33.06% and increases the life span of BESS by 4.48% to 6.34%, depending on the DOD.

In addition, in order to consider the detailed effect of EVs on the system, a practical EVL is required. Therefore, to model the practical EVL profile, an advanced probabilistic modelling is performed that considers uncertain events and practical situations. It considers two most essential conditions, i.e., 1) availability of EV plug-points at EVS, and 2) uncertain behavior of EV owner regarding their leave time duration. Further, a new operating mode, GCD_DRM, is introduced that integrates the concept of V2G and motivates EV owners to participate in DR. In this study, the EVL is modelled for two

operating modes, i.e., ACM and GCD_DRM and their performances are examined while integrated with IEMS. The results reveal that IEMS+ GCD_DRM decreases the operating cost of MG owner and EV aggregator in the range of 5.18% to 7.33% and 19.63% to 21.24% with respect to IEMS+ACM depending on number of EVs. Further, it increases the life span of BESS in the range of 4.76% to 9.71% for the similar case.

Moreover, the performance of IEMS is examined with FLS and both the EV modes individually. It is found that IEMS+FLS+ GCD_DRM is the most economical, sustainable and efficient EMS for the prosumer building (MGO) and the EV aggregator.

Bibliography

[1] H. Ming, B. Xia, K.-Y. Lee, A. Adepoju, S. Shakkottai, and L. Xie, "Prediction and assessment of demand response potential with coupon incentives in highly renewable power systems," Prot. Control Mod. Power Syst., vol. 5, no. 1, p. 12, 2020, doi: 10.1186/s41601-020-00155-x.

[2] Y. Ding et al., "A comprehensive scheduling model for electric vehicles in office buildings considering the uncertainty of charging load," Int. J. Electr. Power Energy Syst., vol. 151, p. 109154, 2023, doi: https://doi.org/10.1016/j.ijepes.2023.109154.

[3] P. Sharma, P. Mishra, and H. D. Mathur, "Optimal energy management in microgrid including stationary and mobile storages based on minimum power loss and voltage deviation," Int. Trans. Electr. Energy Syst., vol. 31, no. 12, p. e13182, 2021, doi: https://doi.org/10.1002/2050-7038.13182.

[4] F. Sheidaei and A. Ahmarinejad, "Multi-stage stochastic framework for energy management of virtual power plants considering electric vehicles and demand response programs," Int. J. Electr. Power Energy Syst., vol. 120, p. 106047, 2020, doi: https://doi.org/10.1016/j.ijepes.2020.106047.

Chapter 7

Closure

7.1. Summary

A microgrid (MG) is a low-voltage electrical network that is developed from the small-scale interconnection of the various distributed energy resources (DERs) and loads. These DERs may include renewable energy sources (RERs), fossil fuel-based traditional generators (TGs) and battery energy storage systems (BESSs). Further, as electric vehicles (EVs) are growing as the potential alternative to fossil fuel-based vehicles, their penetration has substantially increased. Therefore, to achieve stable, optimal, efficient and sustainable operation of MG and to handle the uncertainty associated with load and RERs, an energy management strategy (EMS) is necessary. In this regard, this thesis focuses on the development of EMS for community and prosumer building MG. It explores the performance aspects of BESSs, various modes of EV operation and the impact of demand-side management (DSM) on the developed system.

7.2. Main Contributions

The main contributions of the thesis are as follows:

- A community MG is modelled based on a multi-bus network having various types of DERs and EVS. Further, to obtain the optimal sizing & appropriate placement of DERs together with EVS, an objective function is formulated that minimizes power loss and voltage deviation of the system. It considers voltage-dependent load and different charging patterns modelled as per residential, commercial, and industrial buses.

- For the designed community MG, an optimal energy management strategy (OEMS) is developed that aims at maximum utilization of DERs, promotes energy trading between MG and utility grid, performs peak load management through (governed charging/discharging mode) GCDM of EV operation, and minimizes the dependency of a MG on the utility grid. It is achieved by optimizing the energy exchanged between MG and the utility grid considering minimum total active power loss (TAPL) and total voltage deviation (TVD). The developed OEMS utilizes the coordinated BESS charging/discharging scheduling algorithm, which improves its performance and facilitates its maximum utilization. The proposed OEMS and GCDM of EV operation help in attaining the optimal, efficient, and sustainable operation of the community MG.
- In addition, to evaluate the energy management aspects of a prosumer building MG, a solar PV and BESS based grid-tied MG with EVS is designed, developed and deployed at the building of BITS, Pilani, campus. Further, an IEMS is proposed that focuses on increasing the profit of a prosumer building and improving the operating life span of BESS to achieve optimal and efficient operation of the building. It is achieved by minimizing the formulated cost objective function of MG as per the proposed rule-based algorithm (RBA), which effectively utilizes the BESS and grid power. It involves a non-linear battery degradation model considering calendar and cyclic ageing in terms of static and dynamic degradation factors, respectively, to estimate the practical operating life span of BESS.
- A flexible load shifting (FLS) scheme is formulated for prosumer building MG aiming at shifting the flexible loads from the time slot of a day where the equivalent power (solar PV generation subtracted from the load power) is the maximum to the time slot where it is the minimum. It increases the efficacy of the proposed IEMS by further reducing the operating cost of MG and the degradation factor of BESS, which improves the sustainability and efficiency of the building MG.
- Advanced probabilistic modelling of EVL is performed, which considers practical events, i.e., availability of plug-points and uncertain behavior of EV

owners in terms of time at which EV may leave the EVS. Moreover, a new mode of EV operation is introduced, i.e., governed charging/discharging with demand response mode (GCD_DRM). In addition, the performance of IEMS is examined with the modelled EVL under various modes of EV operation, i.e., ACM and GCD_DRM. Further, to estimate the maximum efficacy of IEMS, the combination of modelled EVL and proposed FLS is studied. The results showed that IEMS+FLS+ GCD_DRM is the most economical, sustainable, and efficient EMS for prosumer building operators and EV aggregators.

7.3. Future Scope

Though the proposed study has shown considerable improvements in performance, there is scope for future research, which is as follows:

- Optimal sizing & appropriate placement of RERs and TG units, together with EVS, is performed for a community MG to minimize power loss and voltage deviation of the system. However, it did not consider the optimal placement and sizing of BESS, which can be considered in future studies.
- The OEMS developed for community MG achieves economical, efficient, and sustainable operation by minimizing a multi-objective function that consists of energy exchanged between MG and utility grid, TAPL and TVD. Further, the direct incorporation of the operation cost function can enhance the performance of OEMS in terms of economical operation.
- In the IEMS proposed for the building, the operation of the BESS and grid power is dependent on the equivalent power, load demand (peak/off-peak), and SOC of BESS, as discussed in RBA. However, it can include grid exchange price to further reduce the operating cost of MG and improve the operating life of BESS,
- The performance of the developed FLS scheme, which is part of DSM, can be augmented by optimally shifting the various flexible loads considering their power ratings, operating hours, flexible time window, and customer comfort.
- Modelling of EVL can be performed using a machine learning prediction model after data collection and analysis. Further, the proposed probabilistic modelling

of EVL can be improved by integrating various demographic, socioeconomic, and weather factors with the considered uncertain events and parameters.

List of Publications

Journal Publications:

- **Pavitra Sharma**, D. Bhattacharjee, H.D. Mathur, P. Mishra, “Dual layer energy management model for optimal operation of a community based microgrid considering electric vehicle penetration” *Scientific Reports*, 14, 17499, July **2024**. https://doi.org/10.1038/s41598-024-68228-7
- **Pavitra Sharma**, K. K. Saini, H. D. Mathur and P. Mishra, "Improved Energy Management Strategy for Prosumer Buildings with Renewable Energy Sources and Battery Energy Storage Systems," *Journal of Modern Power Systems and Clean Energy*, vol. 12, no. 2, pp. 381-392, March **2024**. https://doi.org/10.35833/MPCE.2023.000761
- **Pavitra Sharma**, H.D. Mathur, P. Mishra, R.C. Bansal, “A critical and comparative review of energy management strategies for microgrids”, *Applied Energy*, Volume 327, 120028, ISSN 0306-2619, October **2022**. https://doi.org/10.1016/j.apenergy.2022.120028.
- **Pavitra Sharma**, P. Mishra, and H.D. Mathur, "Optimal Energy Management in Microgrid including Stationary and Mobile Storages based on Minimum Power Loss and Voltage deviation" *International Transactions on Electrical Energy Systems*, Vol. 31, Issue 12, October **2021**. https://doi.org/10.1002/2050-7038.13182

Book Chapters/Conference Publications:

- **Pavitra Sharma**, H.D. Mathur **(2023).** Optimal Siting and Sizing of Renewable Energy Sources in Distribution System. In: Singh, S.N., Jain, N., Agarwal, U., Kumawat, M. (eds) Optimal Planning and Operation of Distributed Energy Resources. Energy Systems in Electrical Engineering. Springer, Singapore.
- **Pavitra Sharma,** D. Sahoo, K.K. Saini, H.D. Mathur, H. Siguerdidjane, **(2023).** Real-Time Data-Based Optimal Power Management of a Microgrid Installed at BITS Supermarket: A Case Study. In: Bansal, H.O., Ajmera, P.K., Joshi, S., Bansal, R.C., Shekhar, C. (eds) Next Generation Systems and Networks. BITS-EEE-CON 2022. Lecture Notes in Networks and Systems, vol 641. Springer, Singapore.
- **Pavitra Sharma**, D. Sahoo, K. K. Saini and H.D. Mathur, "Effect of Environmental Parameters on Performance of Solar Photovoltaic System in Western India," IECON 2023- 49th Annual Conference of the IEEE Industrial Electronics Society, Singapore, Singapore, **2023**, pp. 1-6.
- **Pavitra Sharma**, D. Bhattacharjee, H.D. Mathur, P. Mishra and H. Siguerdidjane, "Novel optimal energy management with demand response for a real-time community microgrid," 2023 IEEE International Conference on Environment and Electrical Engineering and 2023 IEEE Industrial and Commercial Power Systems Europe (EEEIC / I&CPS Europe), Madrid, Spain, **2023**, pp. 1-6.
- K. K. Saini, C. Yadav, **Pavitra Sharma**, and H. D. Mathur, “Real Time Data-based Demand Side Management Techniques for a Microgrid to minify the grid dependency”, in the proceedings of IEEE 14th International Conference on Computing, Communication and Networking Technologies (ICCCNT), IIT Delhi, India, 2023.
- **Pavitra Sharma**, A. K. Mishra, P. Mishra and H.D. Mathur, "Optimal Capacity Estimation and Allocation of Distributed Generation Units with Suitable Placement of Electric Vehicle Charging Stations," *2021 IEEE Region 10 Symposium (TENSYMP)*, Jeju, Korea, Republic of, **2021**, pp. 1-7.

Brief Biography of the Candidate

Pavitra Sharma received the B.Tech. Degree in Power System Engineering from the University of Petroleum & Energy Studies (U.P.E.S.), Dehradun, Uttarakhand, India, and M.E. degree in Power Systems from Thapar Institute of Engineering & Technology (T.I.E.T.), Patiala, Punjab, India, in 2017 and 2019, respectively. She is currently a full-time research scholar pursuing a PhD degree in the Department of Electrical and Electronics Engineering, Birla Institute of Technology and Science (BITS), Pilani-Rajasthan, India. Her research interests include power system optimization, energy management of microgrids, battery energy storage systems, electric vehicle integration and demand-side management. She has authored 5 research articles in peer-reviewed international journals of repute and has published 2 book chapters. Her 11 papers have been published in IEEE-sponsored international and top national conferences.

Brief Biography of the Supervisor

Prof. Hitesh Datt Mathur received a B.E. degree from Nagpur University, Nagpur, India, in 1998; M.E. degree from Malaviya Regional Engineering College, Jaipur, India, in 2000; and a PhD degree from Birla Institute of Technology and Science (BITS) Pilani, India in 2007 and He was Post-Doctoral Fellow in Supelec, Paris, France in 2013. He was also invited as a visiting scientist to Centralesupelec, France in 2015,2019, and 2020.

Currently, He is a Professor in the Department of Electrical and Electronics Engineering, Birla Institute of Technology and Science, Pilani and also heading the School of Interdisciplinary Research and Entrepreneurship (SIRE) at BITS,Pilani. He has teaching and research experience of more than 24 years. Prof. Mathur is the Associate Editor of IET Renewable Power Generation as well as in the editorial board and reviewer of various journals, mainly in the field of electrical power systems and renewable energy.

He is a Senior member of IEEE, a Fellow of the Institution of Engineers (India), a Chartered Engineer and a life member of the Indian Society of Technical Education. He has published more than 90 papers in national/international journals and conference proceedings. His research interests include power system control of isolated and interconnected power systems, power system optimization, automatic generation control and artificial intelligence techniques applications in power systems and distributed generation (DG) with grid interconnection issues. He is handling research projects of various government and non-government organizations such as the Department of Science and Technology, Ministry of Power, Ministry of Human Resource and Development, Department of Biotechnology etc. The projects are related to the area of Energy management through IoT, Renewable source integration, microgrids and Electric vehicle penetration challenges.

Brief Biography of the Co-Supervisor

Dr. Puneet Mishra completed his PhD in Instrumentation and Control Engineering from Netaji Subhas Institute of Technology, University of Delhi, New Delhi, India, in 2017, and his M.E. in Control and Instrumentation Engineering from Delhi College of Engineering, University of Delhi, India in the year 2011. He has been serving as an Assistant Professor in the Department of Electrical and Electronics Engineering at Birla Institute of Technology and Science, Pilani, since December 2017. Prior to this, he served GLA University, Mathura and BIT Mesra as an Assistant Professor. He has published over 55 papers in national/international journals and conference proceedings. His current research interests include Intelligent Control, Fuzzy Adaptive Control, Fractional order control and related fields.